Summer 8-15-2019

High-Density Diffuse Optical Tomography During Passive Movie Viewing: A Platform for Naturalistic Functional Brain Mapping

Andrew Kelsey Fishell
Washington University in St. Louis

WASHINGTON UNIVERSITY IN ST. LOUIS

Division of Biology and Biomedical Sciences
Neurosciences

Dissertation Examination Committee:
Joseph Culver, Chair
Ana María Arbeláez
Nico Dosenbach
Jonathan Peelle
Christopher Smyser

High-Density Diffuse Optical Tomography During Passive Movie Viewing: A Platform for Naturalistic Functional Brain Mapping

by
Andrew Kelsey Fishell

A dissertation presented to
The Graduate School
of Washington University in
partial fulfillment of the
requirements for the degree
of Doctor of Philosophy

August 2019
St. Louis, Missouri

Table of Contents

List of Figures

List of Tables

Acknowledgements

One of the most confusing things about graduate education is the oft-stated goal of training students to become “independent researchers.” I depended heavily on the incredible support, mentorship, and friendship of those around me during my six years as a student, and it is the people who I met who made my graduate education fun, doable, and intellectually rich. While my capabilities as a researcher increased over time, my reliance on those around me for feedback, input, and guidance also increased with time. For this reason, I believe I am graduating from Washington University as a competent, but nonetheless dependent, researcher. Simply put, this dissertation would not have been possible without the extensive support from many people.

I’m not sure what Joe Culver thought when I asked if he would take me as a student, but I am very grateful to have had the opportunity to be mentored by Joe. When I expressed interest in the lab, I also expressed hesitation in my ability to be successful in the lab—I had an extremely limited background in physics, electrical engineering, signal processing, or any of the other topics that seemed central to the lab. I was motivated by in interest in the lab’s techniques, and the surprising realization that you could learn something about the brain by shining light on it. I also thought that it would be amazing to use the lab’s imaging instruments alongside the people who built them. I am thankful for Joe’s open-mindedness, and willingness to work across what some would see as undesirable disciplinary boundaries. When challenges inevitably arose, I was grateful that Joe was always patient, understanding, and confident that we’d arrive at a solution, even if we weren’t quite sure about the specifics.

Joe is an exceptional advisor, and based on my extremely limited work experience, maybe the most interesting boss I will ever have. My three favorite things about Joe are: (1) No matter how you assess it, Joe is extremely creative. Whether you look at his past life as a drummer, or his current funding portfolio, Joe is not afraid to pursue unique and sometimes seemingly absurd opportunities to advance neurophotonics technologies. As my AAdvantage account can affirm, I have benefitted from this creativity as I became exposed to fields and research topics that I would have never imagined as a first-year student interested in neuroimaging. I've particularly enjoyed the opportunity to learn about how clinical research and global health interact through our imaging research sponsored by the Gates Foundation. (2) Whether it's students, collaborators, or staff, Joe surrounds himself with really amazing, kind, and talented people, much to the benefit of the educational environment in the lab. While the research was frequently challenging, the work environment rarely was. (3) Joe is really good at structuring stuff—which is why this list is three items long. I remember when I gave my first conference talk at the fNIRS conference in Paris, which was assigned to me at the last minute. I was both excited and terrified, and Joe helped me structure the talk so I could be confident in my ability to present the talk and focus on being excited for my first ever conference presentation. There has been no shortage of challenges, lessons, and incredible experiences in the Culver Lab, and if I had to choose a lab all over again, there's no doubt I would choose Joe's.

I think one reason that Joe was ok with me joining the lab with little-to-no physics knowledge was because he had a biomedical engineering student named Karla Bergonzi and a post-doc named Adam Eggebrecht (a.k.a. "The Architect") who could teach me the

ways of High-Density Diffuse Optical Tomography. Karla had seemingly unlimited patience for a first-year student (me) who had no idea what was going on. Up until when she graduated, Karla was one of the best role models in the lab, who helped me with everything that a student should know how to do, but doesn't: meeting preparation, poster design, data collection, data analysis, and time management. Most importantly, she is a fantastic travel buddy, and I am extremely grateful for her friendship.

Similarly, despite trying to have a career, Adam was and still is incredibly ok with answering the same question multiple times, explaining concepts that should have stuck from intro physics/math classes, and providing feedback on presentations and manuscripts. Adam also has a knack for developing compelling (and fundable) research narratives, which is a skill that I have both admired and attempted to emulate in my own work. As a perpetually baffled first-year, Adam was one of the few people who actually sat down with me and went over my qualifying exam proposal with me—something that was critical for helping me strengthen my proposal and ultimately pass the exam.

My thesis committee is filled with fantastic role models for rigorous science, and I am grateful to have such a broad set of perspectives represented on my committee. If I had a time machine, I would like to have taken cognitive neuroscience with Jonathan Peelle, my committee chair, when I was an undergrad. The word on the street is that Jonathan is an amazing professor, who is engaging, kind, and extremely knowledgeable. My experiences working with Jonathan are congruent with the word on the street. In addition, Jonathan is a snappy and prolific Twitter user, and an ardent supporter of open, transparent, and reproducible science. The thing I appreciate most about Jonathan is that

he is a fierce advocate for equality, particularly for representation of underrepresented groups in science.

Ana Maria Arbalaez and Chris Smyser are my committee's dynamic duo. Ana Maria and Chris have always made time to give thoughtful feedback whenever I have needed it and have been essential resources as the Culver Lab prepared to begin performing brain imaging research in Colombia. I always looked forward to Chris's sense of humor during weekly meetings, and I also appreciated the fact that Chris and Ana Maria severed as reminders of the clinical motivations for our research—we aren't just here to build cool stuff; we're here to build cool stuff and help people while we're doing it.

In addition to being a professor and physician, Ana Maria has the added distinction of being a travel agent and an international celebrity. Alongside the incredible Marcela Rivera, Ana Maria made sure our trips to Colombia went off without a single hitch. Additionally, Ana Maria and her parents allowed us to convert their incredible home into a neuroimaging lab, and had no hesitation helping us with whatever we needed to get our instrument up and running. It only takes about 5 minutes in the clinics at Centro Medico Imbanaco to realize that Ana Maria is universally adored by the clinicians there. I will always appreciate Ana Maria's endless kindness and support, willingness to jump off a cliff with me, and I will always be inspired by her ability to get anything done, regardless of how impossible it seems.

When I was an undergraduate student in Kathleen McDermott's lab, I was mentored by Steve Nelson, who told me to be on the lookout for a German man in the East Building who had a frightening laugh, because that guy was always on the cutting edge of neuroimaging. That person turned out to be Nico Dosenbach, and Steve Nelson's

assessment turned out to be correct. Like Joe, Nico is one of the more creative scientists I've met, and that creativity has led Nico to some results I really admire. I'm excited to continue cyber-stalking Nico's science to see what's next.

Now I'd like to thank everyone in the Culver Lab, which is an amazingly supportive community and a great place to be a student. Ashley Nielsen is not technically part of the lab but deserves acknowledgement here because of her amazing signal-to-noise, gloriously log-linear light fall off, and ability to watch certain stimuli as many times as needed. Tracy Burns-Yocum (a.k.a. "Torcle", a.k.a. "MT") is one of the reasons I survived the period of grad school I affectionately refer to as "The Fog" (Years 3-5). Tracy is one of the most hilarious people I have ever met, and she made coming to lab easy, even on the most challenging days. I am so grateful for everything she did to help my projects succeed, from collecting data, to helping with analysis, to fixing the cap with me, to listening to haunted house sounds, to playing the tide is high on the beach. I hope she keeps crushing it in graduate school and never has to encounter rimless glasses again.

I am confident that my future officemates will never be as good as the ones I had in grad school. Arefeh Sherafati is inspiring in every sense possible. Arefeh essentially runs all of the lab's clinical neuroimaging projects, from data collection, to light modeling, to data analysis, to teaching others how everything works. I'll always admire her consistently positive attitude, friendliness, warmth, and willingness to lend a second pair of eyes to code or data that seems to be acting up. The thing I'll miss most, however, is taking a break from work to explore our favorite places on Google Maps. I am extremely grateful to Zack Markow for also being a constantly upbeat, friendly, supportive, and entertaining person. One of the best things about Zack is that he's an excellent teacher.

Usually Zack would present a paper for the theory portion of group meeting with a title that I could marginally understand, and by the end of the presentation, I would actually have confidence in my ability to understand the paper! The eternal light of the lab is Kalyan Tripathy, who is a blinding ray of sunshine and enthusiasm. I will always be thankful that Kalyan performed all of my favorite songs (Mambo No. 5) during his karaoke setlist in Ft. Lauderdale. More importantly, we both survived the entertaining chaos that was Tokyo, and now have an endless array of bizarre travel stories.

Ed Richter and Broc Burke are two of the other “adults” in the lab who I have really enjoyed working with, and they both have an amount of technical expertise that makes my head spin. Traveling with Ed is one of my favorite things to do, and because Ed is so incredibly friendly towards everyone we meet, he makes me look good too. Our ~~boondoggles~~ imaging excursions to Cali were always a treat, especially when it was time for lulo. Broc was always up for stimulating conversation (work related or not) and was another person in lab who I could count on to explain something super technical in a way that I could actually understand. (Although I still don’t understand why Broc runs Windows on a Mac… or at least I’ve forgotten.) Broc is an excellent reminder of the potential clinical utility of optical brain imaging and has no shortage of interesting clinical applications that I couldn’t have even possibly imagined.

I regret that Mariel Schroeder and Alexa Svodoba were hired under false pretenses. When they applied for Tracy’s job, they were not told that it also included dealing with me for extended periods of time. Nevertheless, Mariel and Alexa rose to the occasion. I am so glad you both joined the lab, and I will definitely miss being part of the lunch crew. In particular, I want to thank Mariel for nerding out over language acquisition

with me, which was super fun. I hope (and already know) that Mariel and Alexa will both be superstars in graduate school and medical school, respectively. Muriah Wheelock is the lab's fearless senior post-doc, and I am most grateful for her wit. I hope that someday she releases her world's best (worst) figures list, because I think she has great taste in bad figures. Hunter Banks is the fearless junior post-doc and deserves acknowledgment for making me laugh on multiple occasions during a single laser safety presentation. Lindsey Briar did two important thigs for me: keep Kalyan under control and show me (unknowingly via the Box) how to write a paper. I appreciate both things equally.

The Culver Lab is huge and filled with many other incredible people, such as Adam Bauer, Rachel Rahn, Paul Lin, Annie Bice, Chris Tracy, Sean Rafferty, Calamity Svodoba, and Dana Wilhelm, all of whom have contributed to the amazing experience I've had as a graduate student. The list of Culver Lab alumni is also huge, and I certainly would not have made it to the dissertation-writing phase of my life without having some truly incredible role models to show me how to be productive and successful as a graduate student. Thank you to Karla Bergonzi, Inema Orukari, Jon Bumstead, Matt Reisman, Patrick Wright, and Samira Hassanpour.

The Optical Radiology Lab is even larger and filled with other friendly and supportive people. In particular, I would like to thank April Berryman and Dorota Grabowska their kindness and for always being up for a laugh. I would also like to remind April, in a formal, submitted dissertation, that the toner is low. I would like to remind Dorota that it's never too late to spice up life with some Corporate Seasonings, but durian candy will suffice in a pinch. Please reserve the trail mix for April or prepare to face potentially dire consequences.

The best part of being a DBBS student is Sally Vogt, and 100% of neuroscience students agree with me. Sally, thank you for being a never-ending source of encouragement for me, always making time for a chat, and helping me successfully navigate all more challenging portions of my time at WashU. I am incredibly grateful for your patience and everything that you do to keep students happy and on track. I am also grateful to neuroscience program directors past and present, Larry Snyder, Erik Herzog, Tammy Hershey, and Tim Holy, for thoughtfully running the premier training program within DBBS.

As Alex Russo once said, “Friends are… good.” Outside of lab, there has been no shortage of amazing friendships to help me get through the tricky times and celebrate the much more plentiful good times. Now we return to Ashley Nielsen (a.k.a. “Systems”). We began graduate school by frightening each other. Then, we were appropriately recognized as a beautiful seventies couple, premier dancers, and coddlers of La Croix. I am so grateful to have met you, for forming a formidable triad with Shina Seabury, and most importantly, for C-Time (coffee time). Very few people understand C-Time, and that is how it should be. Let the published record show (ahem, Dr. Herzog) that many times, C-Time included discussion of neuroimaging and other scientific topics. Many other times, C-Time was a rambling tribute to incoherence. I will miss you and C-Time, but I am so excited to hear how your post-doc at Northwestern unfolds and to see what awesome things are in store for you.

Ashley is just one of the “Super Six,” a terrifyingly attractive group within the entering neuroscience cohort of 2013. Alex Russo, Krissy Sakers, Amy Clippinger, and Wade Self are all part of why I felt right at home in the neuro program from day one, and

I am so glad to have you as friends during this crazy time. Alex Russo gets a bonus thank you for deciding that “Voxel” was an awesome name for a dog, and for having the best taste in music.

BALSA was an amazing experience because it helped me see the light at the end of the career tunnel and meet like-minded students who shared an entrepreneurial spirit. In particular, I’d like to thank Erica Thomas for being the best president anyone could hope to vice-president for. Another important friend group was the Harry Potter Book Club. While being part of a book club made me feel like a geriatric, the friendships that were formed during the book club helped me emerge from “The Fog,” and our trip to Universal Studios was a trip I will never remember. I would like to formally thank Dana Watt, current titan of industry, and member of the Harry Potter Book Club, for developing our critically acclaimed Elizabeth Holmes impersonation, including the hit single “A Chemistry is Performed; A Readout is Taken.”

Despite all the surprising experimental results I encountered as a student, the most surprising thing that happened to me while I was a student was meeting Jeff Kremer (a.k.a. “MVP”). Jeff was a surprising person to meet because we clicked almost instantaneously, which stands in contrast to the frightening effect that I usually have on people. I’m grateful that you’ve stuck around (another surprise) and for reminding me almost constantly that graduate school was a process that I was capable of seeing through to the end. I’m excited for more surprises, because at this point, I’ve given up on predicting anything.

Ever since I was a child, my parents, Connie and John, have supported my bizarre interests. Developmentalists would be interested to know that my preferred toys as a four-

year-old were a potato and a toothbrush, and I had what I believed was the world's largest collection of disposable cups. Despite these tendencies, my parents' love and support was unconditional, and has only intensified as I've grown up. I am grateful that I can always count on your encouragement, and for you for giving a me sense of personal accountability and curiosity. However, I would like to formally declare at this time that I am done pursuing degrees for the foreseeable future. Finally, my brother, Evan, is just as odd as I am, and despite that, we always seem to figure things out. I'm glad to have you on my side.

It is unclear who in their right mind would still be reading this, but I hope it's clear that my time as a graduate student was a satisfying period in my life almost exclusively due to the people who made this experience worthwhile, fun, and doable. Without them, this wonderful document would not exist.

Andrew Kelsey Fishell

Washington University

August 2019

ABSTRACT OF THE DISSERTATION

High-Density Diffuse Optical Tomography During Passive Movie Viewing:

A Platform for Naturalistic Functional Brain Mapping

by

Andrew Kelsey Fishell

Doctor of Philosophy in Biology and Biomedical Sciences

Neurosciences

Washington University in St. Louis, 2019

Professor Joseph Culver, Chairperson

Human neuroimaging techniques enable researchers and clinicians to non-invasively study brain function across the lifespan in both healthy and clinical populations. However, functional brain imaging methods such as functional magnetic resonance imaging (fMRI) are expensive, resource-intensive, and require dedicated facilities, making these powerful imaging tools generally unavailable for assessing brain function in settings demanding open, unconstrained, and portable neuroimaging assessments. Tools such as functional near-infrared spectroscopy (fNIRS) afford greater portability and wearability, but at the expense of cortical field-of-view and spatial resolution. High-Density Diffuse Optical Tomography (HD-DOT) is an optical neuroimaging modality directly addresses the image quality limitations associated with traditional fNIRS techniques through densely overlapping optical measurements. This thesis aims to establish the feasibility of using HD-DOT in a novel application demanding exceptional portability and flexibility: mapping disrupted cortical activity in chronically malnourished children. I first motivate the need for

dense optical measurements of brain tissue to achieve fMRI-comparable localization of brain function (Chapter 2). Then, I present imaging work completed in Cali, Colombia, where a cohort of chronically malnourished children were imaged using a custom HD-DOT instrument to establish feasibility of performing field-based neuroimaging in this population (Chapter 3). Finally, in order to meet the need for age appropriate imaging paradigms in this population, I develop passive movie viewing paradigms for use in optical neuroimaging, a flexible and rich stimulation paradigm that is suitable for both adults and children (Chapter 4).

Chapter 1: Introduction

1.1 Principles of optical neuroimaging

1.1.1 Measuring cortical hemodynamics with near-infrared light

Optical neuroimaging methods encompass a broad range of techniques that aim to assess the structure and function of the brain using light (Hillman, 2007). These techniques span a broad range of spatial scales, from structures at the cellular level to regions and networks at the systems level, using a variety of contrast agents. These contrast agents are either intrinsic to the tissue of interest (endogenous) or exogenously applied and provide insight into brain function through mechanisms including changes in cellular metabolic state, ionic concentrations, and tissue oxygenation (Ohki, Chung, Ch'ng, Kara, & Reid, 2005; Shoham et al., 1999). The selection an of appropriate optical neuroimaging technique for an experimental question therefore depends on parameters including the organism of interest and the desired source of contrast. Imaging parameters such as the field-of-view and spatial resolution are subsequently constrained by the imaging system.

In humans, a commonly used non-invasive optical brain imaging technique is near-infrared spectroscopy (NIRS) (Scholkmann et al., 2014). This technique relies on the discovery that changes in blood oxygenation are measurable with near-infrared light, which was first demonstrated in felines (Jöbsis, 1977). A NIRS instrument includes a source of near-infrared illumination (approximately 650-1000 nm) and a detector, both of which are positioned on the head. Near-infrared light emitted by the source travels from

the source to the detector through the head, in a path that includes both superficial (i.e. skull and scalp) and cortical tissue (Ferrari & Quaresima, 2012). Critically, relative to small animal imaging systems, which may use visible light, near-infrared light has less scatter and absorption in biological tissues, enabling deeper penetration into the cortical tissue of interest. As near-infrared light enters the head, it is scattered and attenuated by both superficial and cortical tissues. The absorption properties of the chromophores of interest in the near-infrared regime, in this case deoxygenated and oxygenated hemoglobin, mean that changes in light intensity measured by the detector are therefore related to changes in the concentrations of deoxygenated and oxygenated hemoglobin species (Arno Villringer & Chance, 1997). Consequently, this source-detector measurement provides information about the blood oxygenation of the underlying cerebral tissue.

Through a mechanism called neurovascular coupling, changes in neuronal activity result in dilation of local arterioles (Raichle, 1998). This dilation results in a local increase in delivery of oxygenated hemoglobin through an increase cerebral blood flow. The increased oxygenated delivery exceeds the demands rate of neuronal oxygen utilization, meaning that the result of neuronal activity is a surplus of oxygen in the blood surrounding the area of increased neuronal activity. Although the exact mechanisms of this process are still unclear, the changes in blood oxygenation that accompany neuronal activity are a source of intrinsic contrast that is used to indirectly measure brain activity (Lauritzen & Gold, 2003; Logothetis, 2003; Raichle & Mintun, 2006; A. Villringer & Dirnagl, 1995). Consequently, when NIRS techniques are used to measure changes in blood

oxyhemoglobin and deoxyhemoglobin concentration related to brain function, the technique is referred to as functional NIRS (fNIRS).

A typical fNIRS system is comprised of multiple sources and detectors positioned on the head, and to achieve optimal tissue spectroscopy, two or more source wavelengths are used. The light level between a source-detector pair is referred to as a channel or measurement, and the geometry of the source-detector array determines the system's sensitivity to hemodynamics in the underlying cortical tissues. While early fNIRS systems have relied on a relatively small number of measurements to probe hemodynamics in broad swaths of cortex (i.e. entire lobes), more recent fNIRS systems have achieved greater spatial specificity by increasing the number of source-detector measurements, resulting in more precise localization of hemodynamic changes. Even still, the resulting maps of brain activation are topographic images with relatively coarse spatial resolution (approximately 1 cm) and are not depth-resolved (Ferrari & Quaresima, 2012). These image characteristics stand in contrast to other human neuroimaging techniques that measure blood oxygenation to infer changes in neuronal activity, such as functional magnetic resonance imaging (fMRI) and positron emission tomography (PET). These techniques usually result in depth-resolved images of hemodynamics at a higher spatial resolution (Cui, Bray, Bryant, Glover, & Reiss, 2011).

The field-of-view associated with fNIRS instruments also stands in contrast to fMRI and PET fields-of-view, which generally encompass the entire brain. The field-of-view associated with a given fNIRS instrument is directly dependent on the positioning of sources and detectors on the head, as well as the attenuation and scattering of near-

infrared light (Fukui, Ajichi, & Okada, 2003). The result of these two factors is that twofold. First, the source-detector array must be positioned over the cortical regions of interest. Second, due to attenuation and scattering, fNIRS systems can only measure hemodynamics in the superficial cortex. The separation between a source and detector dictates how deeply the associated measurement penetrates the tissue; however, the rapid attenuation of light as it travels through the tissue renders even deep cortical structures such as the insula or operculum inaccessible to these techniques (Dehghani, White, Zeff, Tizzard, & Culver, 2009).

The relationship between source-detector separation and measurement depth means that measurements with a short source-detector separation are biased towards sampling superficial tissues, while longer source-detector separations incorporate sampling of cortical tissues (Gregg, White, Zeff, Berger, & Culver, 2010). In both cases, however, the measurement samples superficial tissues that contain vascular physiology of limited relevance to most neuroscientific questions. Blood flow changes in the scalp, as well as systemic physiology (Franceschini, Fantini, Thompson, Culver, & Boas, 2003) (e.g. respiration, heart rate, vasomotion, and Mayer waves) are components of all fNIRS measurements and must be addressed in order to more closely isolate the measured signal to cortical hemodynamics (Saager & Berger, 2005). One strategy for addressing this nuisance physiology is to incorporate multiple source-detector separations in a source-detector configuration. In doing so, the shorter measurements provide an approximation of nuisance physiology which can then be removed from the deeper

measurements, resulting in fNIRS measurements that more closely report the cortical physiology of interest.

In summary, the components of a functional near-infrared spectroscopy system are sources and detectors of near-infrared light. The light intensity measured by the detector depends on the concentration of oxygenated and deoxygenated hemoglobin, and changes in the concentrations of these chromophores are indirectly related to neuronal activity through neurovascular coupling. The ability of an fNIRS system to generate topographic images of superficial cortical hemodynamics depends critically on the positioning of sources and detectors on the head. In addition to the number and positioning of measurements included in an fNIRS system, which dictate a system's resolution and field-of-view, the separation of source-detector measurements determines how deeply the measurement will sample the underlying tissue. However, all measurements will sample superficial tissue and be sensitive to systemic physiology. Consequently, in the context of performing cognitive neuroscience research, an experimenter using fNIRS must take steps to ensure that the source-detector arrangement is appropriate for the cortical regions of interest and that nuisance physiology is appropriately addressed.

1.1.2 Applications of functional near-infrared spectroscopy

Cognitive neuroscience researchers have a variety of techniques at their disposal for imaging the human brain. The selection of a technique can be constrained by considerations of resolution (temporal and spatial), participant comfort, and participant contraindications (e.g. implanted metal or radiation exposure). Imaging techniques that

rely on neurovascular coupling to indirectly infer brain activity all share a slower temporal sensitivity relative to techniques that measure electrical activity, as the slow hemodynamic response essentially acts as a low-pass filter on faster neuronal impulses (Kim, Richter, & Uğurbil, 1997). Investigators researching questions in which this reduced temporal precision is acceptable might select fNIRS over other brain imaging methods that also infer brain activity through neurovascular coupling, such as fMRI or PET, for both practical and experimental considerations. These considerations provide a framework for describing the applications of fNIRS in human brain research.

1.1.2a Logistical considerations in functional near-infrared spectroscopy

Relative to fMRI and PET, fNIRS instruments are less expensive and demand fewer dedicated resources. Consequently, fNIRS instruments are less expensive to implement, and have enabled imaging in low-resource regions of the world where other neuroimaging techniques would be too expensive to implement (John, Black, & Nelson, 2017). This greater accessibility has enabled researchers to perform assessments of brain function in populations that would otherwise be inaccessible. For instance, low-resource regions of the world generally have higher rates of childhood deprivation, including acute and chronic undernutrition (Tomalski et al., 2013). The low cost and portability associated with fNIRS enables neuroimaging laboratories to be established in the field, in regions where this deprivation is endemic. Indeed, the first field-based functional neuroimaging assessments of childhood malnutrition were performed using a highly portable fNIRS instrument (Lloyd-Fox et al., 2014).

Further, participants in fNIRS experiments are not constrained to a bore, as they are during PET or fMRI scans. Consequently, these instruments open new avenues of clinical neuroimaging, as neuroimaging instruments can be brought to the patient's bedside, instead of transporting patients to stationary neuroimaging instruments (Ferrari, Culver, Hoshi, & Wabnitz, 2016). Further, bedside imaging using a portable and wearable fNIRS instrument enables longitudinal observation of brain function, potentially creating novel strategies for patient monitoring in critical care environments (e.g. stroke intensive care units) (Arenth, Ricker, & Schultheis, 2007; Kassab et al., 2018).

In addition to a bore-free imaging environment, the fNIRS imaging environment is also silent, providing additional enhancements in patient comfort. While the gold-standard of cognitive neuroscience participants, healthy undergraduate students (Henrich, Heine, & Norenzayan, 2010), may not demand exceptionally comfortable imaging environments, other participant populations are sensitive to the constrained and noisy environment posed by other imaging methods. For instance, young children may find enclosed scanner environments too frightening, or they may move to an extent that renders scans unusable. Solutions to this challenge include using mock scanner training, implementing real-time feedback, imaging during sleep, or alleviating anxiety with sedatives (Dosenbach et al., 2017; Greene et al., 2018). However, fNIRS provides an imaging solution that is less prone to these obstacles, enabling imaging of awake, behaving participants in a variety of comfortable settings. Indeed, along with other wearable modalities (e.g. electroencephalography), these methods enable developmentalists to study brain function during performance of tasks assessing developmentally relevant domains such

as language acquisition, motor development, and social development (Aslin & Mehler, 2005; Franceschini et al., 2007; S. Lloyd-Fox, Blasi, & Elwell, 2010).

In summary, fNIRS instruments offer greater portability, lower operational costs, and more open imaging environments than other modalities. These advantages enable functional neuroimaging in settings such as low-resource areas or clinical settings where neuroimaging would have previously been considered cost-prohibitive or impractical.

1.1.2b Experimental considerations in functional near-infrared spectroscopy

Some experimental questions pose constraints on methodological choices that make fNIRS the most appropriate method for a given research topic. For instance, a study assessing perception of auditory stimuli may be confounded by additional noise introduced by the fMRI environment, meaning that cortical responses measured during task performance may not be directly attributable to stimulus processing. In addition, the superficial location of regions related to auditory and linguistic processing make fNIRS an appropriate solution for addressing this confound (Ferrari & Quaresima, 2012; Hassanpour, Eggebrecht, Culver, & Peelle, 2015; Peelle, 2017). Additionally, some patient populations, such as those with cochlear implants or deep brain stimulators are contraindicated for MRI, meaning that a surrogate imaging method is required to study these populations. fNIRS does not pose such contradictions and therefore enables study of populations who otherwise may be unable to undergo functional neuroimaging (Eggebrecht et al., 2014).

Functional neuroimaging modalities are notoriously sensitive to image artifacts induced by head motion (Brigadoi et al., 2014; Power, Barnes, Snyder, Schlaggar, &

Petersen, 2012); however, fNIRS is generally more tolerate to motion artifacts than fMRI. Although the motor system can be studied at a systems-level using passive imaging approaches such as resting-state functional connectivity (Xiong, Parsons, Gao, & Fox, 1999), imaging task-evoked responses to movements is challenging in an environment that is so exquisitely sensitive to head motion . For instance, somatomotor cortex can be functionally localized in the bore using directed movements of the tongue and extremities (Drobyshevsky, Baumann, & Schneider, 2006), but more pronounced movements and natural movements (e.g. walking, speaking) may not be easily accessible using fMRI. fNIRS, as a wearable and portable device, has contributed to motor neuroscience by enabling imaging of the neural underpinnings of these behaviors (Piper et al., 2014; Walsh et al., 2017).

As with motor tasks, social neuroscience using fMRI relies on highly distilled versions of social stimuli, with limited ecological validity. For instance, dyadic conversations imaged with fMRI are generally not face-to-face, and may not even happen in real time, which are experimental designs required to overcome the restrictions of the imaging environment. In contrast, fNIRS enables more ecologically valid measurements of brain activity during naturalistic social interactions that unfold face-to-face and in real time (Quaresima & Ferrari, 2019). An emerging sub-field of hyperscanning even enables imaging of both participants in a dyadic social interaction, extending the field of social neuroscience into even more realistic settings (Liu et al., 2017).

Taken alongside the logistical advantages of portable and wearable optical neuroimaging instruments such as fNIRS, the additional populations and experimental

designs enabled by the unique capabilities of fNIRS offer the opportunity to extend the utility of imaging cortical hemodynamics beyond the bore.

1.1.3 Limitations of functional near-infrared spectroscopy

Despite the numerous applications available to researchers using fNIRS, several caveats limit widespread use of these techniques. As explained in Section 1.1, the image quality characteristics and field-of-view associated with any fNIRS instrument depend on array design and other system specifications such as illumination wavelength (Strangman, Culver, Thompson, & Boas, 2002). Measurement arrays with limited numbers of sources and detectors may be able to detect a change in cortical hemodynamics but may not be able to localize the exact source of the hemodynamic response (White & Culver, 2010b). The relatively coarse localization capability associated with fNIRS is further evident in how researchers display results from fNIRS studies. While topographic, 2-D maps of brain activation are sometimes displayed, activation timecourses that are coarsely attributed to an underlying cortical lobe are also commonly chosen data representation tools (Colier et al., 2001; G. Gratton, Corballis, Cho, Fabiani, & Hood, 1995; Taga, Asakawa, Maki, Konishi, & Koizumi, 2003). This limitation in localization is due to the relatively coarse lateral resolution resulting from sparse sampling of the underlying tissue. Consequently, researchers must take steps to ensure consistent array positioning on participants' heads (Singh, Okamoto, Dan, Jurcak, & Dan, 2005); otherwise, group-level differences could be attributable to localization errors resultant from variability in array placement, rather than the more desirable attribution to genuine differences in brain function.

Another challenge associated with array placement is making *a priori* decisions about field-of-view. With a set number of sources and detectors, experimenters face a tradeoff between field-of-view and lateral resolution, such that an extended field-of-view comes at the expense of localization capability. However, in experimental paradigms without a strong, hypothesis-driven cortical region-of-interest, experimenters may be forced to sacrifice resolution in order to ensure any region(s) implicated in the task are within the instrument's field-of-view. While some tools exist to optimize this tradeoff and eliminate some of the subjectivity (Brigadoi, Salvagnin, Fischetti, & Cooper, 2018; Morais, Balardin, & Sato, 2018), the reality remains that it is often difficult to predict in advance the cortical structures that may be implicated in a task or show between-group differences. Further, in the absence of a highly distilled, uni-modal task, cortical information processing usually implicates a distributed hierarchy of regions (Petersen, Fox, Posner, Mintun, & Raichle, 1988). Consequently, generating a comprehensive image of the cortical activity underlying a task requires both lateral resolution and an extensive field-of-view.

1.2 Principles of high-density diffuse optical tomography

fNIRS instruments with a fixed channel count are not appropriately configured to optimize both lateral resolution and cortical field-of-view, creating a need for more sophisticated solutions that meet these demands for enhanced image quality, while preserving the established uses for optical neuroimaging techniques. High-density diffuse optical tomography (HD-DOT) is an optical neuroimaging methodology that, like fNIRS, performs tissue spectroscopy to measure cortical hemodynamics that are associated with focal

changes in brain activity. The critical advancement from fNIRS is a highly dense array of sources and detectors, which results in a densely overlapping set of optical measurements at multiple source-detector separations (Boas, Chen, Grebert, & Franceschini, 2004). Like fNIRS, the field-of-view is constrained by the positioning of the sources and detectors; however, unlike fNIRS, the tissue within the field-of-view is sampled at a higher lateral resolution and is also depth profiled, enabling tomographic reconstruction of three-dimensional images of brain hemodynamics. Critically, while other diffuse optical tomography (DOT) methods are available, such as time-resolved DOT (Benaron et al., 2000; Selb, Stott, Franceschini, Sorensen, & Boas, 2005), which relies on complex photon gating procedures to depth profile tissue, the following discussion is restricted to DOT techniques that depth resolve tissue using multiple source-detector separations.

1.2.1 High-density diffuse optical tomography instrumentation

A HD-DOT instrument relies on the same underlying instrumentation as an fNIRS instrument. That is, sources illuminate the head (generally at two or more wavelengths) and detectors collect the light emitted from sources. In order to achieve a densely overlapping set of measurements, a larger quantity of sources and detectors are required. And, due to the greatly increased number of measurement channels in an HD-DOT system (sometimes multiple orders of magnitude greater measurement counts than would be obtained with an fNRIS instrument, special considerations must be paid to both the illumination and detection methodologies.

An HD-DOT instrument collects overlapping measurements at multiple source-detector separations. Consequently, the light emitted by one light source will be detected by multiple adjacent detectors, which are positioned at multiple source-detector separations. This measurement bookkeeping in the dense array poses a challenge, as the light collected by a detector at any given point in time must be accurately attributed to the correct source in order to quantify the light level associated with that single source-detector measurement. Solutions to this challenge include spatial, temporal, and frequency encoding patterns that ensure that the light collected by a detector at a given timepoint can be attributed to a known source (Eggebrecht et al., 2014). Spatial and temporal encoding patterns control when and where sources in an array are illuminated, and frequency encoding modulates the illumination of given source at a set frequency, such that a Fourier transform of a detector's output will reveal peaks at the modulation frequencies. Consequently, simultaneously illuminated sources can be unmixed in the frequency domain, given an appropriately designed frequency encoding scheme. These source encoding strategies ensure accurate measurement bookkeeping, which is essential for managing the large number of measurements obtained by an HD-DOT instrument.

In addition to measurement bookkeeping, the multiple source-detector separations in an HD-DOT instrument may span several centimeters. These multiple source-detector separations confer several critical image quality advantages. First, images obtained with HD-DOT are depth-resolved. Second, shorter source-detector measurements provide a dedicated readout of nuisance physiology attributable to scalp hemodynamics, as well as

systemic physiology attributable to pulse, respiration, vasomotion, and Mayer waves (Bumstead, Bauer, Wright, & Culver, 2017; Gregg et al., 2010). This dedicated readout can subsequently be removed from the HD-DOT measurements in order to more accurately isolate cortical physiology of interest. However, due to the rapid attenuation of light through biological tissue, accurate detection of the light intensity at longer measurement distances poses an instrumentation challenge. Consequently, the detection instrumentation chosen for an HD-DOT instrument must retain sufficiently high signal-to-noise across a broad dynamic range (White & Culver, 2010a; Zeff, White, Dehghani, Schlaggar, & Culver, 2007). Otherwise, the deeper cortical measurements associated with longer source detector separations will be at the detector's noise floor for photon detection, rendering the measurements unusable and eliminating the potential image quality improvements conferred by densely overlapping measurements. Avalanche photo diodes and scientific CMOS cameras (Bergonzi et al., 2018) are two detection technologies that have been proven to meet these rigorous specifications.

HD-DOT, through increased measurement density, offers an elegant solution to the image quality challenges associated with standard optical neuroimaging techniques. Although the increased measurement density poses technological challenges, solutions in both source illumination and light detection address these challenges and enable collection of densely overlapping measurements suitable for tomographic image reconstruction.

1.2.2 Tomographic image reconstruction

In HD-DOT, tomographic image reconstruction transforms the set of optical measurements, taken at the surface, into a 3D image of the underlying tissue (Eggebrecht et al., 2014, 2012). This step estimates the desired image of cortical hemodynamics using a finite set of projections, or measurements, that section the tissue of interest. This is an inverse problem that can be expressed as follows,

$$y = A\,x,$$

where at a given timepoint in an acquisition, **y** is a vector of light-level measurements at the surface (i.e. observed with HD-DOT), **x** is the absorption changes within a voxelated, volumetric space (i.e. the image we wish to reconstruct), and **A** is a sensitivity matrix that relates the set observed light-level measurements to the volume that is to be reconstructed. Consequently, is **y** a variable obtained with the HD-DOT instrument, **A** is a variable generated using a forward modeling procedure, and **x** is the variable that must be solved for in order to generate an image.

The sensitivity matrix, **A**, models light propagation through the tissue of interest, which is in this case the head. This forward model requires solving for the light propagation using a model of head anatomy and the positions of the sources and detectors on the head. The head anatomy may be derived from an anatomical image (e.g. MRI or CT) from an individual subject, or it may be derived from an appropriately representative atlas, if no individual anatomical image is available (Ferradal, Eggebrecht, Hassanpour, Snyder, & Culver, 2014). Spatial localization improves the more closely the image of head anatomy matches the actual participant's anatomy, but localization is still acceptable with an atlas-based model.

Briefly, to account for the unique scattering and absorption properties of the tissue compartments a photon will encounter from source to detector, the image of head anatomy is segmented into five tissue compartments (scalp, skull, grey matter, white matter, and cerebrospinal fluid) (Ségonne et al., 2004), and the segmented image is converted into a finite-element mesh, which enables finite-element solutions to modeling light transport through tissue (Jermyn et al., 2013). Once the sources and detectors are positioned onto the mesh, a source-detector measurement's sensitivity is calculated using a finite-element solution to the diffusion approximation to the radiative transport equation (Dehghani et al., 2008). After repeating this procedure for all source-detector measurements in a system (potentially excluding long-distance measurements that are beyond the system's detection sensitivity), this sensitivity matrix is resampled into a voxelated space, which ultimately corresponds to the desired space of the to-be-reconstructed image.

This tomographic reconstruction procedure stands in stark contrast to topographically generated images from fNIRS as it is substantially more computationally and mathematically intensive. However, the resulting reconstructed image of cortical hemodynamics is in a voxelated space, much like images generated with fMRI or PET. While cross-modality comparisons have been completed between fNIRS and fMRI (Duan, Zhang, & Zhu, 2012; Strangman et al., 2002), the anatomical modeling in HD-DOT image reconstruction accounts for tissue-specific optical properties as well as individual head anatomy. Consequently, images reconstructed with HD-DOT should reflect cortical

hemodynamics with greater fidelity than optical neuroimaging techniques that do not include image reconstruction with anatomical light modeling.

Given a set of optical measurements on the surface and a forward model of light transport, the image is then reconstructed by inverting the forward model, such that the above equation, $y = A x$, can be solved for x.

1.2.3 Validation of high-density diffuse optical tomography

Like fNIRS, evaluating the performance of HD-DOT involves generating images of brain activation in controlled task conditions with predictable cortical responses. Images of brain activations reconstructed with HD-DOT-derived measurements can be compared with other studies using the same task paradigm reported using other modalities. An even stronger validation procedure entails collecting subject-matched data under the same task conditions, enabling quantitative evaluation of image quality and localization performance. Work validating HD-DOT has utilized both approaches and has generally shown that images obtained with HD-DOT are highly comparable to images obtained with other modalities (Eggebrecht et al., 2014, 2012). Unlike fNIRS, the resolution enhancements associated with HD-DOT enable detection of boundaries between cortical regions, and the extended field-of-view enables detection of spatially distributed brain responses.

The mammalian brain, and sensorimotor systems in particular, contain topographic maps that have been convergently established across techniques and organisms (Silver & Kastner, 2009). In humans, these maps have been non-invasively studied using neuroimaging techniques (Engel, Glover, & Wandell, 1997; Fox et al., 1986;

Ogawa et al., 1992). For more novel imaging systems such as HD-DOT, these maps can be used to assess the system's mapping performance: The more closely the imaging system recapitulates these known representations, the better the performance of the imaging system. For instance, primary visual cortex, V1, is retinotopically mapped, meaning that adjacent neurons in V1 have receptive fields in the retina that are also adjacent. The topographic map of auditory cortex is arranged such that spatially adjacent neurons represent adjacent sounds in frequency space (Romani, Williamson, & Kaufman, 1982). Likewise, structures responsible for processing other sensory inputs show topographies related to the arrangement of incoming afferents neurons on the corresponding sensory epithelium.

While some of these topographic maps, such as the rhinotopic map in olfaction, are too deep to be accessible with optical neuroimaging methods, other topographic maps are more superficial and are therefore more accessible with HD-DOT. Indeed, using classic retinotopic mapping paradigms established with fMRI and PET, retinotopic organization of visual cortex assessed with HD-DOT recapitulates multiple representations of visual angles and eccentricities within a single hemisphere, highlighting the ability of HD-DOT to meet a classic benchmark of neuroimaging system validation (White & Culver, 2010a; Zeff et al., 2007).

In addition to validating imaging performance using cortical topographic maps, other established task paradigms can be replicated across modalities to quantitatively evaluate spatial overlap between reconstructed activations. For instance, seminal work with PET used a set of increasingly complex language paradigms to image cortical

regions related to tasks as simple as passively listening to spoken words and as complex as imagined speaking of a word related to a visually presented cue (Petersen et al., 1988). Because each more complex task contained processing elements that overlapped with the previous, less complex task, activation images from adjacent tasks in the hierarchy could be subtracted from one another to isolate regions that were specifically recruited as the task complexity increased. Crucially, this task hierarchy recruits a spatially distributed set of regions related to language processing. Over 20 years after the original PET study, participants who underwent both HD-DOT and fMRI with the same suite of tasks revealed activations congruent with the original work that were also highly spatially overlapping across fMRI and HD-DOT (Eggebrecht et al., 2014), providing further distinction between the image quality associated with HD-DOT and other optical neuroimaging modalities such as fNIRS (White & Culver, 2010b).

The imaging of task-evoked responses provides one avenue for interrogating brain function and cross-validating imaging modalities. Imaging the brain at rest provides a complementary approach through resting-state functional connectivity, which reveals that slow patterns of cortical activity measured in the absence of a task are correlated across functionally related systems (Buckner, Krienen, & Yeo, 2013). In other words, a timeseries of brain activity extracted from a region related to visual processing would be correlated with other regions related to visual processing, but uncorrelated with other sensory systems. Regions correlated at rest are therefore “functionally connected,” and thought to reflect the brain’s coactivation history. Despite the nomenclature implying direct

connectivity between regions, functionally connected regions are not necessarily monosynaptically connected.

Functional connectivity provides a powerful technique for assessing all known cortical systems during a single imaging run, and functional connectivity varies across development and disease states, providing a systems-level description of how cortical networks interact across a variety of conditions (Power et al., 2011). Rather than reflecting moment-to-moment changes in mental state or task performance, patterns of functional connectivity are more different across individuals than they are across states (C. Gratton et al., 2018). Finally, because patterns of functional connectivity differ as one traverses an areal boundary, a functional connectivity scan can be used to generate a map of cortical regions, or parcellation, by identifying boundaries where patterns of connectivity abruptly change (Cohen et al., 2008). Consequently, the information garnered during a functional connectivity scan is complementary to task-based imaging. While most of the pioneering work with functional connectivity was completed with fMRI, other modalities have tried to leverage the large amount of information potentially available from functional connectivity assessments by establishing similar sensitivity to correlated patterns of spontaneous brain activity.

Work with HD-DOT during rest has established similar sensitivity to functional connectivity and has also included comparisons to subject-matched fMRI (Eggebrecht et al., 2014). The broad HD-DOT field-of-view maximizes sensitivity to spatially distributed functional systems and extends the fNIRS-based functional connectivity measures that are generally restricted to homotopic connectivity between 1-2 functional systems (Duan

et al., 2012; Lu et al., 2010; Zhang et al., 2010). Regional boundary detection using HD-DOT, in which patterns of abrupt connectivity change indicate a boundary between adjacent regions, match boundaries detected with fMRI, providing yet another indication that image characteristics within the HD-DOT field-of-view are comparable to fMRI.

In summary, through both tasks and functional connectivity scans, work empirically evaluating HD-DOT image performance has successfully demonstrated fMRI-comparable results. This work in humans is further substantiated through convergent simulations demonstrating the improvements in localization accuracy and image localization related to increasing measurement density. Despite the specialized instrumentation associated with increasing the number of sources and detectors to include measurements at multiple source-detector separations, the principal advances and methodological appeals of optical neuroimaging techniques are preserved in HD-DOT instruments, including low cost, limited need for specialized facilities, quiet and open imaging environment, and wearable headgear. Consequently, many of the unique experimental cognitive neuroscience questions that are well suited for fNIRS are also suitable for HD-DOT, with the added benefit of fMRI-comparable images within the field-of-view.

1.3 Applications of high-density diffuse optical tomography

In addition to evaluating the image resolution and spatial localization performance of HD-DOT relative to other benchmark modalities using established neuroimaging paradigms, recent neuroimaging with HD-DOT has begun to demonstrate this technique's suitability for imaging brain function in settings optimized for optical neuroimaging. For instance, a

portable HD-DOT instrument with headgear optimized for neonates was used to demonstrate feasibility of imaging neonates in a critical care environment using functional connectivity scans (Ferradal et al., 2016). This work eliminates the need to transport the infants to an MRI bay, but preserves the potential predictive power of obtaining functional connectivity assessments in infancy and opens the possibility for longitudinal monitoring of functional connectivity in critical care environments (Kassab et al., 2018). Other work has leveraged the silent imaging environment to observe cortical responses related to processing auditorily presented sentences of varying complexity, revealing increased recruitment of speech processing regions to understand more complicated sentences (Hassanpour et al., 2015). Like other optical neuroimaging studies, these recent examples of HD-DOT experiments leverage the unique characteristics of the instrumentation to answer questions that may be inaccessible with other modalities.

1.3.1 Motivation for thesis work

While HD-DOT has been established in healthy young adults, older adults with Parkinson's disease, and neonates, HD-DOT has not yet been established as an imaging modality suitable for children. Consequently, the goal of this thesis is twofold. The first goal is to evaluate the performance of an HD-DOT instrument in imaging task-evoked responses in 7-10-year-old children, using a simple passive word listening task that produces predictable and stereotyped activations. This work was completed in Cali, Colombia in a cohort of chronically malnourished children, in order to secondarily validate that HD-DOT could successfully be used in a field setting, like other portable fNIRS instruments. Having established the feasibility of imaging this age group, the second goal

is to develop richer and more engaging imaging paradigms that are suitable for assessing multiple information processing domains in both school aged children, as well as younger children. This work addresses the gap that currently exists between child-friendly HD-DOT imaging equipment and child-friendly imaging paradigms to accompany the imaging equipment.

However, this work rests on the presupposition that optical measurement density is directly related to attainment of fMRI comparable activations. Prior simulations have shown that sparse measurement grids produce distorted activations (White & Culver, 2010b), but these studies did not include physiological noise that is induced by superficial tissues (Saager & Berger, 2005). Prior work with multi-modal cross validation between fMRI and HD-DOT showed excellent spatial correspondence between the two modalities (Eggebrecht et al., 2014) but did not evaluate whether fewer measurements would produce the same spatial correspondence. Consequently, this work begins with a direct comparison of activations reconstructed using HD-DOT, sparse measurement arrays with no overlapping measurements, and subject-matched fMRI in Chapter 2. By evaluating the performance of imaging grids *in vivo*, including physiological noise and a subject-matched set of reference images, we directly evaluate the extent to which measurement density impacts imaging performance. Characterization of this relationship is especially critical to motivate the continued use of dense measurement arrays in imaging contexts demanding exceptional portability, such as field imaging.

1.3.2 Understanding altered brain development due to malnutrition

Having evaluated the relationship between measurement density and ability to resolve fMRI-comparable activations, Chapter 3 introduces imaging work performed in a cohort of chronically malnourished 7-10-year-old children, following work evaluating childhood malnutrition globally using fNIRS techniques (Lloyd-Fox et al., 2014). Like other work establishing field optical neuroimaging sites, this work establishes feasibility of field imaging using a well-defined task with stereotyped activations, rather than prioritizing identification of deficits related to malnutrition burden. However, as feasibility of imaging is established, and in preparation for imaging younger children who have a greater need for engaging and entertaining imaging paradigms, we also develop child-friendly naturalistic imaging paradigms.

1.3.3 Developing naturalistic brain mapping paradigms

Naturalistic imaging, as it is introduced in Chapter 4, refers to richly stimulating imaging paradigms that incorporate information processing demands that unfold concurrently, as they would in a natural setting outside of the laboratory (Quaresima & Ferrari, 2019). However, operationalized within the context of the laboratory, these richly stimulating paradigms often involve the passive viewing of a feature film or television show (Hasson, Nir, Levy, Fuhrmann, & Malach, 2004). We have developed passive movie viewing paradigms for HD-DOT, demonstrating that responses to these stimuli are both reproducible and decomposable into feature-specific responses. These results set the stage for further study across multiple age groups, as well as applying the same feature-based analysis techniques in truly naturalistic settings (e.g. social interactions) that would be inaccessible to other imaging modalities.

1.4 References

Arenth, P. M., Ricker, J. H., & Schultheis, M. T. (2007). Applications of Functional Near-Infrared Spectroscopy (fNIRS) to Neurorehabilitation of Cognitive Disabilities. *The Clinical Neuropsychologist*, *21*(1), 38–57. https://doi.org/10.1080/13854040600878785

Aslin, R. N., & Mehler, J. (2005). Near-infrared spectroscopy for functional studies of brain activity in human infants: promise, prospects, and challenges. *Journal of Biomedical Optics*, *10*(1), 011009. https://doi.org/10.1117/1.1854672

Benaron, D. A., Hintz, S. R., Villringer, A., Boas, D., Kleinschmidt, A., Frahm, J., … Stevenson, D. K. (2000). Noninvasive functional imaging of human brain using light. *Journal of Cerebral Blood Flow and Metabolism: Official Journal of the International Society of Cerebral Blood Flow and Metabolism*, *20*(3), 469–477. https://doi.org/10.1097/00004647-200003000-00005

Bergonzi, K. M., Burns-Yocum, T. M., Bumstead, J. R., Buckley, E. M., Mannion, P. C., Tracy, C. H., … Culver, J. P. (2018). Lightweight sCMOS-based high-density diffuse optical tomography. *Neurophotonics*, *5*(3), 035006. https://doi.org/10.1117/1.NPh.5.3.035006

Boas, D. A., Chen, K., Grebert, D., & Franceschini, M. A. (2004). Improving the diffuse optical imaging spatial resolution of the cerebral hemodynamic response to brain activation in humans. *Optics Letters*, *29*(13), 1506–1508.

Brigadoi, S., Ceccherini, L., Cutini, S., Scarpa, F., Scatturin, P., Selb, J., … Cooper, R. J. (2014). Motion artifacts in functional near-infrared spectroscopy: A comparison of motion correction techniques applied to real cognitive data. *NeuroImage*, *85*, 181–191. https://doi.org/10.1016/j.neuroimage.2013.04.082

Brigadoi, S., Salvagnin, D., Fischetti, M., & Cooper, R. J. (2018). Array Designer: automated optimized array design for functional near-infrared spectroscopy. *Neurophotonics*, *5*(3), 035010. https://doi.org/10.1117/1.NPh.5.3.035010

Buckner, R. L., Krienen, F. M., & Yeo, B. T. T. (2013). Opportunities and limitations of intrinsic functional connectivity MRI. *Nature Neuroscience*, *16*(7), 832–837. https://doi.org/10.1038/nn.3423

Bumstead, J. R., Bauer, A. Q., Wright, P. W., & Culver, J. P. (2017). Cerebral functional connectivity and Mayer waves in mice: Phenomena and separability. *Journal of Cerebral Blood Flow & Metabolism*, *37*(2), 471–484. https://doi.org/10.1177/0271678X16629977

Cohen, A. L., Fair, D. A., Dosenbach, N. U. F., Miezin, F. M., Dierker, D., Van Essen, D. C., … Petersen, S. E. (2008). Defining functional areas in individual human brains

using resting functional connectivity MRI. *NeuroImage*, *41*(1), 45–57. https://doi.org/10.1016/j.neuroimage.2008.01.066

Colier, W. N., Quaresima, V., Wenzel, R., van der Sluijs, M. C., Oeseburg, B., Ferrari, M., & Villringer, A. (2001). Simultaneous near-infrared spectroscopy monitoring of left and right occipital areas reveals contra-lateral hemodynamic changes upon hemi-field paradigm. *Vision Research*, *41*(1), 97–102.

Cui, X., Bray, S., Bryant, D. M., Glover, G. H., & Reiss, A. L. (2011). A quantitative comparison of NIRS and fMRI across multiple cognitive tasks. *NeuroImage*, *54*(4), 2808–2821. https://doi.org/10.1016/j.neuroimage.2010.10.069

Dehghani, H., Eames, M. E., Yalavarthy, P. K., Davis, S. C., Srinivasan, S., Carpenter, C. M., … Paulsen, K. D. (2008). Near infrared optical tomography using NIRFAST: Algorithm for numerical model and image reconstruction. *Communications in Numerical Methods in Engineering*, *25*(6), 711–732. https://doi.org/10.1002/cnm.1162

Dehghani, H., White, B. R., Zeff, B. W., Tizzard, A., & Culver, J. P. (2009). Depth sensitivity and image reconstruction analysis of dense imaging arrays for mapping brain function with diffuse optical tomography. *Applied Optics*, *48*(10), D137–D143. https://doi.org/10.1364/AO.48.00D137

Dosenbach, N. U. F., Koller, J. M., Earl, E. A., Miranda-Dominguez, O., Klein, R. L., Van, A. N., … Fair, D. A. (2017). Real-time motion analytics during brain MRI improve data quality and reduce costs. *NeuroImage*, *161*, 80–93. https://doi.org/10.1016/j.neuroimage.2017.08.025

Drobyshevsky, A., Baumann, S. B., & Schneider, W. (2006). A rapid fMRI task battery for mapping of visual, motor, cognitive, and emotional function. *NeuroImage*, *31*(2), 732–744. https://doi.org/10.1016/j.neuroimage.2005.12.016

Duan, L., Zhang, Y.-J., & Zhu, C.-Z. (2012). Quantitative comparison of resting-state functional connectivity derived from fNIRS and fMRI: A simultaneous recording study. *NeuroImage*, *60*(4), 2008–2018. https://doi.org/10.1016/j.neuroimage.2012.02.014

Eggebrecht, A. T., Ferradal, S. L., Robichaux-Viehoever, A., Hassanpour, M. S., Dehghani, H., Snyder, A. Z., … Culver, J. P. (2014). Mapping distributed brain function and networks with diffuse optical tomography. *Nature Photonics*, *8*(6), 448–454. https://doi.org/10.1038/nphoton.2014.107

Eggebrecht, A. T., White, B. R., Ferradal, S. L., Chen, C., Zhan, Y., Snyder, A. Z., … Culver, J. P. (2012). A quantitative spatial comparison of high-density diffuse optical tomography and fMRI cortical mapping. *NeuroImage*, *61*(4), 1120–1128. https://doi.org/10.1016/j.neuroimage.2012.01.124

Engel, S. A., Glover, G. H., & Wandell, B. A. (1997). Retinotopic organization in human visual cortex and the spatial precision of functional MRI. *Cerebral Cortex*, *7*(2), 181–192. https://doi.org/10.1093/cercor/7.2.181

Ferradal, S. L., Eggebrecht, A. T., Hassanpour, M., Snyder, A. Z., & Culver, J. P. (2014). Atlas-based head modeling and spatial normalization for high-density diffuse optical tomography: in vivo validation against fMRI. *NeuroImage*, *85 Pt 1*, 117–126. https://doi.org/10.1016/j.neuroimage.2013.03.069

Ferradal, S. L., Liao, S. M., Eggebrecht, A. T., Shimony, J. S., Inder, T. E., Culver, J. P., & Smyser, C. D. (2016). Functional Imaging of the Developing Brain at the Bedside Using Diffuse Optical Tomography. *Cerebral Cortex*, *26*(4), 1558–1568. https://doi.org/10.1093/cercor/bhu320

Ferrari, M., Culver, J. P., Hoshi, Y., & Wabnitz, H. (2016). Special Section Guest Editorial:Clinical near-infrared spectroscopy and imaging of the brain. *Neurophotonics*, *3*(3). https://doi.org/10.1117/1.NPh.3.3.031401

Ferrari, M., & Quaresima, V. (2012). A brief review on the history of human functional near-infrared spectroscopy (fNIRS) development and fields of application. *NeuroImage*, *63*(2), 921–935. https://doi.org/10.1016/j.neuroimage.2012.03.049

Fox, P. T., Mintun, M. A., Raichle, M. E., Miezin, F. M., Allman, J. M., & Van Essen, D. C. (1986). Mapping human visual cortex with positron emission tomography. *Nature*, *323*(6091), 806–809. https://doi.org/10.1038/323806a0

Franceschini, M. A., Fantini, S., Thompson, J. H., Culver, J. P., & Boas, D. A. (2003). Hemodynamic evoked response of the sensorimotor cortex measured noninvasively with near-infrared optical imaging. *Psychophysiology*, *40*(4), 548–560.

Franceschini, M. A., Thaker, S., Themelis, G., Krishnamoorthy, K. K., Bortfeld, H., Diamond, S. G., … Grant, P. E. (2007). Assessment of infant brain development with frequency-domain near-infrared spectroscopy. *Pediatric Research*, *61*(5 Pt 1), 546–551. https://doi.org/10.1203/pdr.0b013e318045be99

Fukui, Y., Ajichi, Y., & Okada, E. (2003). Monte Carlo prediction of near-infrared light propagation in realistic adult and neonatal head models. *Applied Optics*, *42*(16), 2881–2887. https://doi.org/10.1364/AO.42.002881

Gratton, C., Laumann, T. O., Nielsen, A. N., Greene, D. J., Gordon, E. M., Gilmore, A. W., … Petersen, S. E. (2018). Functional Brain Networks Are Dominated by Stable Group and Individual Factors, Not Cognitive or Daily Variation. *Neuron*, *98*(2), 439-452.e5. https://doi.org/10.1016/j.neuron.2018.03.035

Gratton, G., Corballis, P. M., Cho, E., Fabiani, M., & Hood, D. C. (1995). Shades of gray matter: noninvasive optical images of human brain responses during visual stimulation. *Psychophysiology*, *32*(5), 505–509.

Greene, D. J., Koller, J. M., Hampton, J. M., Wesevich, V., Van, A. N., Nguyen, A. L., … Dosenbach, N. U. F. (2018). Behavioral interventions for reducing head motion during MRI scans in children. *NeuroImage*, *171*, 234–245. https://doi.org/10.1016/j.neuroimage.2018.01.023

Gregg, N. M., White, B. R., Zeff, B. W., Berger, A. J., & Culver, J. P. (2010). Brain specificity of diffuse optical imaging: improvements from superficial signal regression and tomography. *Frontiers in Neuroenergetics*, *2*. https://doi.org/10.3389/fnene.2010.00014

Hassanpour, M. S., Eggebrecht, A. T., Culver, J. P., & Peelle, J. E. (2015). Mapping cortical responses to speech using high-density diffuse optical tomography. *NeuroImage*, *117*, 319–326. https://doi.org/10.1016/j.neuroimage.2015.05.058

Hasson, U., Nir, Y., Levy, I., Fuhrmann, G., & Malach, R. (2004). Intersubject Synchronization of Cortical Activity During Natural Vision. *Science*, *303*(5664), 1634–1640. https://doi.org/10.1126/science.1089506

Henrich, J., Heine, S. J., & Norenzayan, A. (2010). The weirdest people in the world? *Behavioral and Brain Sciences*, *33*(2–3), 61–83. https://doi.org/10.1017/S0140525X0999152X

Hillman, E. M. C. (2007). Optical brain imaging in vivo: techniques and applications from animal to man. *Journal of Biomedical Optics*, *12*(5), 051402. https://doi.org/10.1117/1.2789693

Jermyn, M., Ghadyani, H., Mastanduno, M. A., Turner, W., Davis, S. C., Dehghani, H., & Pogue, B. W. (2013). Fast segmentation and high-quality three-dimensional volume mesh creation from medical images for diffuse optical tomography. *Journal of Biomedical Optics*, *18*(8), 86007. https://doi.org/10.1117/1.JBO.18.8.086007

Jöbsis, F. F. (1977). Noninvasive, infrared monitoring of cerebral and myocardial oxygen sufficiency and circulatory parameters. *Science (New York, N.Y.)*, *198*(4323), 1264–1267.

John, C. C., Black, M. M., & Nelson, C. A. (2017). Neurodevelopment: The Impact of Nutrition and Inflammation During Early to Middle Childhood in Low Resource Settings. *Pediatrics*, *139*(Suppl 1), S59–S71. https://doi.org/10.1542/peds.2016-2828H

Kassab, A., Lan, J. L., Tremblay, J., Vannasing, P., Dehbozorgi, M., Pouliot, P., … Nguyen, D. K. (2018). Multichannel wearable fNIRS-EEG system for long-term clinical monitoring. *Human Brain Mapping*, *39*(1), 7–23. https://doi.org/10.1002/hbm.23849

Kim, S.-G., Richter, W., & Uğurbil, K. (1997). Limitations of temporal resolution in functional MRI. *Magnetic Resonance in Medicine*, *37*(4), 631–636. https://doi.org/10.1002/mrm.1910370427

Lauritzen, M., & Gold, L. (2003). Brain Function and Neurophysiological Correlates of Signals Used in Functional Neuroimaging. *Journal of Neuroscience*, *23*(10), 3972–3980. https://doi.org/10.1523/JNEUROSCI.23-10-03972.2003

Liu, Y., Piazza, E. A., Simony, E., Shewokis, P. A., Onaral, B., Hasson, U., & Ayaz, H. (2017). Measuring speaker–listener neural coupling with functional near infrared spectroscopy. *Scientific Reports*, *7*, 43293. https://doi.org/10.1038/srep43293

Lloyd-Fox, S., Blasi, A., & Elwell, C. E. (2010). Illuminating the developing brain: The past, present and future of functional near infrared spectroscopy. *Neuroscience & Biobehavioral Reviews*, *34*(3), 269–284. https://doi.org/10.1016/j.neubiorev.2009.07.008

Lloyd-Fox, Sarah, Papademetriou, M., Darboe, M. K., Everdell, N. L., Wegmuller, R., Prentice, A. M., … Elwell, C. E. (2014). Functional near infrared spectroscopy (fNIRS) to assess cognitive function in infants in rural Africa. *Scientific Reports*, *4*, 4740. https://doi.org/10.1038/srep04740

Logothetis, N. K. (2003). The Underpinnings of the BOLD Functional Magnetic Resonance Imaging Signal. *Journal of Neuroscience*, *23*(10), 3963–3971. https://doi.org/10.1523/JNEUROSCI.23-10-03963.2003

Lu, C.-M., Zhang, Y.-J., Biswal, B. B., Zang, Y.-F., Peng, D.-L., & Zhu, C.-Z. (2010). Use of fNIRS to assess resting state functional connectivity. *Journal of Neuroscience Methods*, *186*(2), 242–249. https://doi.org/10.1016/j.jneumeth.2009.11.010

Morais, G. A. Z., Balardin, J. B., & Sato, J. R. (2018). fNIRS Optodes' Location Decider (fOLD): a toolbox for probe arrangement guided by brain regions-of-interest. *Scientific Reports*, *8*(1), 3341. https://doi.org/10.1038/s41598-018-21716-z

Ogawa, S., Tank, D. W., Menon, R., Ellermann, J. M., Kim, S. G., Merkle, H., & Ugurbil, K. (1992). Intrinsic signal changes accompanying sensory stimulation: functional brain mapping with magnetic resonance imaging. *Proceedings of the National Academy of Sciences*, *89*(13), 5951–5955. https://doi.org/10.1073/pnas.89.13.5951

Ohki, K., Chung, S., Ch'ng, Y. H., Kara, P., & Reid, R. C. (2005). Functional imaging with cellular resolution reveals precise micro-architecture in visual cortex. *Nature*, *433*(7026), 597–603. https://doi.org/10.1038/nature03274

Peelle, J. E. (2017). Optical neuroimaging of spoken language. *Language, Cognition and Neuroscience*, *32*(7), 847–854. https://doi.org/10.1080/23273798.2017.1290810

Petersen, S. E., Fox, P. T., Posner, M. I., Mintun, M., & Raichle, M. E. (1988). Positron emission tomographic studies of the cortical anatomy of single-word processing. *Nature*, *331*(6157), 585–589. https://doi.org/10.1038/331585a0

Piper, S. K., Krueger, A., Koch, S. P., Mehnert, J., Habermehl, C., Steinbrink, J., … Schmitz, C. H. (2014). A wearable multi-channel fNIRS system for brain imaging

in freely moving subjects. *NeuroImage*, *85 Pt 1*, 64–71. https://doi.org/10.1016/j.neuroimage.2013.06.062

Power, J. D., Barnes, K. A., Snyder, A. Z., Schlaggar, B. L., & Petersen, S. E. (2012). Spurious but systematic correlations in functional connectivity MRI networks arise from subject motion. *NeuroImage*, *59*(3), 2142–2154. https://doi.org/10.1016/j.neuroimage.2011.10.018

Power, J. D., Cohen, A. L., Nelson, S. M., Wig, G. S., Barnes, K. A., Church, J. A., … Petersen, S. E. (2011). Functional network organization of the human brain. *Neuron*, *72*(4), 665–678. https://doi.org/10.1016/j.neuron.2011.09.006

Quaresima, V., & Ferrari, M. (2019). Functional Near-Infrared Spectroscopy (fNIRS) for Assessing Cerebral Cortex Function During Human Behavior in Natural/Social Situations: A Concise Review. *Organizational Research Methods*, *22*(1), 46–68. https://doi.org/10.1177/1094428116658959

Raichle, M. E. (1998). Behind the scenes of functional brain imaging: A historical and physiological perspective. *Proceedings of the National Academy of Sciences*, *95*(3), 765–772. https://doi.org/10.1073/pnas.95.3.765

Raichle, M. E., & Mintun, M. A. (2006). Brain Work and Brain Imaging. *Annual Review of Neuroscience*, *29*(1), 449–476. https://doi.org/10.1146/annurev.neuro.29.051605.112819

Romani, G. L., Williamson, S. J., & Kaufman, L. (1982). Tonotopic organization of the human auditory cortex. *Science*, *216*(4552), 1339–1340. https://doi.org/10.1126/science.7079770

Saager, R. B., & Berger, A. J. (2005). Direct characterization and removal of interfering absorption trends in two-layer turbid media. *Journal of the Optical Society of America. A, Optics, Image Science, and Vision*, *22*(9), 1874–1882.

Scholkmann, F., Kleiser, S., Metz, A. J., Zimmermann, R., Mata Pavia, J., Wolf, U., & Wolf, M. (2014). A review on continuous wave functional near-infrared spectroscopy and imaging instrumentation and methodology. *NeuroImage*, *85 Pt 1*, 6–27. https://doi.org/10.1016/j.neuroimage.2013.05.004

Ségonne, F., Dale, A. M., Busa, E., Glessner, M., Salat, D., Hahn, H. K., & Fischl, B. (2004). A hybrid approach to the skull stripping problem in MRI. *NeuroImage*, *22*(3), 1060–1075. https://doi.org/10.1016/j.neuroimage.2004.03.032

Selb, J. J., Stott, J. J., Franceschini, M. A., Sorensen, A. G., & Boas, D. A. (2005). Improved sensitivity to cerebral hemodynamics during brain activation with a time-gated optical system: analytical model and experimental validation. *Journal of Biomedical Optics*, *10*(1), 011013. https://doi.org/10.1117/1.1852553

Shoham, D., Glaser, D. E., Arieli, A., Kenet, T., Wijnbergen, C., Toledo, Y., … Grinvald, A. (1999). Imaging cortical dynamics at high spatial and temporal resolution with novel blue voltage-sensitive dyes. *Neuron*, *24*(4), 791–802.

Silver, M. A., & Kastner, S. (2009). Topographic maps in human frontal and parietal cortex. *Trends in Cognitive Sciences*, *13*(11), 488–495. https://doi.org/10.1016/j.tics.2009.08.005

Singh, A. K., Okamoto, M., Dan, H., Jurcak, V., & Dan, I. (2005). Spatial registration of multichannel multi-subject fNIRS data to MNI space without MRI. *NeuroImage*, *27*(4), 842–851. https://doi.org/10.1016/j.neuroimage.2005.05.019

Strangman, G., Culver, J. P., Thompson, J. H., & Boas, D. A. (2002). A Quantitative Comparison of Simultaneous BOLD fMRI and NIRS Recordings during Functional Brain Activation. *NeuroImage*, *17*(2), 719–731. https://doi.org/10.1006/nimg.2002.1227

Taga, G., Asakawa, K., Maki, A., Konishi, Y., & Koizumi, H. (2003). Brain imaging in awake infants by near-infrared optical topography. *Proceedings of the National Academy of Sciences*, *100*(19), 10722–10727. https://doi.org/10.1073/pnas.1932552100

Tomalski, P., Moore, D. G., Ribeiro, H., Axelsson, E. L., Murphy, E., Karmiloff-Smith, A., … Kushnerenko, E. (2013). Socioeconomic status and functional brain development - associations in early infancy. *Developmental Science*, *16*(5), 676–687. https://doi.org/10.1111/desc.12079

Villringer, A., & Dirnagl, U. (1995). Coupling of brain activity and cerebral blood flow: basis of functional neuroimaging. *Cerebrovascular and Brain Metabolism Reviews*, *7*(3), 240–276.

Villringer, Arno, & Chance, B. (1997). Non-invasive optical spectroscopy and imaging of human brain function. *Trends in Neurosciences*, *20*(10), 435–442. https://doi.org/10.1016/S0166-2236(97)01132-6

Walsh, B., Tian, F., Tourville, J. A., Yücel, M. A., Kuczek, T., & Bostian, A. J. (2017). Hemodynamics of speech production: An fNIRS investigation of children who stutter. *Scientific Reports*, *7*(1), 4034. https://doi.org/10.1038/s41598-017-04357-6

White, B. R., & Culver, J. P. (2010a). Phase-encoded retinotopy as an evaluation of diffuse optical neuroimaging. *NeuroImage*, *49*(1), 568–577. https://doi.org/10.1016/j.neuroimage.2009.07.023

White, B. R., & Culver, J. P. (2010b). Quantitative evaluation of high-density diffuse optical tomography: in vivo resolution and mapping performance. *Journal of Biomedical Optics*, *15*(2), 026006. https://doi.org/10.1117/1.3368999

Xiong, J., Parsons, L. M., Gao, J.-H., & Fox, P. T. (1999). Interregional connectivity to primary motor cortex revealed using MRI resting state images. *Human Brain Mapping*, *8*(2–3), 151–156. https://doi.org/10.1002/(SICI)1097-0193(1999)8:2/3<151::AID-HBM13>3.0.CO;2-5

Zeff, B. W., White, B. R., Dehghani, H., Schlaggar, B. L., & Culver, J. P. (2007). Retinotopic mapping of adult human visual cortex with high-density diffuse optical tomography. *Proceedings of the National Academy of Sciences of the United States of America*, *104*(29), 12169–12174. https://doi.org/10.1073/pnas.0611266104

Zhang, H., Zhang, Y.-J., Lu, C.-M., Ma, S.-Y., Zang, Y.-F., & Zhu, C.-Z. (2010). Functional connectivity as revealed by independent component analysis of resting-state fNIRS measurements. *NeuroImage*, *51*(3), 1150–1161. https://doi.org/10.1016/j.neuroimage.2010.02.080

Chapter 2: Diffuse optical tomography measurement density impacts reconstruction of fMRI-comparable cortical activations

This chapter is being prepared for publication as a journal article. The citation will be:

Burns-Yocum, Tracy M.*, Andrew K. Fishell*, Muriah D. Wheelock, Joseph P. Culver, and Adam T. Eggebrecht. “Diffuse optical tomography measurement density impacts reconstruction of fMRI-comparable cortical activations.”

*Denotes equal contribution.

2.1 Abstract

Functional neuroimaging methods such as MRI and PET enable whole brain imaging in conjunction with outstanding spatial localization of brain activations during task performance. Limitations of these modalities include a need for dedicated and specialized facilities, constrained and noisy imaging environments, and high costs. Other functional neuroimaging techniques, including optical neuroimaging with functional near-infrared spectroscopy, overcome some of these limitations, and provide a tool for performing brain imaging in situations that may demand greater portability or open imaging environments. Despite these advantages, common limitations of optical imaging include a limited cortical field-of-view (FOV) and lower image resolution relative to modalities such as fMRI. However, increasing the number of fNIRS measurements to include overlapping optical measurements at multiple source-detector separations permits tomographic image reconstruction, as incorporated in methods such as high-density diffuse optical tomography (HD-DOT). Consequently, HD-DOT instruments overcome some of the limitations associated with other optical neuroimaging techniques. In this work, we

investigate the effect of varied optical measurement on localization of task-evoked brain responses. Spatial localization is quantified using metrics of image congruency between brain activations measured during three language tasks with fMRI, and subject-matched images reconstructed using with three separate fNIRS optode arrays and one HD-DOT optode array. Brain activations derived using the HD-DOT grid were most congruent with brain activations measured with fMRI across paradigms as quantified by three image similarity metrics, demonstrating that overlapping measurements result in the most fMRI-comparable images. We further investigated two superficial signal regression (SSR) techniques to identify strategies for removing nuisance physiological signal that may interfere with sparse grids' ability to fully localize brain activations. Applying SSR methods to images reconstructed using sparse grids removed unwanted noise and resulted in increased similarity to fMRI.

2.2 Introduction

Human neuroimaging techniques such as functional magnetic resonance imaging (fMRI) and position emission tomography (PET) have enabled researchers and clinicians to non-invasively study brain function across the lifespan in healthy and clinical populations (Davidson, Thomas, & Casey, 2003; Power et al., 2011; Yeo et al., 2011; D. Zhang & Raichle, 2010). These tools enable whole-brain imaging but are large instruments that require experimental participants to remain still in a loud, constrained imaging environment for the duration of the experiment. Wearable neuroimaging tools, such as electroencephalography (EEG) and functional near-infrared spectroscopy (fNIRS) provide an alternative to fMRI and PET, particularly when the experimental question at

hand demands an open, less constrained experimental environment (Pinti et al., n.d.). In particular, fNIRS instruments are quiet, portable, and wearable. In some instances, these optical instruments have generated fMRI-comparable images, highlighting the potential for these techniques to achieve image quality that approaches “gold-standard” techniques in human neuroimaging (Eggebrecht et al., 2014, 2012; Habermehl et al., 2012a).

Experimenters have leveraged the exceptional portability and wearability of fNIRS instruments to perform imaging research that would be difficult to adapt to MRI or PET imaging environments, highlighting the need for human neuroimaging tools that can go beyond the bore. For instance, researchers interested in longitudinal monitoring of clinical patients have used fNIRS instruments to perform bedside scanning in clinical settings, in both adult (Murkin & Arango, 2009) and pediatric populations (Ferradal et al., 2016; Lee, Cooper, & Austin, 2017; Lloyd-Fox, Blasi, & Elwell, 2010). Beyond clinical settings, when experimental questions involve complex environments (Noah et al., 2015; Ono et al., 2015), require participant movement (Miyai et al., 2001; Piper et al., 2014; Suzuki, Miyai, Ono, & Kubota, 2008), or include human social interactions (Hirsch, Zhang, Noah, & Ono, 2017; Liu et al., 2017), fNIRS offers a brain imaging tool unencumbered by bulky, unmovable, and sometimes loud instruments.

fNIRS instruments illuminate the head (scalp, skull, and superficial cortical tissue) with non-ionizing near-infrared light to recover changes in hemoglobin species concentration that occur as a result of local neuronal activity (Bluestone, Abdoulaev, Schmitz, Barbour, & Hielscher, 2001; Boas et al., 2001). Consequently, the signal measured by fNIRS instruments is an indirect, hemodynamic signal of brain activity,

analogous to the blood-oxygen level dependent (BOLD) contrast utilized in fMRI studies. Unlike fMRI, which uses magnetic fields and radio waves to image tissue, fNIRS uses optical measurements obtained with optodes positioned on the participant's head. These optodes either illuminate the head with near-infrared light (sources) or collect light (detectors), and the light level between a given source-detector pair constitutes a single fNIRS measurement. Combined with known tissue absorption and scattering coefficients for the hemoglobin species of interest (e.g. oxyhemoglobin, and deoxyhemoglobin), the light level for a given measurement indicates the hemoglobin concentration in the tissue sampled by the source-detector pair (Bluestone et al., 2001).

The arrangement of source-detector optode pairs, or fNIRS measurements, on the head directly determines a given system's key image quality parameters, including field-of-view, point-spread function, depth sensitivity, and susceptibility to physiological artifacts (Cui, Bray, Bryant, Glover, & Reiss, 2011; White & Culver, 2010). Traditional fNIRS instruments use a sparse measurement configuration, arranging the sources and detectors broadly over the head in order to cover as much of the superficial cortex as possible. Consequently, these sparse grid geometries, while offering substantial cortical coverage, have point-spread functions much broader than fMRI. Larger point-spread functions contribute to mislocalization of reconstructed activations, resulting in activations that may appear artificially distorted (White & Culver, 2010). Further, sparse fNIRS instruments with only one source-detector separation distance cannot depth profile tissue and are therefore susceptible to contamination from vascular physiology in superficial tissues (skull and scalp) that do not reflect neurovascular coupling and are generally of no interest to brain researchers. A critical advantage of sparse measurement

configurations, however, is the need for fewer source and detector optodes, which generally results in a highly portable and wearable instrument.

Dense measurement arrays overcome some of the key image quality challenges faced by sparse arrays. fNIRS techniques that use these arrays, such as high-density diffuse optical tomography (HD-DOT), use a densely packed array of source and detector optodes, resulting in a large number of overlapping measurements at multiple source-detector separations (Eggebrecht et al., 2014; Habermehl, Steinbrink, Müller, & Haufe, 2014; Koch et al., 2010). Because the physical distance between a source and detector determines how deeply into the tissue the resulting measurement will sample, HD-DOT systems achieve depth-resolved images of brain function with point-spread functions that are comparable to images obtained with fMRI (Eggebrecht et al., 2014; Habermehl et al., 2012a). Like other fNIRS instruments with multiple source-detector separations, HD-DOT instruments obtain superficial measurements of blood oxygenation from the skull and scalp that can be removed from deeper measurements, ensuring that the deeper measurements more closely reflect isolated cortical hemodynamics (Gregg, White, Zeff, Berger, & Culver, 2010; Saager & Berger, 2005). The combination of high-resolution lateral sampling (Zeff, White, Dehghani, Schlaggar, & Culver, 2007, p. 200) and depth profiling afforded by the high measurement density enables tomographic reconstruction of images of brain hemodynamics (Dehghani, White, Zeff, Tizzard, & Culver, 2009; Eggebrecht et al., 2014; Gregg et al., 2010; White & Culver, 2010; Zeff et al., 2007). However, a common drawback of dense measurement arrays results from the increased number of source and detector optodes utilized in these systems, which, if unmanaged, results in reduced wearability and ergonomics relative to sparse fNIRS systems.

Images reconstructed with sparse and dense fNIRS arrays have been previously compared using simulations, showing that sparse grids result in lower spatial resolution than dense grids (Habermehl et al., 2012b; Tian, Alexandrakis, & Liu, 2009; White & Culver, 2010; Yamamoto et al., 2002). However, a drawback of many image reconstruction simulations is the lack of superficial physiological noise in the simulation, which is better isolated and removed using dense arrays (Gregg et al., 2010). Other work has used *in vivo* assessments of grid density during a sensorimotor task, showing that a dense grid with 900 optical measurements produces fMRI-comparable images in 7 out of 10 participants (Habermehl et al., 2012b). When the same task was imaged with a sparse measurement array, the resulting images were not tomographically reconstructed, limiting comparability across measurement grids. In the present work, all optical images are reconstructed tomographically, enabling comparison across measurement densities.

The present work extends prior evaluations of grid density through an *in vivo* assessment of fNIRS measurement density. Because many human brain imaging experiments demand high-resolution localization of complex brain functions, we compare images obtained during a set of three previously published language tasks that recruit distinct and distributed cortical regions (Petersen, Fox, Posner, Mintun, & Raichle, 1989), extending prior work using tasks that typically result in single, focal activations. Subsets of the over 1,500 dense HD-DOT measurements are then selected to create three distinct sparse imaging grids, which are used to tomographically reconstruct maps of brain hemodynamics using the same underlying data, crucially eliminating cross-session variance and variance attributable to cap position. We then compare these four (3 sparse, 1 dense) tomographically reconstructed images to subject-matched reference images

obtained with fMRI to evaluate the effect of measurement density on an optical measurement grid's ability to localize fMRI-comparable cortical activations.

2.3 Materials and methods

2.3.1 Participants

The HD-DOT and MRI data used in this study are from a previously published data set (Eggebrecht et al., 2014). All participants gave written informed consent to participate in the experiments, which were conducted under a protocol approved by the Washington University School of Medicine Human Research Protection Office. Participants included 5 healthy, right-handed, native English-speaking adults. Data were acquired with HD-DOT and fMRI on separate days.

2.3.2 Data Acquisition and Stimulus Protocol

During DOT data acquisition, the participants were seated in an adjustable chair facing a 19-inch liquid crystal display monitor positioned 75 cm from the participant's nasion in a sound-isolated imaging chamber. During fMRI acquisition, visual stimuli were presented via a projector onto a screen viewed via a mirror attached to the head coil; auditory stimuli were presented via headphones. The screen resolutions were set such that screens subtended the same solid angles in the fMRI environment as in the DOT imaging room. Stimuli were presented using the Psychophysics Toolbox, V3, in MATLAB (Brainard, 1997).

Data used herein includes three language paradigms designed to map multiple language processing areas (Petersen et al., 1989). Each paradigm consisted of six

blocks, during which 15 single words were presented at a rate of one word per second, followed by 15 seconds of result, during which a fixation cross was displayed on the screen. Word stimuli, all of which were concrete nouns, were either presented visually or aurally, depending on the task. The three tasks in the present study measured responses to aurally presented words ("Hearing Words"), responses to silent reading of visually presented words ("Covert Reading"), and responses during a verb generation task ("Generate Verbs"), during which participants were instructed to imagine themselves speaking a verb that corresponded to the visually presented noun.

2.3.3 HD-DOT instrumentation

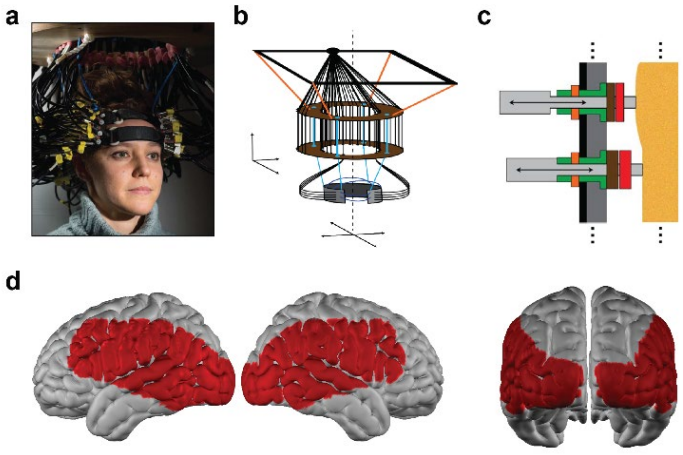

Figure 2.1. HD-DOT instrumentation. A: HD-DOT cap on a participant's head, illustrating the positioning of the dense optode array. **B:** Fiber management schematic, showing how the 188 constituent fibers in the HD-DOT cap are managed using a double halo design, ensuring that the participant's head and neck are not restrained and do not bear any weight of the fibers. **C:** Cross section of the HD-DOT cap, showing how flexible foam rings (brown, red) enable consistent optode coupling with the participant's scalp (tan), regardless of individual differences in head shape. **D:** Representative flat-field reconstruction of the HD-DOT sensitivity matrix, showing regions of superficial cortex in the field-of-view (red). Sensitivity in this image is calculated based on the Montreal Neurological Institute ICBM-152 atlas, meaning that an individual's sensitivity may vary from the group-level field-of-view.

The HD-DOT system (Figure 2.1) has been described in prior work using this instrument (Eggebrecht et al., 2014). Briefly, the HD-DOT system is a continuous-wave instrument with a 96 source and 92 detector array. The sources optodes consisted of light emitting diodes (LEDs) illuminating at 750 and 850 nm, to provide optimal spectroscopic separation of oxygenated and deoxygenated hemoglobin concentrations (Boas et al., 2001). The detector optodes consisted of 92 avalanche photo diode detectors (Hamamatsu C5460-01). The sources and detectors were coupled to the head using 4.2 m long fiber-optic bundles (CeramOptec, 2.5-mm diameter bundles of 50 μm fibers), which are embedded in a semi-rigid imaging cap. The fiber tips extend 3mm beyond the inside of the imaging cap to facilitate combing through hair and to achieve perpendicular optode-scalp coupling, essential for optimal data quality.

The weight of the 188 fibers was managed using an extruded aluminum frame and series of collinear rings surrounding the participant, ensuring that participants do not bear any of the fiber weight. The optode grid geometry results in source-detector separations for first through fourth nearest neighbors of 13 mm (322 measurements), 30 mm (534 measurements), 39 mm (220 measurements), and 47 mm (424 measurements), respectively, with over 1,500 possible measurements per wavelength. Previously published temporal, spatial, and frequency encoded source illimitation patterns enabled the HD-DOT system to achieve an overall framerate of 10 Hz (Eggebrecht et al., 2014). Using image reconstruction procedures as specified below, the measurements were then converted into voxelated movies of brain hemodynamics.

2.3.4 HD-DOT image reconstruction

The full set of source-detector measurements were tomographically reconstructed into voxelated movies of cortical hemodynamics using a previously published HD-DOT processing pipeline (Eggebrecht et al., 2014), implemented in the NeuroDOT toolbox for MATLAB (Eggebrecht, Muccigrosso, & Culver, 2019; Muccigrosso & Eggebrecht, 2018). This pipeline consists of measurement preprocessing, anatomical light modeling, image reconstruction, and tissue spectroscopy. During measurement preprocessing, raw measurements (i.e. light levels for single source-detector pairs) were converted to log-ratio timeseries data by taking the logarithm of the ratio of the instantaneous light level and the source-detector measurement's mean value over the course of the imaging run. Consequently, after the log-ratio procedure, the baseline for a given measurement is the defined as the mean for that measurement.

Next, measurement channels with excessive temporal variance were excluded from further processing, as these measurements were likely contaminated by sources of non-physiological variance (e.g. head motion, poor optode coupling). A threshold of 7.5% was applied to the measurement data, such that channels with a temporal standard deviation greater than 0.075 were excluded from image reconstruction. The measurements that survived this threshold were then temporally filtered to remove long-term drift and physiological signals not related to task performance (e.g. pulse, respiration, vasomotion (Bumstead, Bauer, Wright, & Culver, 2017)). The bandpass filter cutoffs for all runs were set to $0.02 < f < 0.5$ Hz. Next, the superficial signal, or signal originating from scalp and skull hemodynamics, was approximated by averaging the first nearest-neighbor measurements (S-D separation = 13mm) and regressing this global signal from all measurements.

After measurement preprocessing, subject-specific forward models of light propagation were generated using anatomical MRIs obtained during each subject's MRI session (Eggebrecht et al., 2012). These anatomical images were segmented into five non-uniform tissues compartments with tissue specific optical properties: scalp ($\mu_{a,750}$ = 0.017 ; $\mu_{a,850}$ = 0.019; $\mu_{s,750}'$ = 0.74; $\mu_{s,850}'$ = 0.64), skull ($\mu_{a,750}$ = 0.012; $\mu_{a,850}$ = 0.014; $\mu_{s,750}'$ = 0.94; $\mu_{s,850}'$ = 0.84), grey matter ($\mu_{a,750}$ = 0.018; $\mu_{a,850}$ = 0.019; $\mu_{s,750}'$ = 0.84; $\mu_{s,850}'$ = 0.67), white matter ($\mu_{a,750}$ = 0.018; $\mu_{a,850}$ = 0.021; $\mu_{s,750}'$ = 1.19; $\mu_{s,850}'$ = 1.01), and cerebrospinal fluid ($\mu_{a,750}$ = 0.004; $\mu_{a,850}$ = 0.004; $\mu_{s,750}'$ = 0.3; $\mu_{s,850}'$ = 0.3) (Eggebrecht et al., 2014). Using measurements of optode positions relative to the tragus, eyes, nasion, and inion, the optodes were positioned onto the subject-specific anatomy (Eggebrecht et al., 2014, 2012). Finally, using the subject specific anatomy and optode positions, a forward model was generated using NIRFAST (Dehghani et al., 2008), resulting in a wavelength dependent sensitivity matrix with tissue-specific optical properties. This matrix relates relative changes in the ratiometric light-level measurements to relative changes in absorption within the volume. The sensitivity matrix was inverted using Tikhonov regularization with spatially-variant regularization (λ_1 = 0.01; λ_2 = 0.1). Finally, literature-derived spectroscopy values converted the images from differential absorption to differential hemoglobin, resulting in the four dimensional (3 spatial, 1 temporal) movies of three hemodynamic contrasts: oxyhemoglobin (ΔHbO_2), deoxyhemoglobin (ΔHbR) and total hemoglobin (ΔHbT), down-sampled to a final framerate of 1 Hz to reduce data size. Unless otherwise specified, analyses utilized the ΔHbO_2 contrast, which has been previously shown to produce the highest signal-to-noise of the three hemoglobin contrasts (Eggebrecht et al., 2014, 2012; Ferradal et al., 2016).

2.3.5 Tomographic image reconstruction using sparse measurement grids

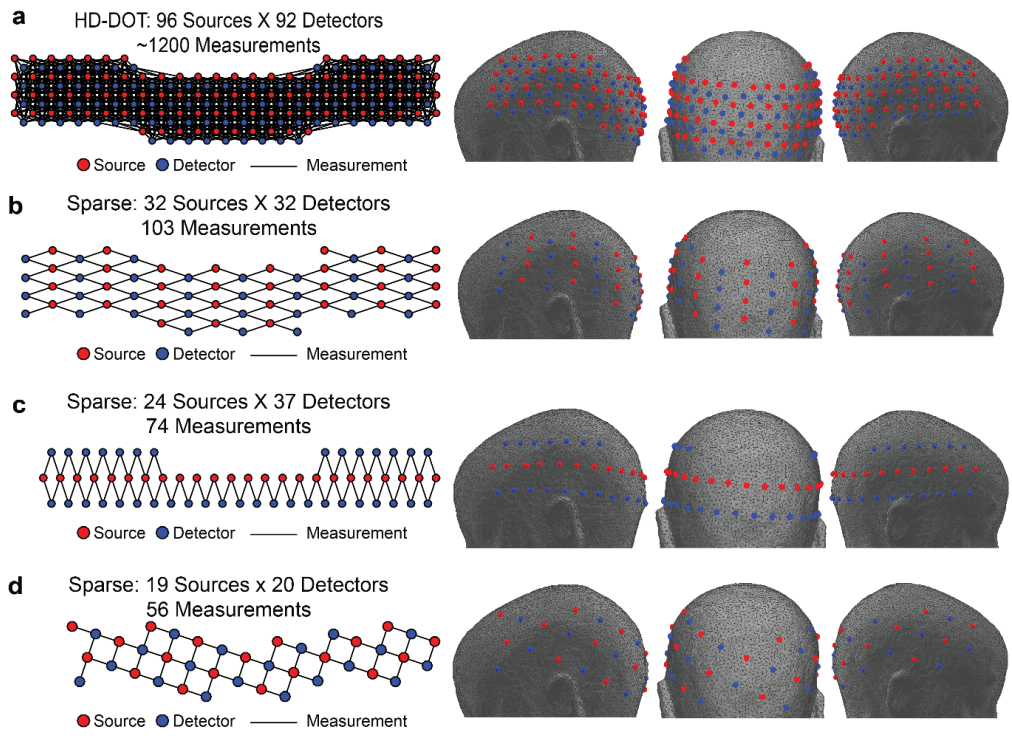

Figure 2.2. HD-DOT and sparse measurement arrays. A: A flattened view of the HD-DOT optode array (left) showing source (red) and detector (blue) optode positions. First through third nearest-neighbor measurements resulting from this arrangement are indicated by black lines resulting in approximately 1200 measurements per wavelength. Optode positions on the head (right) indicate the three-dimensional arrangement of the optodes for this array. **B:** A flattened view of the "horizontal triangular" sparse array (right), which is generated using 32 sources (red) and 32 detectors (blue) selected from the dense array in **Panel A**. This optode configuration results in 103 measurements at a single source-detector separation (30mm). Optode positions on the head (right) indicate the three-dimensional arrangement of the optodes for this array. **C:** A flattened view of the "vertical triangular" sparse array (right), which is generated using 24 sources (red) and 37 detectors (blue) selected from the dense array in **Panel A**. This optode configuration results in 74 measurements at a single source-detector separation (30mm). Optode positions on the head (right) indicate the three-dimensional arrangement of the optodes for this array. **D:** A flattened view of the "square" sparse array (right), which is generated using 19 sources (red) and 20 detectors (blue) selected from the dense array in **Panel A**. This optode configuration results in 56 measurements at a single source-detector separation (30mm). Optode positions on the head (right) indicate the three-dimensional arrangement of the optodes for this array.

To directly assess the effects of measurement density using the same *in vivo* data, three sparse optode grid patterns previously used in simulations evaluating grid density (White & Culver, 2010) were replicated and directly derived from using subsets of measurements from the full 96 source by 92 detector HD-DOT array (Figure 2.2). The full HD-DOT grid contains up to 1,512 possible measurements, per wavelength, within a source-detector separation of 5cm (i.e. first through fourth nearest neighbor measurements).

Each of the three sparse grids were designed such that they only used source-detector measurements at a separation of 30mm, corresponding to the second nearest-neighbor measurements in the full HD-DOT array. The three sparse grid designs included: a horizontal triangular grid (Figure 2.2B; 32 sources, 32 detectors, 103 total measurements); a vertical triangular grid (Figure 2.2C; 24 sources, 37 detectors, 74 total measurements); and a square grid (Figure 2.2D; 19 sources, 20 detectors, 56 total measurements).

Tomographic image reconstruction using the sparse grids followed the image reconstruction procedures described in Section 2.3.4, except instead of using the full set of possible HD-DOT source-detector measurements, measurements were restricted to include only source-detector pairs contained within a given grid pattern. However, due to uniformity of source-detector separations within each of the sparse grids, superficial signal regression using the average of all usable first-nearest neighbor measurements was not possible. Consequently, sparse images were tomographically reconstructed without superficial signal regression. To further characterize the effects of superficial

signal regression in sparse grids, alternative methods for nuisance physiology removal schemes in sparse grid reconstruction were utilized, as described in Section 2.3.6.

Crucially, all sparse and dense images reconstructed for a given subject were reconstructed using the same underlying data, eliminating variance attributable movement, cap fit, and task performance, as well as variance related to imaging the same participant across multiple task repetitions and disparate imaging sessions. As a result, differences in activation localization across the sparse and dense image reconstructions are more likely to be attributable to optode positioning and measurement density.

2.3.6 Superficial signal regression using sparse measurement grids

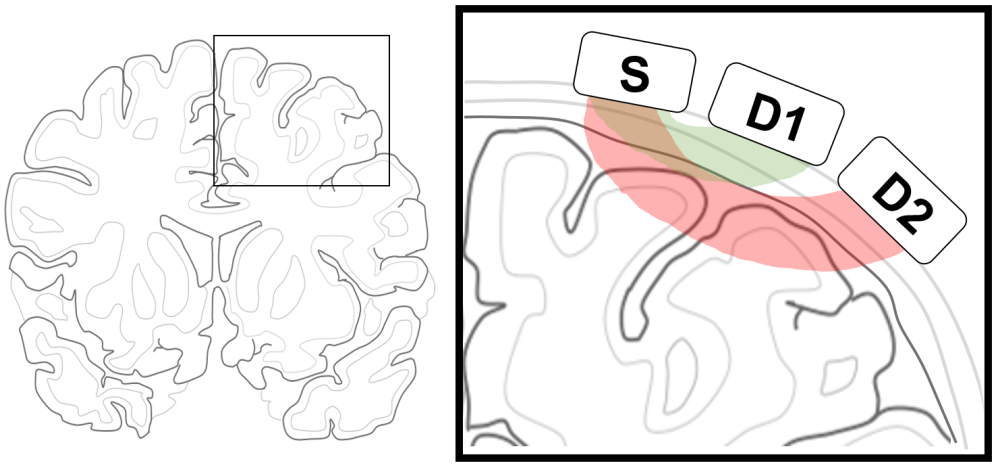

Figure 2.3. Superficial signal regression in high-density diffuse optical tomography. Superficial signal regression (SSR) as implemented in HD-DOT is designed to approximate and remove signals related to systemic physiology that is unrelated to the cortical hemodynamics of interest. SSR approximates this nuisance signal by averaging all first nearest-neighbor measurements (i.e. measurement between source, **S**, and detector, **D1**, with sensitivity indicated in red) which have sensitivity biased towards superficial tissues. By removing this superficial signal from measurements with greater source-detector separation (i.e. measurement between source, **S**, and detector, **D2**, with sensitivity indicated in green), measurements with greater depth sensitivity can more specifically probe deeper, cortical tissues of interest.

As light in a single measurement travels from the source optode to the detector optode, the measured light level contains contributions from superficial, systemic physiology such as respiration and heartbeat. These systemic signals are distinct from the deeper, focal changes in cortical hemodynamics related to neurovascular coupling (Huppert, Diamond, Franceschini, & Boas, 2009; Saager & Berger, 2005). As described in Section 2.3.4 superficial signal regression is a strategy for removing the contribution of superficial signals to optical measurements, resulting in measurements that more closely reflect variance related to cortical hemodynamics (Figure 2.3). The superficial signal was approximated by averaging all first nearest-neighbor measurements (separation = 13mm), which have a sensitivity that is heavily weighted towards the superficial tissue. This approximation of superficial physiology is then regressed from all source-detector measurements (Gregg et al., 2010; Zeff et al., 2007), which is a common technique in HD-DOT image reconstruction (Eggebrecht et al., 2014, 2012; Hassanpour, Eggebrecht, Culver, & Peelle, 2015; Hassanpour, Eggebrecht, Peelle, & Culver, 2017).

Because the sparse grids described in Section 2.3.5 lack measurements at a short source-detector separation, superficial signal regression was initially not performed in tomographic image reconstruction using these arrays. However to further investigate the effects of superficial signal regression on sparsely reconstructed images, the sparse reconstruction was repeated using two superficial signal regression strategies that may be available to researchers using sparse optode arrays: (1) Regress using the first nearest-neighbor average from the full HD-DOT grid to evaluate the effect of including a short source-detector separation in a sparse measurement array and (2) regress using

the average of all clean measurements in the sparse arrays, which is analogous to regressing the global signal from the data.

2.3.7 fMRI acquisition and processing

MRI scans were collected on a Siemens Trio 3T scanner. Anatomical T1-weighted MPRAGE (echo time (TE) = 3.13 ms, repetition time (TR) = 2,400 ms, flip angle = 8°, 1 × 1 × 1 mm isotropic voxels) and T2-weighted (TE = 84 ms, flip angle = 120°, 1 × 1× 4 mm voxels) scans were taken at each session. Functional images were collected during performance of the three language paradigms described in Section 2.2 using a series of asymmetric gradient spin-echo echo-planar (EPI) sequences (TE = 27 ms, TR = 2,000 ms, flip angle = 90°, 4 × 4 × 4 mm voxels) to measure the Blood Oxygen Level Dependent contrast.

Importantly, to enable comparison between fMRI and HD-DOT-derived maps of brain activations, the fMRI data were smoothed using a 13 mm FWHM Gaussian kernel to match the HD-DOT point-spread-function (Eggebrecht et al., 2014). Further, to account for the larger field-of-view afforded by fMRI, the fMRI datasets were spatially masked to match the HD-DOT field-of-view. As described in prior work, this field-of-view masking procedure limits the cortical field-of-view to approximately the outer 10 mm of cortex (Eggebrecht et al., 2014, p. 2).

2.3.8 Block analysis of task data

In order to generate spatial maps of brain activation during the three language paradigms used in this work, images of brain hemodynamics during task were contrasted with images of brain activity during fixation (i.e. no task). As in previous work utilizing HD-DOT

during performance of these language tasks, the response magnitude was computed using a voxelwise paired t-statistic, contrasting the task image with the fixation image across subjects.

2.3.9 Image comparison metrics

The result of the HD-DOT image reconstruction, sparse image reconstruction, subject-matched fMRI acquisition, and block analysis was set of five activation maps, per subject, per task. The set of five images consisted of 1 image obtained through HD-DOT reconstruction, 3 sparsely reconstructed images, and 1 subject-matched fMRI image. Because the goal of this work was to evaluate agreement between reference images obtained with fMRI and images reconstructed using sparse and dense measurement sets, three image agreement metrics were used to quantify image agreement: Dice's coefficient, overlap percentage, and spatial correlation. These metrics were chosen to provide distinct but convergent information about image agreement across the reconstruction schemes.

Dice's coefficient is a region-based similarity coefficient that was calculated using T-maps thresholded at 50% of the maximum value for the fMRI and optical T-maps. Voxels that survive the threshold were considered to be "activated," and Dice's coefficient is computed as the ratio of the number of overlapping activated voxels between the two maps as compared with the total number of activated voxels. Values of Dice's coefficient range from 0 (no agreement) to 1 (total agreement).

The overlap percentage is calculated by identifying the strongest contiguous regions of activation in two activation maps (i.e. one fMRI image and one optical image),

after thresholding each image at 50% of the maximum. Then, the percentage of voxels in one activated region that spatially correspond with the activated region in the second image is calculated.

Unlike Dice's coefficient and overlap percentage, spatial correlation does not use any thresholding in the maps, and therefore provides a measure of agreement across the entire FOV between images from multiple modalities. The spatial correlation is computed as Pearson's product-moment correlation coefficient between two images. As with all Pearson product-moment correlation coefficients, values range from -1 (anti-correlation) to 0 (no correlation) to 1 (perfect correlation).

All image agreement metrics were computed between either a sparsely or densely reconstructed image and fMRI. A pairwise T-test was used to test for significant differences between image agreement metrics for pairs of reconstructed optical images, resulting in a total of 6 pairwise comparisons between the 1 dense and 3 sparse reconstructions. Thus, a Bonferroni-corrected alpha value was set to 0.0083 for all pairwise comparisons ($\alpha = 0.05/6$).

2.4 Results

Our primary question was how the number of measurements in an optical imaging array affects the reconstruction of activations that spatially concur with activations obtained using a high-resolution, whole-brain imaging modality, fMRI. For each of the three language paradigms used in this study, we used either the full set of HD-DOT measurements ("Dense Array") or subsets of HD-DOT measurements ("Sparse Arrays") to compute metrics of image agreement between the optical arrays and fMRI. All three

metrics indicated the highest agreement between fMRI-derived activation maps and activation maps reconstructed using the dense, HD-DOT array. In this section, we first consider group-level responses across all three language processing task across sparse and dense reconstruction schemes. We then evaluate the effect of incorporating superficial signal regression into the sparse reconstruction scheme on the image agreement metrics.

2.4.1 Group-level analysis

2.4.1a Hearing words

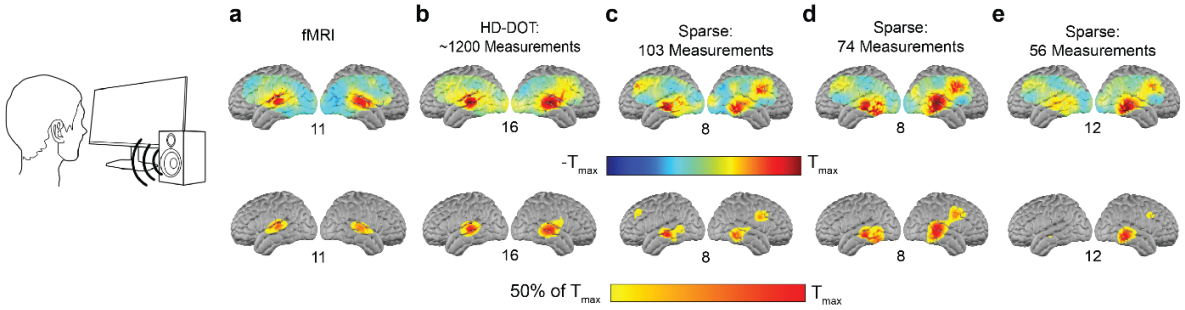

Figure 2.4. Activations related to the hearing words task. During the hearing words task, participants passively listen to words presented over a speaker. **A:** Using fMRI, group-level activations related to this task were computed using a block design analysis and localized to bilateral superior temporal gyrus. Unthresholded maps (top) are scaled to the maximum T-value for image, indicated below each image. Thresholded maps (bottom) are thresholded at 50% of the maximum T-value and scaled to the image's maximum T-value. **B:** Group-level activations reconstructed using the dense HD-DOT array. **C:** Group-level activations reconstructed using the sparse horizontal triangular array, with 103 source-detector measurements. **D:** Group-level activations reconstructed using the sparse vertical triangular array, with 74 source-detector measurements. **E:** Group-level activations reconstructed using the sparse square array, with 56 source-detector measurements. Image agreement metrics for maps in **Panel A** and **Panels B-E** are reported in **Table 2.1**.

The Hearing Words task required participants to listen to sequences of spoken concrete nouns. Both thresholded and unthresholded fMRI maps revealed that this task produces bilateral activations centered on the superior temporal gyrus, as shown by the T-maps presented in Figure 2.4A. Of the four optical reconstruction schemes (Figure 2.4B-E), the maps reconstructed using the HD-DOT array produced activation maps with the highest spatial agreement with fMRI activations. Like the fMRI-derived maps, the activations reconstructed with HD-DOT resulted in focal loci of activation on each hemisphere. Quantitatively, the image agreement metrics (Table 2.1) confirm that the HD-DOT reconstructions most closely recapitulate the fMRI activations, as the Dice's Coefficient (0.59), percent overlap (73%), and spatial correlation (r = 0.48) for the HD-DOT metrics were significantly greater for the dense reconstruction compared to the three sparse reconstructions (Figure 2.4F-G). There were no significant differences between image agreement metrics for any pairs of sparse measurement grids.

Grid Type	Dice's Coefficient	Overlap Percentage	Spatial Correlation
HD-DOT	0.46 (± 0.05)	0.77 (± 0.04)	0.48 (± 0.04)
Sparse: 103 Measurements	0.32 (± 0.06)	0.55 (± 0.10)	0.22 (± 0.11)
Sparse: 74 Measurements	0.35 (± 0.06)	0.64 (± 0.10)	0.28 (± 0.04)
Sparse: 56 Measurements	0.33 (± 0.06)	0.66 (± 0.10)	0.28 (± 0.08)

Table 2.1. Image agreement metrics for the hearing words task. Image agreement metrics between sparsely/densely reconstructed images and subject-matched fMRI for the hearing words task. Values reported are the group means and SEM for each reconstruction scheme and metric.

2.4.1b Covert reading

The Covert Reading task required participants read sequences of visually presented concrete nouns. This task resulted in activations centered in occipital cortex, as shown by fMRI (Figure 2.5A). Like the passive word listening task, the images reconstructed using HD-DOT resulted in the greatest agreement with the fMRI-based images, as indicated by the three image agreement metrics (Figure 2.5F). However, for this task, images reconstructed using the sparse arrays also recovered focal activations in occipital cortex, as indexed by the moderate agreement between the three sparse arrays and fMRI across the image agreement metrics (Table 2.2).

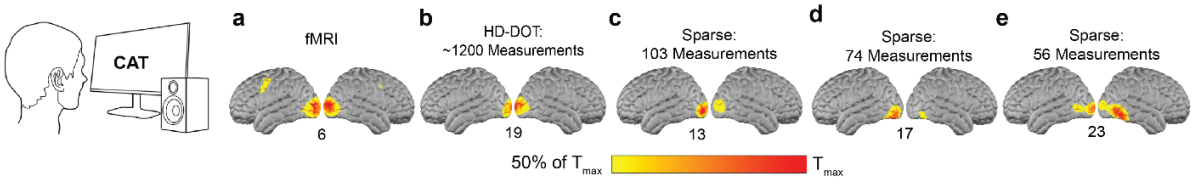

Figure 2.5. Activations related to the reading words task. During the reading words task, participants passively read words presented on a monitor. **A:** Using fMRI, group-level activations related to this task were computed using a block design analysis and primarily localized to bilateral occipital cortex. Thresholded maps are thresholded at 50% of the maximum T-value and scaled to the image's maximum T-value, which is reported below each image. **B:** Group-level activations reconstructed using the dense HD-DOT array. **C:** Group-level activations reconstructed using the sparse horizontal triangular array, with 103 source-detector measurements. **D:** Group-level activations reconstructed using the sparse vertical triangular array, with 74 source-detector measurements. **E:** Group-level activations reconstructed using the sparse square array, with 56 source-detector measurements. Image agreement metrics for maps in **Panel A** and **Panels B-E** are reported in **Table 2.2**.

Grid Type	Dice's Coefficient	Overlap Percentage	Spatial Correlation
HD-DOT	0.68 (± 0.03)	0.82 (± 0.04)	0.46 (± 0.08)
Sparse: 103 Measurements	0.60 (± 0.06)	0.79 (± 0.04)	0.36 (± 0.09)
Sparse: 74 Measurements	0.61 (± 0.06)	0.74 (± 0.06)	0.39 (± 0.07)
Sparse: 56 Measurements	0.55 (± 0.08)	0.65 (± 0.09)	0.33 (± 0.11)

Table 2.2. Image agreement metrics for the reading words task. Image agreement metrics between sparsely/densely reconstructed images and subject-matched fMRI for the reading words task. Values reported are the group means and SEM for each reconstruction scheme and metric.

2.4.1c Generate verbs

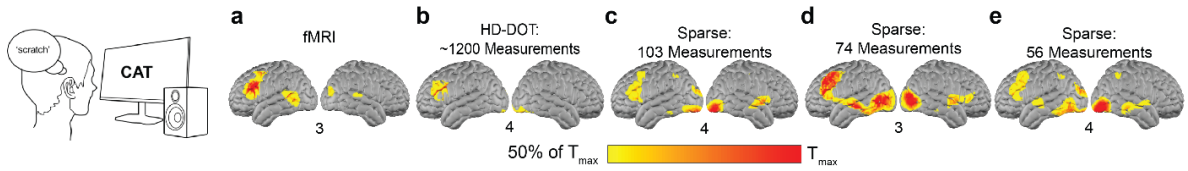

Figure 2.6. Activations related to the verb generation task. During the verb generation task, participants imagined themselves speaking a verb related to a cue word presented on a monitor. **A:** Using fMRI, group-level activations related to this task were computed using a block design analysis and primarily localized to bilateral occipital cortex. Thresholded maps are thresholded at 50% of the maximum T-value and scaled to the image's maximum T-value, which is reported below each image. **B:** Group-level activations reconstructed using the dense HD-DOT array. **C:** Group-level activations reconstructed using the sparse horizontal triangular array, with 103 source-detector measurements. **D:** Group-level activations reconstructed using the sparse vertical triangular array, with 74 source-detector measurements. **E:** Group-level activations reconstructed using the sparse square array, with 56 source-detector measurements. Image agreement metrics for maps in **Panel A** and **Panels B-E** are reported in **Table 2.3**.

In the Generate Verbs paradigm participants covertly spoke verbs related to visually presented concrete nouns, resulting in spatially distributed brain activations related to reading the cue word and generating a novel word in response to the cue. While both sparsely and densely reconstructed images of brain activation during this task resulted in detection of spatially distributed responses (Figure 2.6), the dense HD-DOT grid most resulted in images with the greatest spatial agreement with fMRI, as quantified by both Dice's coefficient and percent overlap. In this case, the sparsely reconstructed responses, while spatially distributed, were both enlarged and included regions not detected with fMRI, resulting in lower Dice's coefficients and overlap percentages relative to the dense reconstruction, which produced more focal and spatially concordant responses. Further, the three sparse grids showed substantial variance across participants for Dice's coefficient and percent overlap, indicating that activation localization performance for the sparse reconstructions varied considerably from individual to individual (Table 2.3).

Grid Type	Dice's Coefficient	Overlap Percentage	Spatial Correlation
HD-DOT	0.29 (± 0.16)	0.35 (± 0.19)	0.08 (± 0.08)
Sparse: 103 Measurements	0.12 (± 0.14)	0.16 (± 0.18)	0.05 (± 0.11)
Sparse: 74 Measurements	0.10 (± 0.10)	0.12 (± 0.12)	0.12 (± 0.12)
Sparse: 56 Measurements	0.11 (± 0.12)	0.20 (± 0.21)	0.06 (± 0.10)

Table 2.3. Image agreement metrics for the verb generation task. Image agreement metrics between sparsely/densely reconstructed images and subject-matched fMRI for the verb generation task. Values reported are the group means and SEM for each reconstruction scheme and metric.

However, for this task, the spatial correlation between reconstructed images and subject-matched fMRI did not reveal superior performance for any of the reconstruction schemes.

2.4.2 Applying superficial signal regression to sparsely reconstructed images

Initially, image reconstruction using the three sparse measurement grids did not include a superficial signal regression step, as these measurement grids did not include measurement pairs at a shorter source-detector separation that was suitable for approximating the superficial signal regression. However, some sparse optode arrays do include multiple measurement distances, and the global average of measurements at a longer source-detector separation may also capture superficial nuisance physiology. To account for these possibilities, the sparsely reconstructed images were reprocessed to evaluate two superficial signal regression schemes. The first scheme approximated the superficial signal using the average of the first nearest-neighbor measurements from the full HD-DOT grid, as is done in standard HD-DOT processing. The second scheme did not incorporate an additional source-detector separation and instead approximated the superficial signal using the average of all clean (i.e. below the 7.5% temporal variance threshold described in Section 2.3.4) measurements in the sparse array.

Relative to sparsely reconstructed images from the hearing words task with no superficial signal regression (Figure 2.4), sparsely reconstructed images with superficial signal regression resulted in greater agreement with subject-matched fMRI (Figure 2.7). As quantified in Tables 2.4 and 2.5, the trend of greater agreement with activations obtained with fMRI is captured by the three image agreement metrics. Consequently,

incorporating an approximation of nuisance physiology into image reconstruction results in improved agreement with reference images obtained using fMRI.

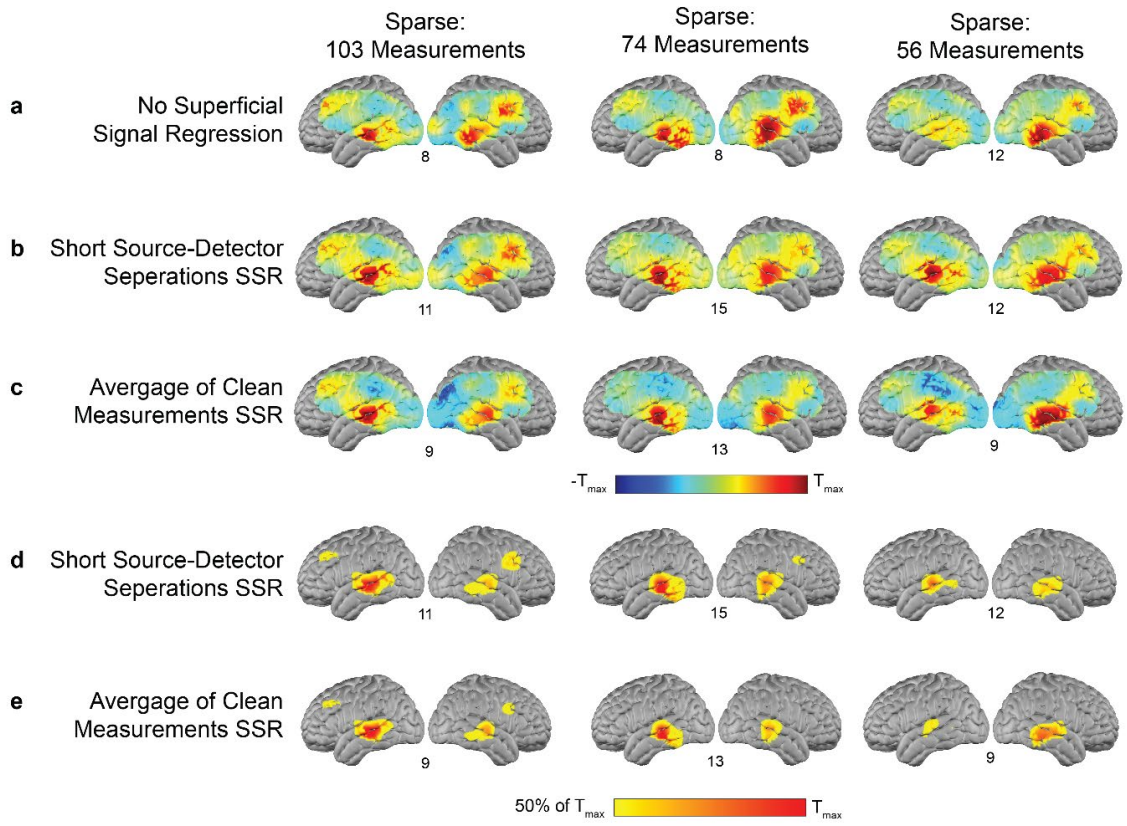

Figure 2.7. Sparsely reconstructed images with two superficial signal regression schemes. Sparse images from the hearing words task were reconstructed two superficial signal regression (SSR) strategies. **A:** Reconstructed images from the three sparse grids with no SSR. **B:** Reconstructed images from the three sparse grids using a superficial nuisance signal approximated using the first nearest-neighbor measurements from the full HD-DOT grid. **C:** Reconstructed images from the three sparse grids using a superficial nuisance signal approximated using the average of all clean measurements used in sparse reconstruction. Maps in **A-C** are unthresholded and scaled to each image's maximum T-value, which is reported below each individual image. **D:** Thresholded view of the map presented in **Panel B**. **E:** Thresholded view of the map presented in **Panel C**. Maps in **D-E** are thresholded at 50% of each image's maximum T-value and scaled to each image's maximum T-value, which is reported below each individual image.

Grid Type	Dice's Coefficient		Overlap Percentage		Spatial Correlation	
	Mean	% Chg	Mean	% Chg	Mean	% Chg
HD-DOT	0.46 (± 0.05)	-	0.77 (± 0.04)	-	0.48 (± 0.04)	-
Sparse: 103 Measurements	0.42 (± 0.09)	30.0	0.58 (± 0.09)	5.4	0.33 (± 0.7)	50.8
Sparse: 74 Measurements	0.40 (± 0.08)	13.2	0.56 (± 0.10)	-11.9	0.33 (± 0.6)	17.6
Sparse: 56 Measurements	0.44 (± 0.06)	31.7	0.64 (± 0.08)	-3.1	0.35 (±0.04)	23.4

Table 2.4. Hearing words SSR image agreement metrics. Sparse images were reconstructed using superficial signal regression (SSR) based on a superficial signal approximated using the mean of clean first-nearest neighbor measurements from the full HD-DOT measurement grid. Values reported are the group means and SEM for each reconstruction scheme and metric. Percent change indicates the percent increase/decrease of the image agreement metric with superficial signal regression relative to image agreement metrics for non-SSR images, reported in Table 2.1.

Grid Type	Dice's Coefficient		Overlap Percentage		Spatial Correlation	
	Mean	% Chg	Mean	% Chg	Mean	% Chg
HD-DOT	0.46 (± 0.05)	-	0.77 (± 0.04)	-	0.48 (± 0.04)	-
Sparse: 103 Measurements	0.46 (± 0.07)	42.4	0.63 (± 0.05)	14.6	0.35 (± 0.07)	59.9
Sparse: 74 Measurements	0.39 (± 0.08)	10.4	0.56 (± 0.11)	-11.9	0.35 (± 0.05)	24.7
Sparse: 56 Measurements	0.44 (± 0.06)	31.7	0.66 (± 0.08)	-0.1	0.35 (± 0.05)	23.4

Table 2.5 Hearing words SSR image agreement metrics. Sparse images were reconstructed using superficial signal regression (SSR) based on using the mean of all clean measurements. Values reported are the group means and SEM for each reconstruction scheme and metric. Percent change indicates the percent increase/decrease of the image agreement metric with superficial signal regression relative to image agreement metrics for non-SSR images, reported in Table 2.1.

2.5 Discussion

In this work, we assessed the agreement between activations reconstructed with four optical imaging grids of varying measurement density and activations obtained with subject-matched fMRI data. Across three language processing paradigms, a dense measurement array is most likely to result in maps of brain activation in spatial agreement with fMRI, as quantified by three image agreement metrics. We further demonstrate that approximating and removing nuisance physiology, either with a short source-detector measurement or global measurement average, is one strategy for improving agreement between sparsely reconstructed images and subject-matched fMRI.

Prior work has assessed grid densities in simulations, in the absence of physiological noise, demonstrating that grids with overlapping measurements more reliably localize functional activations as compared to sparse measurement grids (Habermehl et al., 2012b; Tian et al., 2009; White & Culver, 2010; Yamamoto et al., 2002). This work extends this work evaluating activation localization capability by using *in vivo* data from both HD-DOT and fMRI, enabling further evaluation of the effect of nuisance physiology on localization capability. An advantage of using a dense measurement array such as HD-DOT is that sparsely reconstructed images can be obtained from the same dataset, simply by restricting the reconstruction to include predetermined measurement sets that comprise sparse arrays. By utilizing the same underlying data for all reconstructions, common sources of variance such as array position and task performance/attentiveness are mitigated. Consequently, differences in localization

performance across reconstruction schemes can more confidently be attributed to measurement density.

The sparse grids consistently had low spatial agreement with fMRI for all three language paradigms, including poorly localized activations and spurious secondary activations. This discrepancy is a result of their grid arrangement, which places all source-detector pairs equidistant from one another. The HD-DOT array, which permits over 1,500 measurements at both wavelengths allows for surface profiling and more accurate localization at three different depths that is not possible with unidistant sparse grids (Dehghani et al., 2009; Gregg et al., 2010). These benefits of a dense array lead to reliable high-quality data over a wider FOV. Relatively good agreement is found between HD-DOT and subject-matched fMRI data for all the paradigms and image quality metrics.

For the functional brain areas probed in this paper, sparse grids with 30 mm source-detector separation and no superficial signal regression typically generate images with lower spatial agreement fMRI than images reconstructed with dense grids incorporating multiple source-detector separations. Failing to account for superficial nuisance physiology means that the images reconstructed using sparse arrays are contaminated with noise unrelated to stimulus driven brain responses(Diamond et al., 2005; Huppert et al., 2009). Superficial signal regression is a useful strategy for approximating and removing unwanted physiological noise in optical data, as shown by prior work(Gregg et al., 2010; Saager & Berger, 2005) incorporating a measurements with a shorter source-detector separation, biasing the physiologic origin of the measured signal to superficial tissues.

We investigated two strategies for incorporating superficial signal regression into sparse reconstruction schemes and found that these strategies generally improve agreement between sparsely reconstructed images and subject-matched fMRI, as shown in Figure 2.7. The first strategy incorporated first nearest-neighbor measurements obtained with the full HD-DOT grid, and used these measurements to approximate the superficial signal, highlighting the utility of including optical measurements at multiple source-detector separations (Gregg et al., 2010; Saager & Berger, 2005). The second strategy averaged the unidistant measurements already included in the sparse arrays to approximate systemic nuisance physiology (Pfeifer, Scholkmann, & Labruyère, 2017; Saager & Berger, 2005). This superficial signal regression strategy does not require overlapping measurements, allowing this technique to be more easily implemented in existing instruments with unidistant measurements.

One limitation of this study is the focus on task-evoked responses during language processing paradigms. Two of the language paradigms, hearing words and reading words, were presented in a single sensory modality, and resulted in bilateral activations in a focal brain region related to that sensory modality (i.e. visual or auditory cortex). In these cases, the sparsely reconstructed images resulted in activations that were often partially overlapping or adjacent to activations imaged with fMRI, in addition to other activations that were not present in the subject-matched fMRI data. This finding highlights that sparse arrays may be suitable detecting activations for paradigms in which experimenters have an *a priori* hypothesis about the brain region of interest, with the caveat that exact localization of a cortical response may depend on the optode geometry. Indeed, novel tools now exist for fNIRS researchers to optimize optode arrays given a

constrained set of *a priori* regions of interest (Brigadoi, Salvagnin, Fischetti, & Cooper, 2018), potentially automating this time consuming and often subjective process. The other paradigm used in this work, covert verb generation, recruited spatially distributed responses related to reading the cue word and generating a response to the cue. In this paradigm, the sparsely reconstructed images showed the lowest agreement with subject-matched fMRI, emphasizing that grid density is a particularly important consideration for localization of multiple, spatially distributed cortical activations.

Other imaging paradigms, such as resting-state functional connectivity also measure spatially distributed brain activity, but in the absence of task performance, to assess patterns of correlated brain hemodynamics. These patterns of correlated hemodynamics reflect coactivation patterns between regions, revealing functionally related networks of brain regions. Prior work with fNIRS has used functional connectivity techniques to image a subset of these functional networks (e.g. somatomotor and sensory systems) (Lu et al., 2010; H. Zhang et al., 2010), generally limited by the fNIRS instrument's field-of-view. Work with HD-DOT demonstrates that a broader cortical field-of-view paired with higher lateral resolution enables sampling of a greater number of cortical systems. Further, regional changes in connectivity associated with crossing borders between regions are detectable using both fMRI and HD-DOT (Cohen et al., 2008; Eggebrecht et al., 2014). In contrast, simultaneous fNIRS and fMRI assessments functional connectivity focused on two functional systems and assessed both modalities' sensitivity to patterns of bilateral homotopic connectivity (Duan, Zhang, & Zhu, 2012), underscoring the need for higher resolution and larger fields-of-view to assess more complex network structure. Consequently, the relationship between optical measurement

density and sensitivity to spatially distributed patterns of functional connectivity is an important future direction for future grid density assessments.

Due to the reduced channel count, sparse arrays that use fiber optics are more lightweight and wearable than their fiber-based dense counterparts. However, the tradeoff between wearability and spatial resolution is being mitigated by advances in optical neuroimaging technology that either use novel detection methods to enable use of lighter weight fiber bundles, or eliminate fiber optics altogether (Bergonzi et al., 2018; Chitnis et al., 2016). Consequently, future optical neuroimaging instrumentation may not be as susceptible to the tradeoff between portability/wearability and image quality and may more readily achieve the fMRI-quality spatial localization afforded by dense measurement arrays. The potential for highly portable and wearable instruments that do not sacrifice fMRI-comparable localization capability represents a critical advancement in optical neuroimaging technology, enabling researchers to fully leverage the potential advantages of optical neuroimaging, including imaging of complex behaviors in naturalistic environments or high-resolution longitudinal monitoring of clinical populations.

2.6 References

Bergonzi, K. M., Burns-Yocum, T. M., Bumstead, J. R., Buckley, E. M., Mannion, P. C., Tracy, C. H., … Culver, J. P. (2018). Lightweight sCMOS-based high-density diffuse optical tomography. *Neurophotonics*, *5*(3), 035006. https://doi.org/10.1117/1.NPh.5.3.035006

Bluestone, A., Abdoulaev, G., Schmitz, C., Barbour, R., & Hielscher, A. (2001). Three-dimensional optical tomography of hemodynamics in the human head. *Optics Express*, *9*(6), 272–286.

Boas, D. A., Gaudette, T., Strangman, G., Cheng, X., Marota, J. J., & Mandeville, J. B. (2001). The accuracy of near infrared spectroscopy and imaging during focal changes in cerebral hemodynamics. *NeuroImage*, *13*(1), 76–90. https://doi.org/10.1006/nimg.2000.0674

Brainard, D. H. (1997). The Psychophysics Toolbox. *Spatial Vision*, *10*(4), 433–436.

Brigadoi, S., Salvagnin, D., Fischetti, M., & Cooper, R. J. (2018). Array Designer: automated optimized array design for functional near-infrared spectroscopy. *Neurophotonics*, *5*(3), 035010. https://doi.org/10.1117/1.NPh.5.3.035010

Bumstead, J. R., Bauer, A. Q., Wright, P. W., & Culver, J. P. (2017). Cerebral functional connectivity and Mayer waves in mice: Phenomena and separability. *Journal of Cerebral Blood Flow & Metabolism*, *37*(2), 471–484. https://doi.org/10.1177/0271678X16629977

Chitnis, D., Cooper, R. J., Dempsey, L., Powell, S., Quaggia, S., Highton, D., … Everdell, N. L. (2016). Functional imaging of the human brain using a modular, fibre-less, high-density diffuse optical tomography system. *Biomedical Optics Express*, *7*(10), 4275–4288. https://doi.org/10.1364/BOE.7.004275

Cohen, A. L., Fair, D. A., Dosenbach, N. U. F., Miezin, F. M., Dierker, D., Van Essen, D. C., … Petersen, S. E. (2008). Defining functional areas in individual human brains using resting functional connectivity MRI. *NeuroImage*, *41*(1), 45–57. https://doi.org/10.1016/j.neuroimage.2008.01.066

Cui, X., Bray, S., Bryant, D. M., Glover, G. H., & Reiss, A. L. (2011). A quantitative comparison of NIRS and fMRI across multiple cognitive tasks. *NeuroImage*, *54*(4), 2808–2821. https://doi.org/10.1016/j.neuroimage.2010.10.069

Davidson, M. C., Thomas, K. M., & Casey, B. J. (2003). Imaging the developing brain with fMRI. *Mental Retardation and Developmental Disabilities Research Reviews*, *9*(3), 161–167. https://doi.org/10.1002/mrdd.10076

Dehghani, H., Eames, M. E., Yalavarthy, P. K., Davis, S. C., Srinivasan, S., Carpenter, C. M., … Paulsen, K. D. (2008). Near infrared optical tomography using NIRFAST: Algorithm for numerical model and image reconstruction. *Communications in Numerical Methods in Engineering*, *25*(6), 711–732. https://doi.org/10.1002/cnm.1162

Dehghani, H., White, B. R., Zeff, B. W., Tizzard, A., & Culver, J. P. (2009). Depth sensitivity and image reconstruction analysis of dense imaging arrays for mapping brain function with diffuse optical tomography. *Applied Optics*, *48*(10), D137–D143. https://doi.org/10.1364/AO.48.00D137

Diamond, S. G., Huppert, T. J., Kolehmainen, V., Franceschini, M. A., Kaipio, J. P., Arridge, S. R., & Boas, D. A. (2005). Physiological system identification with the Kalman filter in diffuse optical tomography. *Medical Image Computing and Computer-Assisted Intervention: MICCAI ... International Conference on Medical Image Computing and Computer-Assisted Intervention*, *8*(Pt 2), 649–656.

Duan, L., Zhang, Y.-J., & Zhu, C.-Z. (2012). Quantitative comparison of resting-state functional connectivity derived from fNIRS and fMRI: A simultaneous recording study. *NeuroImage*, *60*(4), 2008–2018. https://doi.org/10.1016/j.neuroimage.2012.02.014

Eggebrecht, A. T., Ferradal, S. L., Robichaux-Viehoever, A., Hassanpour, M. S., Dehghani, H., Snyder, A. Z., … Culver, J. P. (2014). Mapping distributed brain function and networks with diffuse optical tomography. *Nature Photonics*, *8*(6), 448–454. https://doi.org/10.1038/nphoton.2014.107

Eggebrecht, A. T., Muccigrosso, D., & Culver, J. P. (2019). NeuroDOT: an extensible Matlab toolbox for streamlined optical brain mapping (Conference Presentation). *Optical*

Tomography and Spectroscopy of Tissue XIII, *10874*, 108741F. https://doi.org/10.1117/12.2510526

Eggebrecht, A. T., White, B. R., Ferradal, S. L., Chen, C., Zhan, Y., Snyder, A. Z., … Culver, J. P. (2012). A quantitative spatial comparison of high-density diffuse optical tomography and fMRI cortical mapping. *NeuroImage*, *61*(4), 1120–1128. https://doi.org/10.1016/j.neuroimage.2012.01.124

Ferradal, S. L., Liao, S. M., Eggebrecht, A. T., Shimony, J. S., Inder, T. E., Culver, J. P., & Smyser, C. D. (2016). Functional Imaging of the Developing Brain at the Bedside Using Diffuse Optical Tomography. *Cerebral Cortex*, *26*(4), 1558–1568. https://doi.org/10.1093/cercor/bhu320

Gregg, N. M., White, B. R., Zeff, B. W., Berger, A. J., & Culver, J. P. (2010). Brain specificity of diffuse optical imaging: improvements from superficial signal regression and tomography. *Frontiers in Neuroenergetics*, *2*. https://doi.org/10.3389/fnene.2010.00014

Habermehl, C., Holtze, S., Steinbrink, J., Koch, S. P., Obrig, H., Mehnert, J., & Schmitz, C. H. (2012a). Somatosensory activation of two fingers can be discriminated with ultrahigh-density diffuse optical tomography. *Neuroimage*, *59*(4), 3201–3211. https://doi.org/10.1016/j.neuroimage.2011.11.062

Habermehl, C., Holtze, S., Steinbrink, J., Koch, S. P., Obrig, H., Mehnert, J., & Schmitz, C. H. (2012b). Somatosensory activation of two fingers can be discriminated with ultrahigh-density diffuse optical tomography. *Neuroimage*, *59*(4), 3201–3211. https://doi.org/10.1016/j.neuroimage.2011.11.062

Habermehl, C., Steinbrink, J., Müller, K.-R., & Haufe, S. (2014). Optimizing the regularization for image reconstruction of cerebral diffuse optical tomography. *Journal of Biomedical Optics*, *19*(9), 96006. https://doi.org/10.1117/1.JBO.19.9.096006

Hassanpour, M. S., Eggebrecht, A. T., Culver, J. P., & Peelle, J. E. (2015). Mapping cortical responses to speech using high-density diffuse optical tomography. *NeuroImage*, *117*, 319–326. https://doi.org/10.1016/j.neuroimage.2015.05.058

Hassanpour, M. S., Eggebrecht, A. T., Peelle, J. E., & Culver, J. P. (2017). Mapping effective connectivity within cortical networks with diffuse optical tomography. *Neurophotonics*, *4*(4), 041402. https://doi.org/10.1117/1.NPh.4.4.041402

Hirsch, J., Zhang, X., Noah, J. A., & Ono, Y. (2017). Frontal temporal and parietal systems synchronize within and across brains during live eye-to-eye contact. *NeuroImage*, *157*, 314–330. https://doi.org/10.1016/j.neuroimage.2017.06.018

Huppert, T. J., Diamond, S. G., Franceschini, M. A., & Boas, D. A. (2009). HomER: a review of time-series analysis methods for near-infrared spectroscopy of the brain. *Applied Optics*, *48*(10), D280-298.

Koch, S. P., Habermehl, C., Mehnert, J., Schmitz, C. H., Holtze, S., Villringer, A., … Obrig, H. (2010). High-resolution optical functional mapping of the human somatosensory cortex. *Frontiers in Neuroenergetics*, *2*, 12. https://doi.org/10.3389/fnene.2010.00012

Lee, C. W., Cooper, R. J., & Austin, T. (2017). Diffuse optical tomography to investigate the newborn brain. *Pediatric Research*, *82*(3), 376–386. https://doi.org/10.1038/pr.2017.107

Liu, Y., Piazza, E. A., Simony, E., Shewokis, P. A., Onaral, B., Hasson, U., & Ayaz, H. (2017). Measuring speaker–listener neural coupling with functional near infrared spectroscopy. *Scientific Reports*, *7*, 43293. https://doi.org/10.1038/srep43293

Lloyd-Fox, S., Blasi, A., & Elwell, C. E. (2010). Illuminating the developing brain: the past, present and future of functional near infrared spectroscopy. *Neuroscience and Biobehavioral Reviews*, *34*(3), 269–284. https://doi.org/10.1016/j.neubiorev.2009.07.008

Lu, C.-M., Zhang, Y.-J., Biswal, B. B., Zang, Y.-F., Peng, D.-L., & Zhu, C.-Z. (2010). Use of fNIRS to assess resting state functional connectivity. *Journal of Neuroscience Methods*, *186*(2), 242–249. https://doi.org/10.1016/j.jneumeth.2009.11.010

Miyai, I., Tanabe, H. C., Sase, I., Eda, H., Oda, I., Konishi, I., … Kubota, K. (2001). Cortical Mapping of Gait in Humans: A Near-Infrared Spectroscopic Topography Study. *NeuroImage*, *14*(5), 1186–1192. https://doi.org/10.1006/nimg.2001.0905

Muccigrosso, D., & Eggebrecht, A. (2018). NeuroDOT: A New Neuroimaging Toolbox for DOT. *Biophotonics Congress: Biomedical Optics Congress 2018 (Microscopy/Translational/Brain/OTS) (2018), Paper OW4C.7*, OW4C.7. https://doi.org/10.1364/OTS.2018.OW4C.7

Murkin, J. M., & Arango, M. (2009). Near-infrared spectroscopy as an index of brain and tissue oxygenation. *British Journal of Anaesthesia*, *103 Suppl 1*, i3-13. https://doi.org/10.1093/bja/aep299

Noah, J. A., Ono, Y., Nomoto, Y., Shimada, S., Tachibana, A., Zhang, X., … Hirsch, J. (2015). fMRI Validation of fNIRS Measurements During a Naturalistic Task. *Journal of Visualized Experiments : JoVE*, (100). https://doi.org/10.3791/52116

Ono, Y., Noah, J. A., Zhang, X., Nomoto, Y., Suzuki, T., Shimada, S., … Hirsch, J. (2015). Motor learning and modulation of prefrontal cortex: an fNIRS assessment. *Journal of Neural Engineering*, *12*(6), 066004. https://doi.org/10.1088/1741-2560/12/6/066004

Petersen, S. E., Fox, P. T., Posner, M. I., Mintun, M., & Raichle, M. E. (1989). Positron Emission Tomographic Studies of the Processing of Singe Words. *Journal of Cognitive Neuroscience*, *1*(2), 153–170. https://doi.org/10.1162/jocn.1989.1.2.153

Pfeifer, M. D., Scholkmann, F., & Labruyère, R. (2017). Signal Processing in Functional Near-Infrared Spectroscopy (fNIRS): Methodological Differences Lead to Different Statistical Results. *Frontiers in Human Neuroscience*, *11*, 641. https://doi.org/10.3389/fnhum.2017.00641

Pinti, P., Tachtsidis, I., Hamilton, A., Hirsch, J., Aichelburg, C., Gilbert, S., & Burgess, P. W. (n.d.). The present and future use of functional near-infrared spectroscopy (fNIRS) for cognitive neuroscience. *Annals of the New York Academy of Sciences*, *0*(0). https://doi.org/10.1111/nyas.13948

Piper, S. K., Krueger, A., Koch, S. P., Mehnert, J., Habermehl, C., Steinbrink, J., … Schmitz, C. H. (2014). A wearable multi-channel fNIRS system for brain imaging in freely moving subjects. *NeuroImage*, *85 Pt 1*, 64–71. https://doi.org/10.1016/j.neuroimage.2013.06.062

Power, J. D., Cohen, A. L., Nelson, S. M., Wig, G. S., Barnes, K. A., Church, J. A., … Petersen, S. E. (2011). Functional network organization of the human brain. *Neuron*, *72*(4), 665–678. https://doi.org/10.1016/j.neuron.2011.09.006

Saager, R. B., & Berger, A. J. (2005). Direct characterization and removal of interfering absorption trends in two-layer turbid media. *Journal of the Optical Society of America. A, Optics, Image Science, and Vision*, *22*(9), 1874–1882.

Suzuki, M., Miyai, I., Ono, T., & Kubota, K. (2008). Activities in the frontal cortex and gait performance are modulated by preparation. An fNIRS study. *NeuroImage*, *39*(2), 600–607. https://doi.org/10.1016/j.neuroimage.2007.08.044

Tian, F., Alexandrakis, G., & Liu, H. (2009). Optimization of probe geometry for diffuse optical brain imaging based on measurement density and distribution. *Applied Optics*, *48*(13), 2496–2504. https://doi.org/10.1364/AO.48.002496

White, B. R., & Culver, J. P. (2010). Quantitative evaluation of high-density diffuse optical tomography: in vivo resolution and mapping performance. *Journal of Biomedical Optics*, *15*(2), 026006. https://doi.org/10.1117/1.3368999

Yamamoto, T., Maki, A., Kadoya, T., Tanikawa, Y., Yamada, Y., Okada, E., & Koizumi, H. (2002). Arranging optical fibres for the spatial resolution improvement of topographical images. *Physics in Medicine and Biology*, *47*(18), 3429–3440. https://doi.org/10.1088/0031-9155/47/18/311

Yeo, B. T. T., Krienen, F. M., Sepulcre, J., Sabuncu, M. R., Lashkari, D., Hollinshead, M., … Buckner, R. L. (2011). The organization of the human cerebral cortex estimated by intrinsic functional connectivity. *Journal of Neurophysiology*, *106*(3), 1125–1165. https://doi.org/10.1152/jn.00338.2011

Zeff, B. W., White, B. R., Dehghani, H., Schlaggar, B. L., & Culver, J. P. (2007). Retinotopic mapping of adult human visual cortex with high-density diffuse optical tomography. *Proceedings of the National Academy of Sciences of the United States of America*, *104*(29), 12169–12174. https://doi.org/10.1073/pnas.0611266104

Zhang, D., & Raichle, M. E. (2010). Disease and the brain's dark energy. *Nature Reviews. Neurology*, *6*(1), 15–28. https://doi.org/10.1038/nrneurol.2009.198

Zhang, H., Zhang, Y.-J., Lu, C.-M., Ma, S.-Y., Zang, Y.-F., & Zhu, C.-Z. (2010). Functional connectivity as revealed by independent component analysis of resting-state fNIRS measurements. *NeuroImage*, *51*(3), 1150–1161. https://doi.org/10.1016/j.neuroimage.2010.02.080

Chapter 3: Portable, field-based neuroimaging using high-density diffuse optical tomography

This chapter is being submitted for publication as an invited journal article. The citation will be:

Fishell, A.K., Claudia P. Valdés, Tracy M. Burns-Yocum, Arefeh Sherafati, Edward J. Richter, Margarita Torres, Adam T. Eggebrecht, Christopher D. Smyser, Ana María Arbeláez, Joseph P. Culver. "Portable, field-based neuroimaging using high-density diffuse optical tomography." NeuroImage (2019).

3.1 Abstract

Behavioral and cognitive tests in children with malnutrition have revealed malnutrition-related deficits that persist throughout the lifespan, but long-term effects of malnutrition have not been extensively examined. These findings have motivated recent neuroimaging investigations, which use highly portable functional near-infrared spectroscopy (fNIRS) instruments to meet the demands of brain imaging experiments in low-resource environments and enable longitudinal investigations of brain function in the context of long-term malnutrition. However, the limited cortical field-of-view and image quality limitations associated with fNIRS instruments necessitate higher-resolution imaging tools that preserve portability, wearability, and ergonomics. In this work, we introduce high-density diffuse optical tomography (HD-DOT), an optical neuroimaging modality that produces fMRI-comparable images of brain function, in a field setting. Our results evaluate the performance of a custom HD-DOT instrument for assessing brain function in a cohort of malnourished children in Cali, Colombia. In addition to demonstrating portability and wearability, we show the HD-DOT instrument's sensitivity to distributed brain responses using a sensory processing task and measurement of homotopic

functional connectivity. Task-evoked responses to the passive word listening task produce activations localized to bilateral superior temporal gyrus, resembling previously published work using this paradigm. Evaluating this localization performance across sparse and dense reconstruction schemes indicates that greater localization consistency is associated with a dense array of overlapping measurements. These results set the stage for additional avenues of investigation, including identifying and characterizing a child's individual malnutrition burden and eventually contributing to intervention development.

3.2 Introduction

Despite increased efforts focused upon reducing the prevalence of childhood malnutrition and the high mortality rates associated with this condition, the deleterious effect of malnutrition on brain development is a pressing global health concern (Chugani, Phelps, & Mazziotta, 1987; Goyal, Hawrylycz, Miller, Snyder, & Raichle, 2014; Kuzawa et al., 2014; Thompson & Nelson, 2001). During the first decade of life, the human brain has exceptional nutritional and metabolic requirements as the brain undergoes critical structural and functional changes, including neuronal development, synaptogenesis, and synaptic remodeling (Goyal & Raichle, 2013; Murthy & Desiraju, 1991; Thompson & Nelson, 2001; Wiggins, 1982). Thus, if nutrients are scarce and energetic demands are unmet during this critical period, trajectories of brain development can be irreversibly compromised, leading to life-altering deficits (Black et al., 2019; S. Grantham-McGregor et al., 2007; Liu, Raine, Venables, Dalais, & Mednick, 2003).

Correlational studies of weight gain during early childhood show that weight gain during the first two years of life is related to subsequent performance in school (Martorell, 1999; Martorell et al., 2010). Additional studies show a relationship between malnutrition status and attainment of WHO-established motor milestones, social behaviors, and linguistic abilities (Barrett, Radke-Yarrow, & Klein, 1982; Iannotti et al., 2016). Interventional studies have directly assessed the effect of various therapeutic feeding regimens and supplements on subsequent neurodevelopmental outcomes, establishing a causal link between childhood malnutrition and brain development (Cusick & Georgieff, 2012; S. M. Grantham-McGregor, Powell, Walker, & Himes, 1991; McKay, Sinisterra, McKay, Gomez, & Lloreda, 1978). If malnutrition is unaddressed during childhood, the long-term sequelae of malnutrition include cognitive, behavioral, and social deficits throughout the lifespan (Liu et al., 2003; Prado & Dewey, 2014). In turn, these lifelong consequences impact social and economic development on a national scale (Hoddinott, Maluccio, Behrman, Flores, & Martorell, 2008).

Malnutrition-related deficits revealed using behavioral assessments raise additional questions about the neurological changes underlying behavioral differences between typically developing and malnourished children (Nelson, 2015; Raizada & Kishiyama, 2010). Assessing compromised brain development in regions where malnutrition is highly prevalent requires careful selection of methods that are both sensitive to a child's malnutrition burden and practical to implement in low-resource settings. Widely used neuroimaging modalities, such as magnetic resonance imaging (MRI), can elucidate typical and atypical developmental trajectories, but are often poorly

suited for global neuroimaging contexts due to the limited portability, need for specialized facilities, and high cost associated with these methods (Estep et al., 2014; Greene et al., 2016; JL, n.d.; Smyser et al., 2010; Smyser, Snyder, & Neil, 2011; Smyser et al., 2013). To address the need for neuroimaging studies in these environments, researchers have turned to more portable optical neuroimaging instrumentation. These highly portable tools, including electroencephalography (EEG) (Jensen et al., 2019), functional near-infrared spectroscopy (fNIRS) (Lloyd-Fox et al., 2019; Lloyd-Fox et al., 2016, 2014), and diffuse correlation spectroscopy (DCS) (Roberts et al., 2017), effectively create mobile neuroimaging laboratories that can be deployed virtually anywhere, eliminating practical constraints imposed by costly and immobile neuroimaging facilities.

These neuroimaging methods have begun to address the urgent need for portable and inexpensive tools for assessing brain function in low-resource settings. In addition to establishing these methods in new regions where neuroimaging research may be unfamiliar, investigators using these highly portable techniques must also achieve results demonstrating high-quality data and risk sensitivity in the population(s) of interest. To date, research based in The Gambia, Guinea-Bissau, and Bangladesh supports the feasibility for using these tools to perform field-based brain imaging experiments, and some recent results show altered cortical physiology related to early adversity and malnutrition (Jensen et al., 2019; Lloyd-Fox et al., 2016; Roberts et al., 2017). However, one significant challenge associated with these methods is the tradeoff between cortical field-of-view and portability, as increasing an instrument's cortical coverage generally increases the physical size of the instrument.

High-density diffuse optical tomography (HD-DOT) is an optical neuroimaging modality that, like fNIRS, uses near-infrared light to measure tissue oxygenation, resulting in an indirect measure of neuronal activity analogous to the blood oxygen level dependent (BOLD) signal obtained with fMRI. However, unlike fNIRS, HD-DOT utilizes a densely overlapping measurement array, which produces depth resolved images of cortical hemodynamics with point-spread functions comparable to fMRI (Eggebrecht et al., 2014, 2012). With a broad cortical field-of-view, HD-DOT enables measurement of spatially distributed brain function, eliminating the need to configure source/detector arrays for *a priori* cortical regions of interest. While HD-DOT has successfully mapped distributed brain function using both task-evoked responses and resting-state functional connectivity in healthy adults, adults with Parkinson's, and neonates in the intensive care unit, HD-DOT has not yet been established as an imaging modality suitable for applications demanding highly portable instruments, such as on-site studies of childhood malnutrition (Eggebrecht et al., 2014; Ferradal et al., 2016; White & Culver, 2010a, 2010b).

The goal of this work is to evaluate the performance of a field-optimized HD-DOT system. We used both task-evoked responses and functional connectivity measures to demonstrate feasibility of imaging chronically malnourished children recruited as part of a larger study investigating the effects of malnutrition on brain development and cognition in Cali, Colombia. Task-evoked responses to a passive auditory processing task were used to evaluate response localization performance and data quality in this novel cohort. Assessment of homotopic functional connectivity was used to evaluate sensitivity to distributed brain function, setting the stage for future assessments of malnutrition burden

across multiple cortical systems, using this powerfully predictive imaging paradigm (Wheelock et al., 2018). Our results demonstrate that a high channel count can be preserved in a portable, field-ready optical neuroimaging system and can confer the image quality and localization improvements associated with tomographically reconstructed images of brain function in a non-laboratory setting.

3.3 Methods

3.3.1 Participants

Participants in this experiment were recruited from the urban and peri-urban regions surrounding Cali, Colombia. Families were primarily recruited from community health and educational programs established by the Cali Department of Health, the Malnutrition Rehabilitation Program for the municipality, and some school lunch programs. In accordance with experimental protocols approved by the Human Research Protection Offices at Washington University and the Centro Medico Imbanaco Ethics Committee, caregivers gave written consent and participants gave verbal assent to participate in the study. All participants had normal physical examinations and were not acutely ill at the time of study. No participants had a personal history of premature birth, diabetes, chronic disease, psychiatric, or neurological conditions. In total, a cohort of 30 participants completed the HD-DOT experiments. After completing the HD-DOT experiments, participants were excluded primarily due to poor cap fit and/or excessive motion (N=13), leaving a total of 17 participants (Mean age = 8.4 years; 9 females, 8 males) included in the subsequent analyses (Table 3.1).

N	17		
Sex	8 male; 9 female		
	Mean	**SD**	**Range**
Age (years)	8.4	0.9	7 – 10
Head Circumference (cm)	51.4	1.7	49 – 54.4
Height (cm)	128	6.0	118.5 - 140
Weight (kg)	24.2	4.7	18.2 – 33
Height-for-Age (WHO Z-Score)	-0.5	1.1	-2.44 – 1.31
Weight-for-Age (WHO Z-Score)	-0.9	1.2	-3.64 – 0.95

Table 3.1. Demographic information. Demographic information for participants included in HD-DOT analyses.

3.3.2 Experimental procedures and stimuli

Participants underwent an HD-DOT cap fit procedure lasting approximately 5-10 minutes. Cap fit was optimized for a given participant using real-time displays of measurement light level, optode signal-to-noise, and optode-scalp coupling coefficients. This procedure ensured that the greatest possible number of measurements would be retained for subsequent analysis. Following cap fit, participants completed two experimental paradigms: passive word listening and passive movie viewing. Participants alternated between the two paradigms until three repetitions of each paradigm were acquired or the experimenter judged that the participant began to move excessively or became too fatigued to continue with the experiment. All stimuli were presented using a liquid crystal display monitor positioned at eye-level in front of the seated participant, as well as a speaker positioned in front of the participant.

3.3.2a Passive word listening

Following previously published procedures (Eggebrecht et al., 2014), during the passive word listening task, participants listened to lists of spoken Spanish concrete nouns in a

block design. Words were presented at a rate of 1 word/second for 15 seconds, followed by 15 seconds of silence. During a single 3-minute run, participants listened to 6 blocks of words (90 words in total). The passive word listening task was chosen because it has been previously published with both fMRI and HD-DOT (Eggebrecht et al., 2014), producing reliable activations to a sensory stimulus. Further, this task was not hypothesized to show any malnutrition-related effects, underscoring that this task was intended to generate activation maps consistent with previous studies (Eggebrecht et al., 2014), enabling assessment of data quality, image reconstruction procedures, instrument performance, and localization capabilities.

3.3.2b Passive movie viewing

During a passive movie viewing run, participants were instructed to sit still and quietly watch an unedited, continuous 10-minute segment from *Buscando a Nemo* (*Finding Nemo*). Participants viewed one of two clips, lasting from either (00:45-10:45) or (10:45-20:45). The passive movie viewing task was chosen because it enabled acquisition of a continuous, 10-minute measurement of brain activity, permitting subsequent analysis of functional connectivity, which can be related to subsequent outcomes in pediatric populations (Wheelock et al., 2018). Critically, in pediatric populations, functional connectivity measured during periods of quiet fixation resulted in greater head movement relative to functional connectivity assessed during movie viewing (Greene et al., 2018; Vanderwal, Kelly, Eilbott, Mayes, & Castellanos, 2015). Therefore, passive movie viewing was chosen in order to maximize the number of usable functional connectivity datasets.

3.3.3 High-density diffuse optical tomography instrumentation

3.3.3a Design specifications

The HD-DOT instrument built for field use in these experiments (Figure 3.1) followed design specifications for previously published HD-DOT instruments (Eggebrecht et al., 2014, 2012), but was optimized to have a smaller footprint in a single self-contained console, in order to maximize portability and usability. The instrument used in this work was a custom-built continuous wave instrument, consisting of 48 LED sources illuminating the head at two wavelengths (λ = 750 nm and 850 nm), and 30 avalanche photodiodes (Hamamatsu C5460-01), coupled to the head using fiber-optic bundles (2.5-mm diameter bundles of 50 μm fibers).

The weight of the 78 fibers was managed using a custom-built, collapsible support made of extruded aluminum, ensuring that the participant's head did not bear any weight from the fibers. Fiber tips were positioned on the scalp using a custom-built neoprene imaging cap, which maintained an optode geometry such that first-through third-nearest neighbor separations were 13, 29, and 39 mm, respectively. Temporal, frequency, and spatial encoding of the source illumination pattern achieved an overall HD-DOT framerate of 10 Hz. As in other optical neuroimaging systems, a measurement consists of the light level between a single source-detector pair. The total number of first- through third-nearest neighbor measurements afforded by this array configuration was 324 measurements per wavelength (116 first nearest neighbor, 158 second nearest neighbor, 50 third nearest neighbor). These measurements were converted into volumetric, voxelated movies of brain hemodynamics using the image reconstruction procedures described in Section 3.3.4.

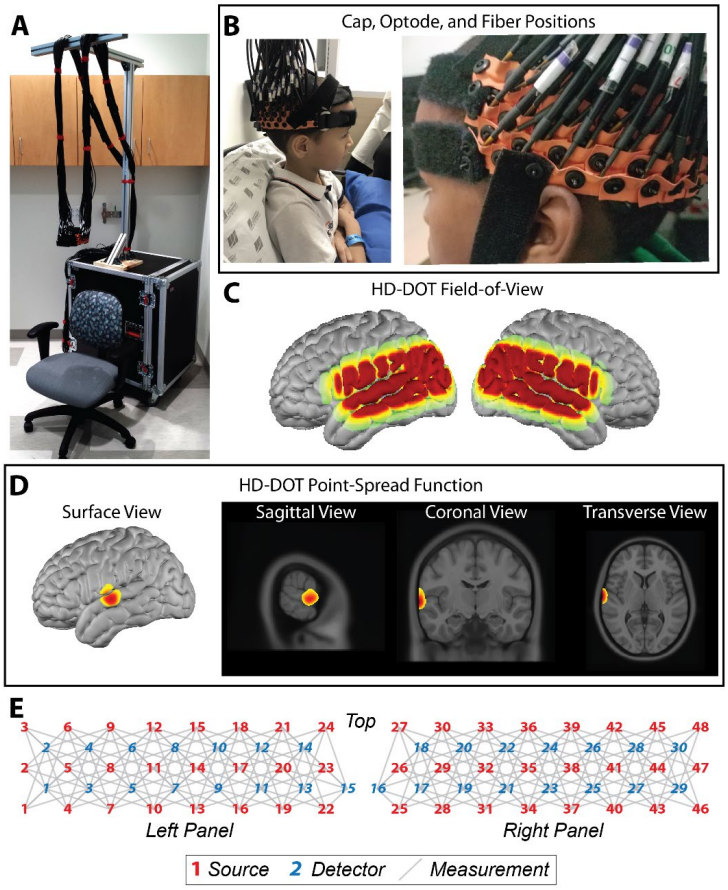

Figure 3.1. HD-DOT instrumentation. A: The HD-DOT instrument used in these experiments is a portable, self-contained instrument containing all opto-electronic equipment needed for the 30 detector by 48 source system. The instrument includes a removable fiber support system, ensuring that the participant's head bears no weight from the fibers, and the overall footprint for this system is 76×55 cm. **B:** HD-DOT cap position on two participants in Cali, Colombia. **C:** The field-of-view based on optode positions, projected on to the surface of the MNI atlas. **D:** Simulated point-spread function for the HD-DOT system, shown on the cortical surface and volumetric slices of the MNI atlas. **E:** Optode layout for both panels of the HD-DOT cap, including sources (red numbers), detectors (blue numbers), and first through third nearest-neighbor measurements (grey lines).

3.3.3b Instrument setup

Critical considerations for imaging instruments used in non-laboratory settings included factors such as portability, fast setup, and ease of use, which are not necessarily

considerations for fixed instruments that remain in laboratory environments. The large channel count on the field HD-DOT system used in this work necessitated a design that facilitated easy imaging by a variety of users. Consequently, the instrument was designed to be encased in a commercially available equipment cart (Gator G-TOUR16UCA-24D), which had a footprint of 76 x 55 cm. This design enabled the HD-DOT instrument to be easily transported and positioned at the imaging site at Centro Medico Imbanaco. Of note, the HD-DOT instrument was ready for imaging after 4 hours of setup on site and training new HD-DOT users was complete after 5 working days of guided imaging, highlighting the ease of use associated with this HD-DOT instrument.

3.3.4 Image reconstruction

3.3.4a Measurement pre-processing and anatomical light modeling

As previously published using existing HD-DOT systems, image reconstruction occurs in five steps: light-level measurement pre-processing, anatomical light modeling, image reconstruction, spectroscopy and spatial normalization (Eggebrecht et al., 2014, 2014). To begin, raw detector light levels were converted to a time-series of log-ratio data, using the mean of a given measurement as the baseline. An initial quality control step identified measurements with excessive noise by excluding any measurement with a temporal variance exceeding 7.5%, as this excessive variance was more likely to reflect nuisance variance (e.g. head motion) than it was to reflect variance related to cortical hemodynamics (Eggebrecht et al., 2014). Subsequently, the measurements that passed the variance threshold were then high-pass filtered (passive word listening cutoff: $f > 0.02$ Hz; passive movie viewing cutoff: $f > 0.009$ Hz). Next, nuisance signals resulting from

systemic or superficial (i.e. scalp and skull) physiology were approximated using the average of all first nearest neighbor measurements, which provided the most superficial penetration into the tissue. This superficial signal was regressed out of all measurements. Finally, the measurements were low-pass filtered (passive word listening cutoff: $f < 0.5$ Hz; passive movie viewing cutoff: $f < 0.08$ Hz).

Anatomical light modeling requires either a subject-specific segmented anatomical mesh or an atlas-based anatomy. In these experiments, an age appropriate atlas-based model was used, in order to eliminate the need for subject-specific anatomy obtained with costlier and frequently unavailable modalities such as MRI or CT. Using atlas-based forward modeling has been previously shown to result in reasonable individual and group-level localization errors on the order of millimeters (Ferradal, Eggebrecht, Hassanpour, Snyder, & Culver, 2014). A non-linear ICBM152 atlas from the Montreal Neurological Institute was for image reconstruction in this work. This atlas is segmented into five tissue compartments in order to account for the unique optical properties of each: skull, scalp, grey matter, white matter, and cerebrospinal fluid. Using this atlas anatomy combined with the positions of the 30 detector and 48 source optodes, a sensitivity matrix was generated using NIRFAST (Dehghani et al., 2008) for each wavelength. The sensitivity matrix was subsequently inverted using Tikhonov regularization, and spectroscopy was performed using literature-derived values (Bluestone, Abdoulaev, Schmitz, Barbour, & Hielscher, 2001).

The output of the image reconstruction procedure was volumetric time-series data, down-sampled from 10 Hz to 1 Hz for three hemoglobin contrasts: oxyhemoglobin

(ΔHbO_2), deoxyhemoglobin (ΔHbR) and total hemoglobin (ΔHbT). All analyses performed on these images utilize the oxyhemoglobin (ΔHbO_2) contrast, unless otherwise specified (e.g. see Appendix Figure 3.8 for results with ΔHbO_2, ΔHbR, and ΔHbT.)

3.3.4b Head motion quantification

To quantify the amount of head motion present during an imaging run, we leveraged the inherent covariance induced by head motion across optical measurements. The temporal variance across measurements was quantified using the Global Variance in the Temporal Derivative (GVTD) (Sherafati, Eggebrecht, Burns-Yocum, & Culver, 2017). For a given run, GVTD was computed over a matrix with *j* measurements and *i* timepoints, y_{ji}. The squared temporal derivative,

$$(y_{ji} - y_{j(i-1)})^2$$

was then computed. Finally, to generate a single timeseries quantifying GVTD over the course of the run, the root mean square was taken over the temporal derivative of all measurements, such that GVTD, *g*, for timepoint *i,* is expressed as,

$$g_i = \sum_{j=1}^{n} \frac{1}{n} \sqrt{(y_{ji} - y_{j(i-1)})^2}$$

This metric is analogous to the DVARS metric used to assess head motion in fMRI datasets (Smyser et al., 2010), and enables comparison of head motion related variance across data collected across sites, instruments, and cohorts as shown in Figure 3.7 (Appendix).

3.3.5 Image analysis

3.3.5a Passive word listening

The passive word listening task delivered auditory stimulation in a block design, with alternating blocks of stimulation (“On”) and no stimulation (“Off”). Consequently, the magnitude of the cortical response to the stimulus was calculated by comparing the voxel-wise responses during the On and Off conditions. During each 30-second block, the stimulus was on for 15 seconds, followed by 15 seconds of silence. All blocks from a single participant were then averaged to produce a single volumetric movie containing the block-averaged response to the stimulus. The difference between voxelwise responses during the On and Off conditions was estimated by averaging seconds 10-19 of the block (“On”) and contrasting that response to seconds 20-29 of the block (“Off”). A random effects t-statistic was computed across participants to assess the magnitude of the contrast between conditions.

3.3.5b Passive movie viewing

Oxyhemoglobin timeseries obtained during passive movie viewing were filtered to the functional connectivity band ($0.009 < f < 0.08$) in order to examine patterns of oxyhemoglobin fluctuation representing correlated, or functionally connected, brain regions (Vanderwal, Eilbott, & Castellanos, 2018). As in previous work using HD-DOT to measure functional connectivity, a seed-based approach was used to assess patterns of homotopic, or bilateral, connectivity (Ferradal et al., 2016). Seeds consisted of 12 spheres (radius 5 = mm) placed across the HD-DOT field-of-view. For each seed, the oxyhemoglobin signal was extracted by averaging the ΔHbO_2 signal for all voxels within the sphere, to generate a single time-series for the seed. This time-series was then cross-correlated with every other seed to produce a correlation matrix showing the functional

connectivity between pairs of seed regions. To assess functional connectivity between a single seed and all voxels within the field-of-view, a spatial map of Pearson product-moment correlations was generated by cross correlating the seed ΔHbO_2 timeseries with the voxelwise ΔHbO_2 timecourses from across the entire field-of-view. Individual correlation maps were then converted to a normally distributed statistic using the Fisher's z-transformation. Finally, group-average connectivity maps were generated by averaging individual z-transformed seed maps across all subjects.

3.3.6 Sparse array reconstruction and analysis

The HD-DOT measurement array results in a densely overlapping set of measurements, which produces depth-resolved images of brain function with a point-spread function comparable to images obtained with fMRI. However, sparser measurement arrays are often favored over dense arrays due to the reduced channel count, which results in a smaller instrument with fewer fibers affixed to the participant's head. We evaluated the effect of measurement density by reconstructing passive word listening data using a sparse array. A sparse array was constructed by selecting a subset of second nearest neighbor measurements from the larger set of HD-DOT measurements to achieve a measurement count comparable with other fNIRS systems used for global health applications (Lloyd-Fox et al., 2014). These sparse array measurements were selected to have the same lateral coverage as the HD-DOT array, but with no overlapping source-detector measurements. The resulting simulated sparse array consisted of 16 measurements per hemisphere, for a total of 32 measurements at a 29-millimeter separation.

Measurement processing, image reconstruction, and image analysis followed the same procedures outlined in Sections 3.3.4a and 3.3.5a, with one notable exception. Because the sparse measurement array did not contain any measurement pairs with a short source-detector separation, no superficial signal regression was performed. Without measurements with a short source-detector separation, the superficial nuisance signal cannot be approximated. Consequently, images reconstructed using the simulated sparse array do not include any superficial signal regression.

Spatial overlap maps were used to quantify the agreement between passive word listening activations reconstructed using the dense and sparse reconstruction schemes, leveraging the reliability of the activations produced by the passive word listening paradigm (see Figure 3.10, Appendix). To compute spatial overlap of activations across individual maps, each participant's dense and sparse block-averaged passive word listening maps were thresholded at 25% of the maximum voxel value for each map. Individual maps were then binarized such that any voxel meeting or surpassing the threshold was set to 1, and all remaining voxels were set to 0. The activation overlap was then computed by summing across individual activation maps for dense and sparse reconstructions separately.

To compute the spatial overlap between individual activation maps and the group-averaged activation map, individual maps were again thresholded and binarized as described above. The spatial overlap between the dense/sparse activation maps and the respective dense or sparse group-average map was computed by the conjunction between the two binarized images. Summing across individual conjunction images

resulted in a map showing the extent to which the dense and sparse reconstruction schemes produced individual passive word listening activations consistent with the group average response.

3.4 Results

3.4.1 Wearability and data quality

On average, participants completed approximately 26 minutes of imaging, including two repetitions of the passive word listening task (3-minute duration), and two repetitions of the passive movie viewing (10-minute duration). Combined with short breaks between imaging runs and 5-10 minutes for initial cap fit, participants in this study wore the HD-DOT cap for approximately 40 minutes per session, indicating the tolerability of HD-DOT imaging in this cohort of 7-9-year-old children with no prior experience participating in brain imaging experiments.

Scan duration provided an indicator for participant comfort and instrument ergonomics. In addition, we assessed measurement data quality using a battery of readouts generated during image reconstruction (Figure 3.2). These readouts ensure that only high-quality measurements are used in reconstruction, mitigating the deleterious effects of including measurements contaminated by poor optode-scalp coupling or head motion. As shown in Figure 3.2, HD-DOT measurements are of sufficient quality across the entire field-of-view, resulting in cortical coverage at three source-detector separations. Finally, signal-to-noise at the participant's pulse frequency (Figure 3.2, E) verified that

measurements were sensitive to vascular physiology. These rigorous quality control measurements ensure that the reconstructed images provided a high-fidelity readout of brain function.

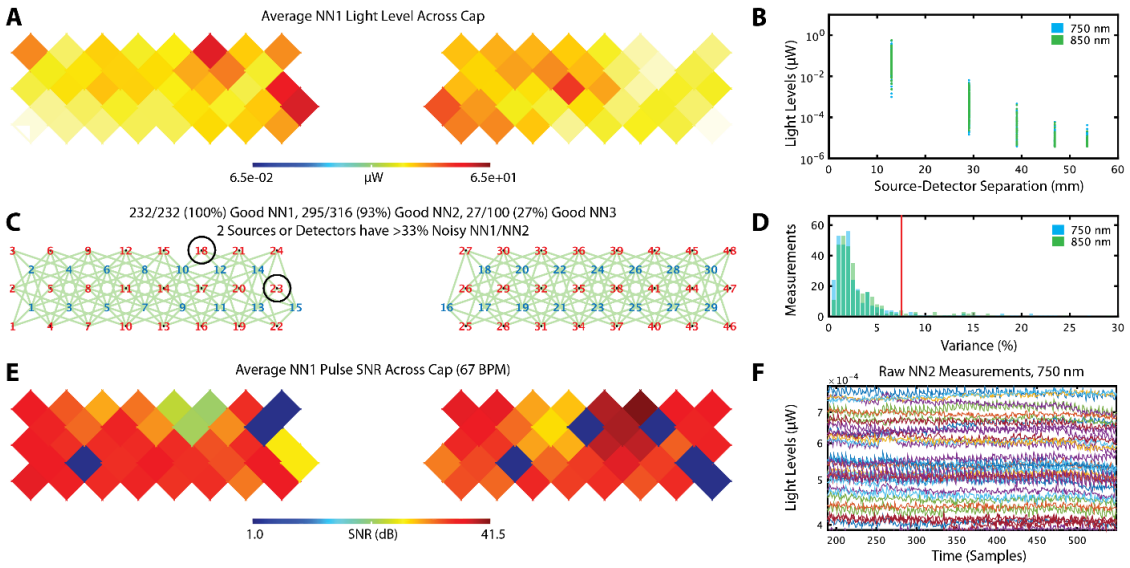

Figure 3.2. Data quality. The data quality report generated during image reconstruction indicates the measurement quality obtained during a single scan and includes multiple measurement quality assessments used to determine the usability of a scan in real-time. This report was generated from a representative subject during a passive word listening acquisition. **A:** The average light level for first nearest neighbor (NN1) measurements across the two panels of the HD-DOT cap indicated relatively strong light levels across the cap. **B:** A plot of light level as a function of source-detector separation (i.e. measurement distance) showed log-linear light falloff, as would be expected in biological tissue. **C:** The plot of measurement retention for this acquisition showed measurements retained for subsequent image reconstruction (green lines), as well as optodes where at least 33% of measurements were rejected (black circles). **D:** The histogram of measurement-wise temporal variance indicated that most measurements are below the temporal variance threshold (7.5%, red line) imposed on measurements to exclude measurements contaminated by movement or poor optode coupling. **E:** The signal-to-noise for first nearest-neighbor measurements showed, in general, strong signal-to-noise ratio at the participant's pulse frequency, indicating good sensitivity to vascular physiology needed to image cortical hemodynamics. **F:** A plot of individual second nearest-neighbor measurements showed sensitivity to the participant's pulse, and a lack of global variance across measurements that could be associated with global noise introduced by head motion.

Measurement retention as a function of source detector separation was relatively consistent across the cohort (Figure 3.6, Appendix), with an average of 94% of first nearest-neighbor measurements, 77% of second nearest-neighbor measurements, and 24% of third nearest-neighbor measurements retained per participant. Further, using GVTD, as described in Section 3.3.4b, to quantify head-motion induced variance in each dataset (Figure 3.7, Appendix) shows that data quality quantified using this metric is comparable to HD-DOT data quality across multiple sites, instruments, and age groups.

3.4.2 Task-evoked responses

Group-averaged oxyhemoglobin activation maps from the passive word listening paradigm are displayed in Figure 3.3. This group average map contains activation data from 17 individual participants, who in total completed 46 runs of the passive word listening task. The group average map (Figure 3.3, A) reveals elevated oxyhemoglobin concentration in bilateral superior temporal gyrus, the same cortical region activated by this task in prior work (Eggebrecht et al., 2014). Further, the time course of the hemodynamic response (Figure 3.3, B) shows the expected elevation in oxyhemoglobin concentration, including a brief hemodynamic lag (approximately 4 seconds) between stimulus onset and hemodynamic response onset.

We used a t-statistic to contrast the voxelwise brain responses between the stimulus On/Off conditions to assess the contrast-to-noise achieved in this paradigm (Figure 3.3, F-G). Further, inspection of single-subject maps (Figure 3.9, Appendix) that

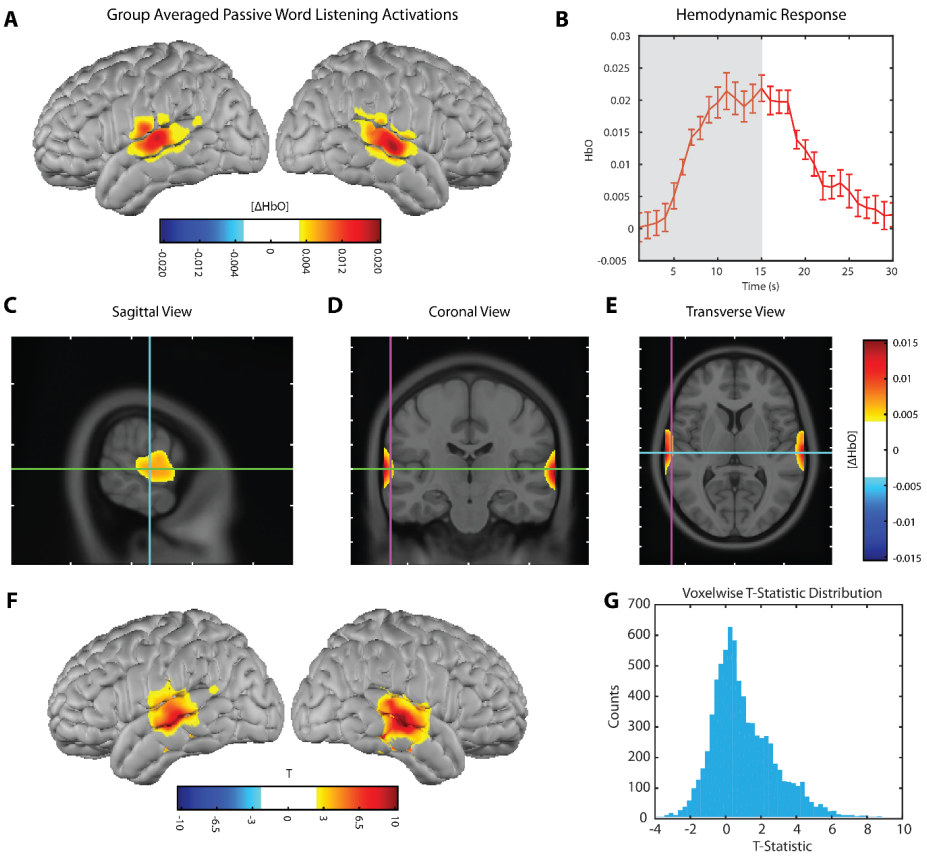

Figure 3.3. Passive word listening activations. A: Block averaged oxy-hemoglobin activations associated with the passive word listening task averaged across the entire cohort of participants. Activation locations were in agreement with previously published HD-DOT results using this task, showing bilateral activations on superior temporal gyrus. **B:** The block averaged oxy-hemoglobin time course extracted from left superior temporal gyrus showed a stimulus-related activation. The shaded area represents the stimulation epoch, in which participants listened to concrete Spanish nouns at a rate of 1 word/second. Error bars are S.E.M. across participants. **C:** A volumetric map of the oxyhemoglobin activation shows depth-resolved images of the surface projection shown in **Panel A**. Crosshairs indicate the location of the voxel used to plot the timecourse displayed in **Panel B**. **F:** Random effects T map showing the contrast between "On" and "Off" stimulation periods. **G:** Voxelwise distribution of T-statistics shown in **Panel F**.

comprise the group average indicated that the topography of the activation--bilateral responses centered on the superior temporal gyrus--was observable from a single run of the passive word listening task (i.e. 3 minutes of data). Finally, repeating the block

average analysis with all three hemoglobin contrasts obtainable with the HD-DOT instrument, ΔHbO_2, ΔHbR, and ΔHbT, produced both convergent maps and activation timecourses (Figure 3.8, Appendix), further verifying image quality and spectroscopy performance via the ratios between the three contrasts (Zeff, White, Dehghani, Schlaggar, & Culver, 2007).

3.4.3 Task-evoked responses with sparse array reconstruction

To evaluate the effect of reconstructing images of brain activation with a sparse array, we reconstructed images of ΔHbO_2 during passive word listening with a subset of second nearest neighbor measurements from the full set of HD-DOT measurements. Measurements were selected such that they spanned a field-of-view comparable to the HD-DOT field-of-view, but with no overlapping measurements (Figure 3.4, A). A single subject's passive word listening responses for the sparse array (Figure 3.4, B-C) and dense array (Figure 3.4, E-F) revealed an effect of measurement density on the localization of the passive word listening response in the reconstructed images.

While the sparse reconstruction reveals a pattern of bilateral activations near the superior temporal gyrus, the shape and magnitude of these responses differed from the responses reconstructed using the dense measurement array. For example, comparing the right hemisphere activations between sparse and dense reconstructions revealed that measurement density affected the spatial extent and magnitude of the reconstructed oxyhemoglobin concentration change. Importantly, these images were produced with the same underlying data—the variance between sparse and dense reconstructions cannot

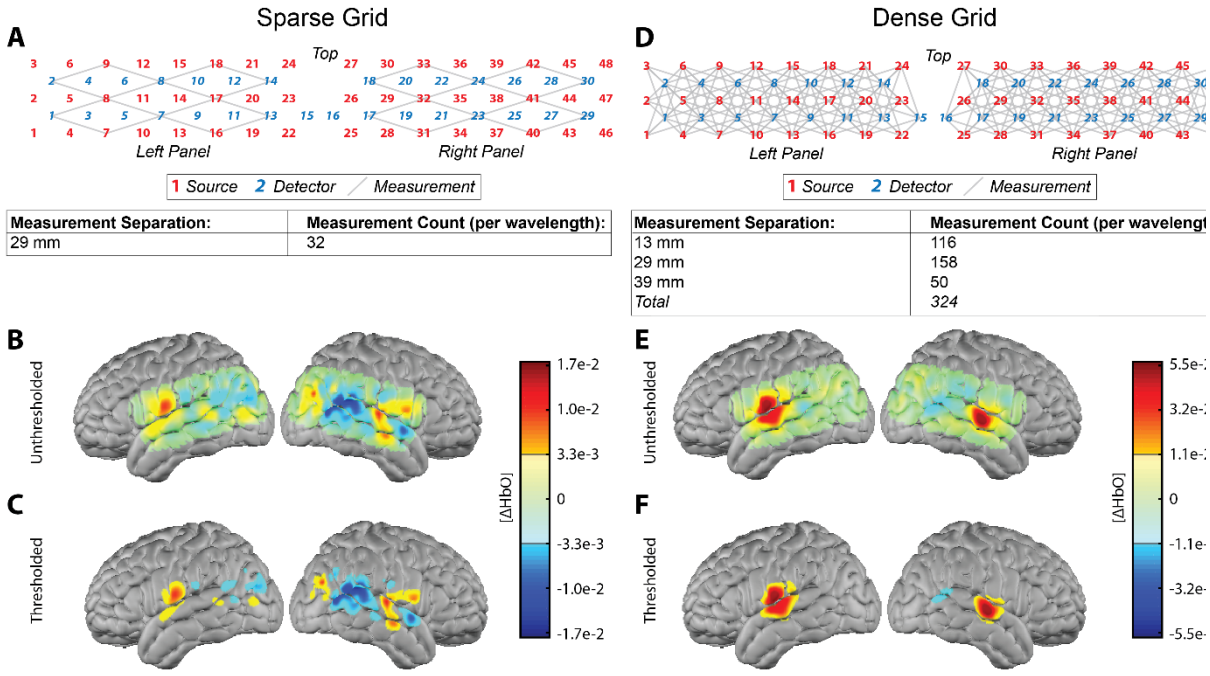

Figure 3.4. Sparse and dense image reconstruction. A: The sparse measurement grid used to reconstruct tomographic images of brain function using a measurement count more typical of field-based fNIRS instruments. Sources (red) and detectors (blue) show optode locations in the full HD-DOT optode array. The subset of HD-DOT measurements used to reconstruct sparse-measurement fNIRS images are indicated by grey lines. All 32 measurements were at a single source-detector separation of 29 mm. **B:** Unthresholded oxy-hemoglobin activations reconstructed using sparse measurements obtained during the passive word listening task. **C:** Thresholded image of data shown in **Panel B**. **D:** The full HD-DOT optode array includes 324 measurements at 3 source-detector separations, which were subsequently used for tomographic image reconstruction of the same data shown in **Panels B, C**. **E:** Unthresholded oxy-hemoglobin activations reconstructed using dense measurements obtained during the passive word listening task (i.e. the same data used for sparse reconstruction). **F:** Thresholded image of data shown in **Panel E**.

be attributed to variance driven by analyzing data derived from different cap fits, different imaging sessions, or different participants.

Across all participants, the dense reconstruction scheme resulted in more consistent localization of passive word listening activations across participants (Figure 3.10, Appendix). While both reconstruction schemes produced group-averaged bilateral

activations, greater spatial consistency was observed between individual activation maps reconstructed using a dense array of optical measurements. Further, individual maps reconstructed using the dense array showed greater overlap with the group-averaged activation map, further underscoring that an individual activation map reconstructed using a dense measurement array has a higher likelihood of consistently localizing the activation to the same region of superior temporal gyrus than maps reconstructed using a sparse measurement array.

3.4.4 Bilateral functional connectivity

We assessed bilateral, or homotopic, functional connectivity using a set of twelve seed regions (Figure 3.5, A) that spanned the HD-DOT field-of-view. The seed set included seeds in superior temporal gyrus (auditory), the middle temporal lobe, visual cortex, and the temporal-parietal junction (Figure 3.5, G). Seed positions were informed by prior functional connectivity analyses using HD-DOT and constrained by the present instrument's field-of-view (Ferradal et al., 2016). The correlation matrix between seed pairs (Figure 3.5, B) and individual voxelwise seed maps (Figure 3.5, C-F) display the z-transformed correlation value, representing the magnitude of the correlation between a pair of oxyhemoglobin timetraces.

Bilateral connectivity is quantified through the correlation coefficient between homotopic seed pairs and is evident through elevated off-diagonal correlations in the correlation matrix (Figure 3.5, B). Seed maps (Figure 3.5, C-F) show the spatial extent of bilateral connectivity for four seeds with the highest homotopic connectivity, with the highest correlation values present on the ipsilateral hemisphere, near the seed region.

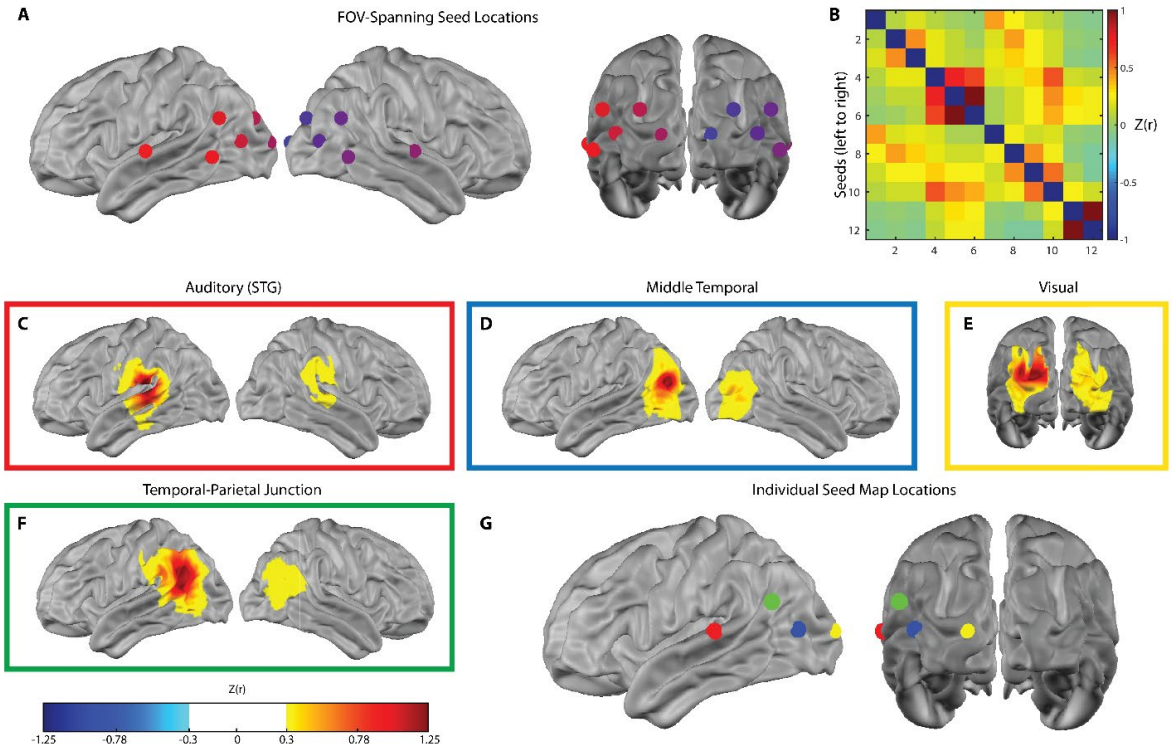

Figure 3.5. Homotopic functional connectivity. Homotopic functional connectivity was assessed using a seed-based approach. **A:** Location of the 12 seeds spanning the HD-DOT field-of-view used in the functional connectivity analysis. **B:** Correlation matrix displaying the Fisher z-transformed correlation magnitudes for pairwise seed correlations. **C-F:** Seed maps showing z-transformed correlation coefficients for four of the seeds with the strongest bilateral connectivity. Seed maps were generated by computing the Pearson correlation between the Pearson correlation between the oxy-hemoglobin timeseries extracted from the 5-mm radius spherical seed and every voxel in the field of view. **G:** Seed locations for the seed maps shown in **Panels C-F**; the colors of the seed map outlines correspond to the color of the seed.

However, areas with elevated correlations were observed in the corresponding region on the contralateral hemisphere, highlighting the capability of the field HD-DOT instrument to sample connectivity in multiple, distributed regions throughout the field-of-view.

3.5 Discussion

High-density diffuse optical tomography instruments use a large channel count and dense, overlapping optical measurements to produce fMRI-comparable images of cortical hemodynamics during tasks and rest (Eggebrecht et al., 2014, 2012). In this work, an HD-DOT system was used for the first time to image brain function in a cohort of malnourished children in Cali, Colombia. Like other work investigating the effects early malnutrition on brain function, imaging this population was feasible due to the utilization of a portable and wearable optical neuroimaging modality, as low-resource settings where malnutrition is endemic demand imaging tools that can function in the absence of expensive, dedicated infrastructure (Lloyd-Fox et al., 2016, 2014; Roberts et al., 2017). Here, HD-DOT was used to measure task-evoked responses and homotopic functional connectivity in Cali, Colombia, establishing the capability of measuring spatially distributed brain function in a portable HD-DOT instrument.

Optical imaging has been used globally to perform neuroimaging assessments in settings that would not be reachable with imaging modalities that require dedicated infrastructure. fNIRS and DCS-based studies of childhood malnutrition have assayed various aspects of brain function hypothesized to be impacted by malnutrition in the first 1000 days of life, including executive functioning and social processing (Lloyd-Fox et al., 2019; Lloyd-Fox et al., 2016, 2014; Roberts et al., 2017). These studies incorporate cross-culturally appropriate, risk sensitive imaging paradigms to provide insight into malnutrition-related deviances in developmental trajectories (Lloyd-Fox et al., 2019). While these studies focused on younger participants (i.e. < 2 years), continued

investigation of the older children in the present cohort will provide complementary insight into the effects of long-term malnutrition over the course of childhood.

Like other work introducing field imaging instruments in novel settings, the focus of the imaging performed in this work was to obtain maps of brain function in good agreement with previously published HD-DOT results, rather than investigating potential group-level differences between typically-developing and malnourished children (Lloyd-Fox et al., 2014). Indeed, the images obtained with the HD-DOT instrument introduced in this work agreed with previous HD-DOT work performed with other instruments, across multiple sites, in both healthy adults and neonates (Eggebrecht et al., 2014; Ferradal et al., 2016). This finding indicated that the instrument design, channel count, and optode configuration successfully managed the tradeoff between portability and cortical coverage (i.e. sensitivity to multiple cortical regions).

The sensitivity to homotopic functional connectivity established in this analysis sets the stage for using this powerfully predictive measurement in future analyses that are more targeted at identifying correlates of malnutrition burden (Estep et al., 2014; Smyser et al., 2011, 2013). Prior work using fetal and infant fMRI demonstrates the emergence of bilateral FC over development, highlighting the utility of this measure in future assessments of a child's developmental status (Smyser et al., 2010; Thomason et al., 2013). Importantly, the functional connectivity scans collected in this work were during passive movie viewing conditions. While this condition means that functional connectivity results from this work may not be directly comparable to results obtained during rest (i.e. passive fixation), movie viewing is a powerful tool to enhance subject compliance during

functional connectivity scans and reduce the pernicious effects of head motion (Greene et al., 2018; Vanderwal et al., 2018, 2015).

Future analyses with this dataset may leverage the rich, multimodal content of the movie stimulus by filtering the data to a band more appropriate for measuring task-evoked responses (e.g. $0.02 < f < 0.5$ Hz). Evaluating the task-evoked responses during movie viewing opens additional analytic possibilities, including assessing synchronized brain responses during passive movie viewing (Hasson, Nir, Levy, Fuhrmann, & Malach, 2004). Critically, prior work using fMRI has shown that the extent to which an individual exhibits synchronized brain responses during passive movie viewing is related to mathematical and linguistic ability, and also varies between typical and atypical development (Byrge, Dubois, Tyszka, Adolphs, & Kennedy, 2015; Cantlon & Li, 2013; Moraczewski, Chen, & Redcay, 2018). Consequently, this study establishes a foundation for incorporating these powerful analyses in ongoing assessments of malnutrition burden.

A key difference between the HD-DOT system introduced in this work and other fNIRS systems is the density of optical measurements. The system introduced in this work provides coverage of both hemispheres, using a total of 78 optodes, resulting in up to 324 measurements per wavelength, enabling tomographic image reconstruction. In contrast, an fNIRS system may have an order of magnitude fewer measurements and limited cortical coverage; consequently, topographic analysis of brain function is often favored over analyzing tomographically reconstructed images (Everdell et al., 2005; Lloyd-Fox et al., 2014). In this work, we directly compared tomographically reconstructed images using both sparse and dense measurement configurations. While both

configurations detected a hemodynamic signal change associated with stimulus presentation, the localization of the resulting signal change varied as a function of grid density, with consistently localized brain activations most prominently evident in the dense reconstructions. Accordingly, an instrument's channel count is a critical consideration in experiments demanding both detection *and* localization of brain activations.

While prior work with simulations and *in-vivo* comparisons of grid density show that increasing grid density improves image quality characteristics including the system's point-spread function and localization error (Habermehl et al., 2012; Tian, Alexandrakis, & Liu, 2009; White & Culver, 2010b; Yamamoto et al., 2002), one key limitation of the sparse and dense measurement comparison presented here is the lack of a "ground truth" image for evaluating the quality of the two reconstruction schemes used in this work. Consequently, follow- up work will require comparing the images resulting from sparse and dense image reconstruction schemes using subject-matched images obtained using a reference modality, such as fMRI.

In addition to the imaging results presented in this work, our results highlight the usability of the HD-DOT instrument in non-laboratory contexts. After four hours of setup, the HD-DOT instrument was ready for imaging, and posed no infrastructure requirements beyond electricity. New users learned to perform cap fit and data collection procedures within a week of supervised imaging. This manageable learning curve is a significant advantage of optical neuroimaging instruments relative to other imaging modalities (e.g.

MRI), and is likely a contributing factor to the burgeoning use of these instruments in the field.

3.6 Conclusions

The present work establishes HD-DOT as an optical neuroimaging modality suitable for investigations of brain function in low-resource contexts that demand portable instruments, while maintaining cortical coverage and image resolution associated with less portable modalities. Reconstructing subject-matched data with fewer measurements revealed that optical measurement density is a contributing factor in reconstructing consistently localized brain activations. Finally, the combination of task-evoked and functional connectivity maps evaluated in this work set the stage for targeted investigations of the developing brain in the context of childhood malnutrition, including identifying and characterizing a child's risk to foster future intervention development (Raizada & Kishiyama, 2010).

3.7 Appendix

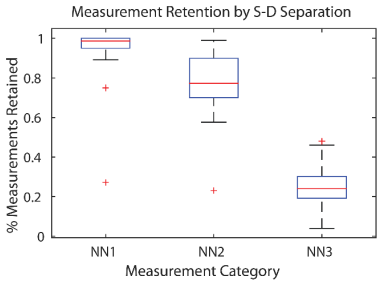

Figure 3.6. Group-level measurement retention. Boxplots show the percentage of measurements retained as a function of measurement density. (NN1 = first nearest neighbor, 13 mm source-detector separation; NN2 = second nearest neighbor, 29 mm source detector separation; NN3 = third nearest neighbor, 39 mm source detector separation).

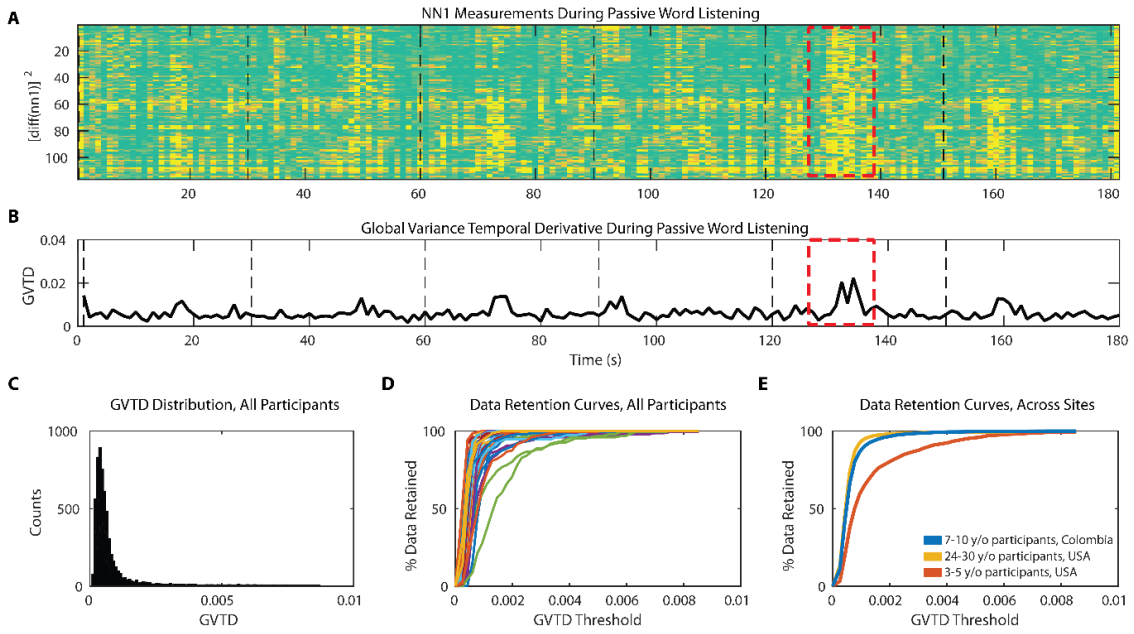

Figure 3.7. Quantifying global measurement variance across participants and sites. A: Matrix (measurements x time) displaying the squared first derivative of first nearest neighbor measurements, obtained during a 3-minute passive word listening run. The dashed red box indicates a period of global measurement variance, likely attributable to a head movement. **B:** A timeseries showing the Global Variance Temporal Derivative (GVTD) is generated by taking the root mean square of the squared first derivative of all measurements (i.e. **Panel A**). Spikes in the GVTD measure (dashed red box) correspond to epochs of global measurement variance. **C:** The distribution of GVTD values for all passive word listening runs (N = 46) obtained in the cohort. **D:** Data quality can be assessed by imposing a GVTD threshold, such that timepoints with GVTD values above the threshold are censored from analysis. As the threshold is relaxed (x-axis), the percentage of data retained (y-axis) increases. Consequently, steeply rising curves are indicative of higher quality datasets. Individual curves in this panel represent data retention for all 17 participants in this cohort. **E:** Data retention curves for 3 passive word listening datasets, collected across sites and HD-DOT instruments: 7-10-year-old participants in Colombia (blue, present dataset); young adults in the USA (yellow, unpublished data); 3-5-year-old participants (red, unpublished data). The data retention curve for participants in this study shows that data quality in Colombia is closely matched to data collected in more traditional laboratory settings.

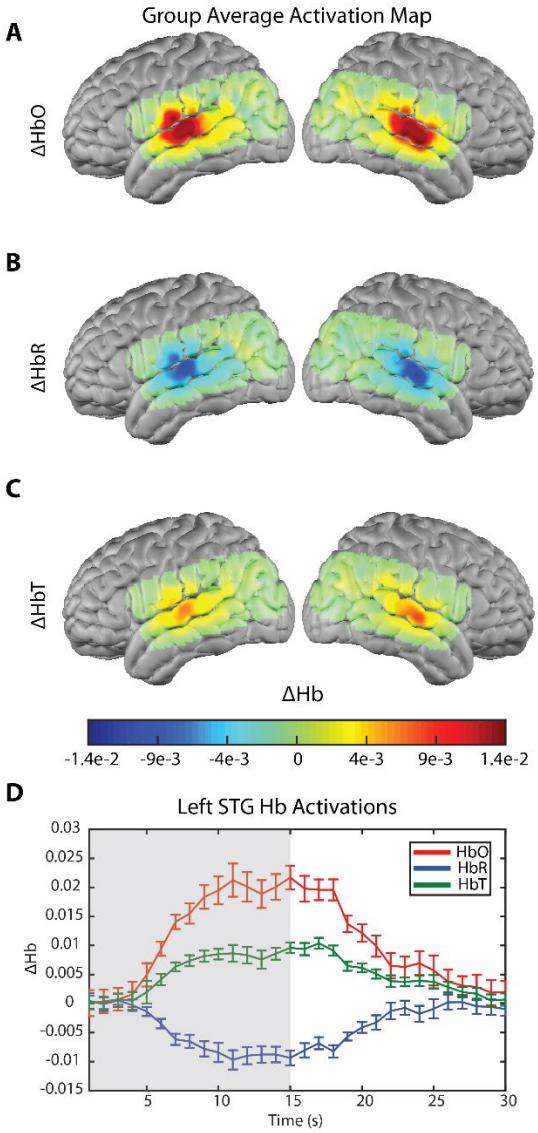

Figure 3.8. Passive word listening activations with all hemoglobin contrasts. A-C: Activation maps from the passive word listening task using oxy-hemoglobin (**A**), deoxy-hemoglobin (**B**), and total hemoglobin (**C**) contrasts. **D:** Timecourses show the temporal dynamics of activation in the left superior temporal gyrus. The shaded portion indicates the stimulation period, during which participants passively listened to concrete Spanish nouns presented at a rate of 1 word/second. Error bars indicate S.E.M.

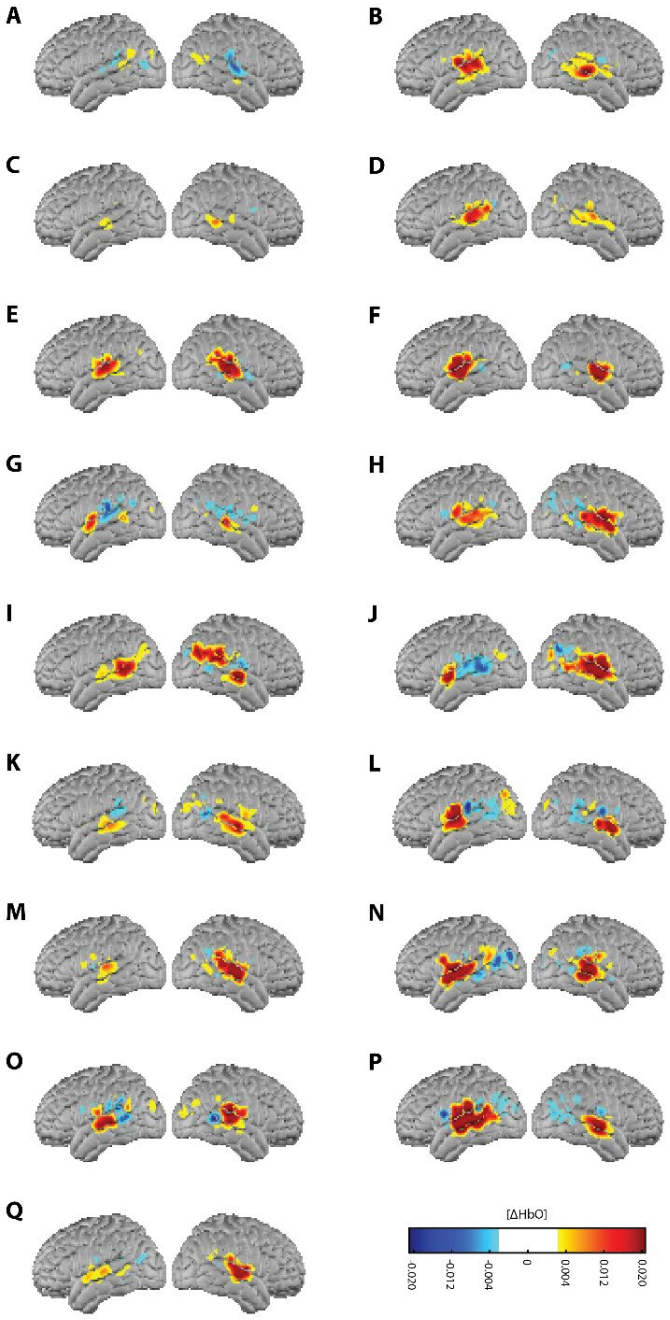

Figure 3.9. Single-subject passive word listening activations. A-Q: Single-subject maps from the group-level map of passive word listening activations shown in **Figure 3.3**.

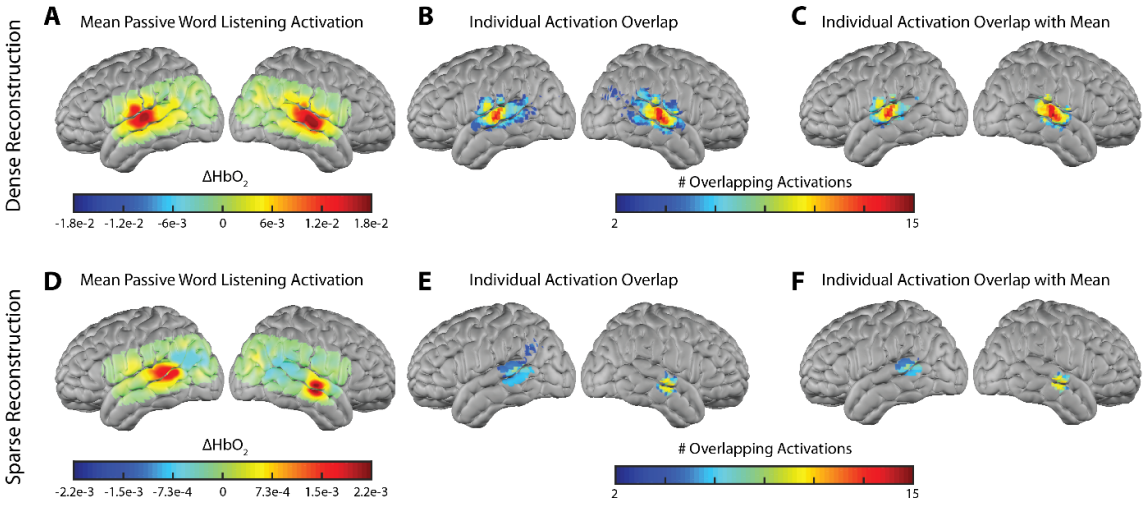

Figure 3.10. Quantification of activation overlap between sparse and dense HD-DOT image reconstruction schemes. A: Block-averaged oxy-hemoglobin activation across all participants, reconstructed using the dense measurement grid for the passive word listening task. **B:** After thresholding and binarizing individual activation maps at 25% of the maximum oxy-hemoglobin value, the overlap between individual's densely reconstructed activation map was computed by summing the binarized images, showing consistent overlap between individual participants. **C:** Masking the image in **Panel B** by a thresholded and binarized group average image shows that well over half of the participants in the study show activations within the bounds of the densely-reconstructed group average. **D:** Block-averaged oxy-hemoglobin activation across all participants, reconstructed using the sparse measurement grid for the passive word listening task. **E:** After thresholding and binarizing individual activation maps at 25% of the maximum oxy-hemoglobin value, the overlap between individual's sparsely reconstructed activation map was computed by summing the binarized images, showing limited overlap between individual participants. **F:** Masking the image in **Panel E** by a thresholded and binarized group average image shows that while the group average for sparsely reconstructed activations produces bilateral activations, most participants' activations do not fall within the bounds of the sparsely-reconstructed group average.

3.8 Acknowledgements

I am extremely grateful to families in Cali, Colombia who volunteered to participate in this study. I further wish to thank the Cali Department of Health for facilitating participant

recruitment. The imaging studies in Cali would not have been possible without the tireless effort and incredible dedication of Marcela Rivera. Drs. William Escobar and Eduardo Bueno provided essential support with the imaging studies at Centro Medico Imbanaco. The following funding sources (associated with study investigators) supported the work: NIH R01EB009223, R01NS090874, R21NS098020, R21DC015884, U01EB027005, Bill & Melinda Gates Foundation OPP1184813; K02 NS089852; Children's Discovery Institute; McDonnell Center for Systems Neuroscience.

3.9 References

Barrett, D. E., Radke-Yarrow, M., & Klein, R. E. (1982). Chronic malnutrition and child behavior: Effects of early caloric supplementation on social and emotional functioning at school age. *Developmental Psychology*, *18*(4), 541–556. https://doi.org/10.1037/0012-1649.18.4.541

Black, M. M., Yimgang, D. P., Hurley, K. M., Harding, K. B., Fernandez-Rao, S., Balakrishna, N., … Nair, K. M. (2019). Mechanisms linking height to early child development among infants and preschoolers in rural India. *Developmental Science*, e12806. https://doi.org/10.1111/desc.12806

Bluestone, A., Abdoulaev, G., Schmitz, C., Barbour, R., & Hielscher, A. (2001). Three-dimensional optical tomography of hemodynamics in the human head. *Optics Express*, *9*(6), 272–286.

Byrge, L., Dubois, J., Tyszka, J. M., Adolphs, R., & Kennedy, D. P. (2015). Idiosyncratic Brain Activation Patterns Are Associated with Poor Social Comprehension in Autism. *Journal of Neuroscience*, *35*(14), 5837–5850. https://doi.org/10.1523/JNEUROSCI.5182-14.2015

Cantlon, J. F., & Li, R. (2013). Neural Activity during Natural Viewing of Sesame Street Statistically Predicts Test Scores in Early Childhood. *PLOS Biology*, *11*(1), e1001462. https://doi.org/10.1371/journal.pbio.1001462

Chugani, H. T., Phelps, M. E., & Mazziotta, J. C. (1987). Positron emission tomography study of human brain functional development. *Annals of Neurology*, *22*(4), 487–497. https://doi.org/10.1002/ana.410220408

Cusick, S. E., & Georgieff, M. K. (2012). Nutrient Supplementation and Neurodevelopment: Timing Is the Key. *Archives of Pediatrics & Adolescent Medicine*, *166*(5), 481–482. https://doi.org/10.1001/archpediatrics.2012.199

Dehghani, H., Eames, M. E., Yalavarthy, P. K., Davis, S. C., Srinivasan, S., Carpenter, C. M., … Paulsen, K. D. (2008). Near infrared optical tomography using NIRFAST: Algorithm for numerical model and image reconstruction. *Communications in Numerical Methods in Engineering*, *25*(6), 711–732. https://doi.org/10.1002/cnm.1162

Eggebrecht, A. T., Ferradal, S. L., Robichaux-Viehoever, A., Hassanpour, M. S., Dehghani, H., Snyder, A. Z., … Culver, J. P. (2014). Mapping distributed brain function and networks with diffuse optical tomography. *Nature Photonics*, *8*(6), 448–454. https://doi.org/10.1038/nphoton.2014.107

Eggebrecht, A. T., White, B. R., Ferradal, S. L., Chen, C., Zhan, Y., Snyder, A. Z., … Culver, J. P. (2012). A quantitative spatial comparison of high-density diffuse optical tomography and fMRI cortical mapping. *NeuroImage*, *61*(4), 1120–1128. https://doi.org/10.1016/j.neuroimage.2012.01.124

Estep, M. E., Smyser, C. D., Anderson, P. J., Ortinau, C. M., Wallendorf, M., Katzman, C. S., … Shimony, J. S. (2014). Diffusion tractography and neuromotor outcome in very preterm children with white matter abnormalities. *Pediatric Research*, *76*(1), 86–92. https://doi.org/10.1038/pr.2014.45

Everdell, N. L., Gibson, A. P., Tullis, I. D. C., Vaithianathan, T., Hebden, J. C., & Delpy, D. T. (2005). A frequency multiplexed near-infrared topography system for imaging functional activation in the brain. *Review of Scientific Instruments*, *76*(9), 093705. https://doi.org/10.1063/1.2038567

Ferradal, S. L., Eggebrecht, A. T., Hassanpour, M., Snyder, A. Z., & Culver, J. P. (2014). Atlas-based head modeling and spatial normalization for high-density diffuse optical tomography: in vivo validation against fMRI. *NeuroImage*, *85 Pt 1*, 117–126. https://doi.org/10.1016/j.neuroimage.2013.03.069

Ferradal, S. L., Liao, S. M., Eggebrecht, A. T., Shimony, J. S., Inder, T. E., Culver, J. P., & Smyser, C. D. (2016). Functional Imaging of the Developing Brain at the Bedside Using Diffuse Optical Tomography. *Cerebral Cortex*, *26*(4), 1558–1568. https://doi.org/10.1093/cercor/bhu320

Goyal, M. S., Hawrylycz, M., Miller, J. A., Snyder, A. Z., & Raichle, M. E. (2014). Aerobic glycolysis in the human brain is associated with development and neotenous gene expression. *Cell Metabolism*, *19*(1), 49–57. https://doi.org/10.1016/j.cmet.2013.11.020

Goyal, M. S., & Raichle, M. E. (2013). Gene expression-based modeling of human cortical synaptic density. *Proceedings of the National Academy of Sciences*, *110*(16), 6571–6576. https://doi.org/10.1073/pnas.1303453110

Grantham-McGregor, S., Cheung, Y. B., Cueto, S., Glewwe, P., Richter, L., & Strupp, B. (2007). Developmental potential in the first 5 years for children in developing countries. *Lancet*, *369*(9555), 60–70. https://doi.org/10.1016/S0140-6736(07)60032-4

Grantham-McGregor, S. M., Powell, C. A., Walker, S. P., & Himes, J. H. (1991). Nutritional supplementation, psychosocial stimulation, and mental development of stunted children: the Jamaican Study. *Lancet (London, England)*, *338*(8758), 1–5.

Greene, D. J., Church, J. A., Dosenbach, N. U. F., Nielsen, A. N., Adeyemo, B., Nardos, B., … Schlaggar, B. L. (2016). Multivariate pattern classification of pediatric Tourette syndrome using functional connectivity MRI. *Developmental Science*, *19*(4), 581–598. https://doi.org/10.1111/desc.12407

Greene, D. J., Koller, J. M., Hampton, J. M., Wesevich, V., Van, A. N., Nguyen, A. L., … Dosenbach, N. U. F. (2018). Behavioral interventions for reducing head motion during MRI scans in children. *NeuroImage*, *171*, 234–245. https://doi.org/10.1016/j.neuroimage.2018.01.023

Habermehl, C., Holtze, S., Steinbrink, J., Koch, S. P., Obrig, H., Mehnert, J., & Schmitz, C. H. (2012). Somatosensory activation of two fingers can be discriminated with ultrahigh-density diffuse optical tomography. *Neuroimage*, *59*(4), 3201–3211. https://doi.org/10.1016/j.neuroimage.2011.11.062

Hasson, U., Nir, Y., Levy, I., Fuhrmann, G., & Malach, R. (2004). Intersubject Synchronization of Cortical Activity During Natural Vision. *Science*, *303*(5664), 1634–1640. https://doi.org/10.1126/science.1089506

Hoddinott, J., Maluccio, J. A., Behrman, J. R., Flores, R., & Martorell, R. (2008). Effect of a nutrition intervention during early childhood on economic productivity in Guatemalan adults. *Lancet (London, England)*, *371*(9610), 411–416. https://doi.org/10.1016/S0140-6736(08)60205-6

Iannotti, L., Jean Louis Dulience, S., Wolff, P., Cox, K., Lesorogol, C., & Kohl, P. (2016). Nutrition factors predict earlier acquisition of motor and language milestones among young children in Haiti. *Acta Paediatrica (Oslo, Norway: 1992)*, *105*(9), e406-411. https://doi.org/10.1111/apa.13483

Jensen, S. K. G., Kumar, S., Xie, W., Tofail, F., Haque, R., Petri, W. A., & Nelson, C. A. (2019). Neural correlates of early adversity among Bangladeshi infants. *Scientific Reports*, *9*(1), 3507. https://doi.org/10.1038/s41598-019-39242-x

JL, G. J. and R. (n.d.). Structural MRI of pediatric brain development: what have we learned and where are we going? - PubMed - NCBI. Retrieved March 31, 2019, from https://www.ncbi.nlm.nih.gov/pubmed/20826305

Kuzawa, C. W., Chugani, H. T., Grossman, L. I., Lipovich, L., Muzik, O., Hof, P. R., … Lange, N. (2014). Metabolic costs and evolutionary implications of human brain development. *Proceedings of the National Academy of Sciences of the United States of America*, *111*(36), 13010–13015. https://doi.org/10.1073/pnas.1323099111

Liu, J., Raine, A., Venables, P. H., Dalais, C., & Mednick, S. A. (2003). Malnutrition at age 3 years and lower cognitive ability at age 11 years: independence from psychosocial adversity. *Archives of Pediatrics & Adolescent Medicine*, *157*(6), 593–600. https://doi.org/10.1001/archpedi.157.6.593

Lloyd-Fox, S., Blasi, A., McCann, S., Rozhko, M., Katus, L., Mason, L., … Elwell, C. E. (2019). Habituation and novelty detection fNIRS brain responses in 5- and 8-month-old infants: The Gambia and UK. *Developmental Science*, *0*(0), e12817. https://doi.org/10.1111/desc.12817

Lloyd-Fox, S., Moore, S., Darboe, M., Prentice, A., Papademetriou, M., Blasi, A., … Elwell, C. E. (2016). fNIRS in Africa & Asia: an Objective Measure of Cognitive Development for Global Health Settings. *The FASEB Journal*, *30*(1_supplement), 1149.18-1149.18. https://doi.org/10.1096/fasebj.30.1_supplement.1149.18

Lloyd-Fox, S., Papademetriou, M., Darboe, M. K., Everdell, N. L., Wegmuller, R., Prentice, A. M., … Elwell, C. E. (2014). Functional near infrared spectroscopy (fNIRS) to assess cognitive function in infants in rural Africa. *Scientific Reports*, *4*, 4740. https://doi.org/10.1038/srep04740

Martorell, R. (1999). The Nature of Child Malnutrition and Its Long-Term Implications. *Food and Nutrition Bulletin*, *20*(3), 288–292. https://doi.org/10.1177/156482659902000304

Martorell, R., Horta, B. L., Adair, L. S., Stein, A. D., Richter, L., Fall, C. H. D., … Consortium on Health Orientated Research in Transitional Societies Group. (2010). Weight gain in the first two years of life is an important predictor of schooling outcomes in pooled analyses from five birth cohorts from low- and middle-income countries. *The Journal of Nutrition*, *140*(2), 348–354. https://doi.org/10.3945/jn.109.112300

McKay, H., Sinisterra, L., McKay, A., Gomez, H., & Lloreda, P. (1978). Improving cognitive ability in chronically deprived children. *Science (New York, N.Y.)*, *200*(4339), 270–278.

Moraczewski, D., Chen, G., & Redcay, E. (2018). Inter-subject synchrony as an index of functional specialization in early childhood. *Scientific Reports*, *8*(1), 2252. https://doi.org/10.1038/s41598-018-20600-0

Murthy, K. D., & Desiraju, T. (1991). Synapses in developing cingulate and hippocampal cortices in undernourished rats. *Neuroreport*, *2*(8), 433–436.

Nelson, C. A. (2015). An international approach to research on brain development. *Trends in Cognitive Sciences*, *19*(8), 424–426. https://doi.org/10.1016/j.tics.2015.05.008

Prado, E. L., & Dewey, K. G. (2014). Nutrition and brain development in early life. *Nutrition Reviews*, *72*(4), 267–284. https://doi.org/10.1111/nure.12102

Raizada, R. D. S., & Kishiyama, M. M. (2010). Effects of Socioeconomic Status on Brain Development, and How Cognitive Neuroscience May Contribute to Levelling the Playing Field. *Frontiers in Human Neuroscience*, *4*. https://doi.org/10.3389/neuro.09.003.2010

Roberts, S. B., Franceschini, M. A., Krauss, A., Lin, P.-Y., Braima de Sa, A., Có, R., … Muentener, P. (2017). A Pilot Randomized Controlled Trial of a New Supplementary Food Designed to Enhance Cognitive Performance during Prevention and Treatment of Malnutrition in Childhood. *Current Developments in Nutrition*, *1*(11). https://doi.org/10.3945/cdn.117.000885

Sherafati, A., Eggebrecht, A. T., Burns-Yocum, T. M., & Culver, J. P. (2017). A global metric to detect motion artifacts in optical neuroimaging data (Conference Presentation). *Neural Imaging and Sensing*, *10051*, 1005112. https://doi.org/10.1117/12.2252417

Smyser, C. D., Inder, T. E., Shimony, J. S., Hill, J. E., Degnan, A. J., Snyder, A. Z., & Neil, J. J. (2010). Longitudinal analysis of neural network development in preterm infants. *Cerebral Cortex (New York, N.Y.: 1991)*, *20*(12), 2852–2862. https://doi.org/10.1093/cercor/bhq035

Smyser, C. D., Snyder, A. Z., & Neil, J. J. (2011). Functional connectivity MRI in infants: exploration of the functional organization of the developing brain. *NeuroImage*, *56*(3), 1437–1452. https://doi.org/10.1016/j.neuroimage.2011.02.073

Smyser, C. D., Snyder, A. Z., Shimony, J. S., Blazey, T. M., Inder, T. E., & Neil, J. J. (2013). Effects of white matter injury on resting state fMRI measures in prematurely born infants. *PloS One*, *8*(7), e68098. https://doi.org/10.1371/journal.pone.0068098

Thomason, M. E., Dassanayake, M. T., Shen, S., Katkuri, Y., Alexis, M., Anderson, A. L., … Romero, R. (2013). Cross-Hemispheric Functional Connectivity in the Human Fetal Brain. *Science Translational Medicine*, *5*(173), 173ra24-173ra24. https://doi.org/10.1126/scitranslmed.3004978

Thompson, R. A., & Nelson, C. A. (2001). Developmental science and the media. Early brain development. *The American Psychologist*, *56*(1), 5–15.

Tian, F., Alexandrakis, G., & Liu, H. (2009). Optimization of probe geometry for diffuse optical brain imaging based on measurement density and distribution. *Applied Optics*, *48*(13), 2496–2504. https://doi.org/10.1364/AO.48.002496

Vanderwal, T., Eilbott, J., & Castellanos, F. X. (2018). Movies in the magnet: Naturalistic paradigms in developmental functional neuroimaging. *Developmental Cognitive Neuroscience*. https://doi.org/10.1016/j.dcn.2018.10.004

Vanderwal, T., Kelly, C., Eilbott, J., Mayes, L. C., & Castellanos, F. X. (2015). Inscapes: A movie paradigm to improve compliance in functional magnetic resonance imaging. *NeuroImage*, *122*, 222–232. https://doi.org/10.1016/j.neuroimage.2015.07.069

Wheelock, M. D., Austin, N. C., Bora, S., Eggebrecht, A. T., Melzer, T. R., Woodward, L. J., & Smyser, C. D. (2018). Altered functional network connectivity relates to motor development in children born very preterm. *NeuroImage*, *183*, 574–583. https://doi.org/10.1016/j.neuroimage.2018.08.051

White, B. R., & Culver, J. P. (2010a). Phase-encoded retinotopy as an evaluation of diffuse optical neuroimaging. *NeuroImage*, *49*(1), 568–577. https://doi.org/10.1016/j.neuroimage.2009.07.023

White, B. R., & Culver, J. P. (2010b). Quantitative evaluation of high-density diffuse optical tomography: in vivo resolution and mapping performance. *Journal of Biomedical Optics*, *15*(2), 026006. https://doi.org/10.1117/1.3368999

Wiggins, R. C. (1982). Myelin development and nutritional insufficiency. *Brain Research*, *257*(2), 151–175.

Yamamoto, T., Maki, A., Kadoya, T., Tanikawa, Y., Yamada, Y., Okada, E., & Koizumi, H. (2002). Arranging optical fibres for the spatial resolution improvement of topographical images. *Physics in Medicine and Biology*, *47*(18), 3429–3440. https://doi.org/10.1088/0031-9155/47/18/311

Zeff, B. W., White, B. R., Dehghani, H., Schlaggar, B. L., & Culver, J. P. (2007). Retinotopic mapping of adult human visual cortex with high-density diffuse optical tomography. *Proceedings of the National Academy of Sciences of the United States of America*, *104*(29), 12169–12174. https://doi.org/10.1073/pnas.0611266104

Chapter 4: Mapping brain function during naturalistic viewing using high-density diffuse optical tomography

This chapter has been re-submitted with revisions to a journal for publication. The citation will be:

Fishell, A.K., Tracy M. Burns-Yocum, Karla M. Bergonzi, Adam T. Eggebrecht, Joseph P. Culver. “Mapping brain function during naturalistic viewing using high-density diffuse optical tomography.” Scientific Reports (2019).

4.1 Abstract

Naturalistic stimuli, such as movies, more closely recapitulate “real life” sensory processing and behavioral demands relative to paradigms that rely on highly distilled and repetitive stimulus presentations. The rich complexity inherent in naturalistic stimuli demands an imaging system capable of measuring spatially distributed brain responses, and analysis tools optimized for unmixing responses to concurrently presented features. In this work, the combination of passive movie viewing with high-density diffuse optical tomography (HD-DOT) is developed as a platform for naturalistic brain mapping. We imaged healthy young adults during free viewing of a feature film using HD-DOT and observed reproducible, synchronized cortical responses across a majority of the field-of-view, most prominently in hierarchical cortical areas related to visual and auditory processing, both within and between individuals. In order to more precisely interpret broad patterns of cortical synchronization, we extracted visual and auditory features from the movie stimulus and mapped the cortical responses to the features. The results demonstrate the sensitivity of HD-DOT to evoked responses during naturalistic viewing,

and that feature-based decomposition strategies enable functional mapping of naturalistic stimulus processing, including human-generated speech.

4.2 Introduction

Optical neuroimaging techniques enable functional brain imaging in naturalistic settings unavailable to imaging modalities with highly constrained imaging environments such as functional magnetic resonance imaging (fMRI) (Matusz, Dikker, Huth, & Perrodin, 2018; Yücel, Selb, Huppert, Franceschini, & Boas, 2017). For instance, functional near-infrared spectroscopy (fNIRS) enables functional brain imaging of social interactions or unconstrained movements (Hirsch, Zhang, Noah, & Ono, 2017; Liu et al., 2017; Miyai et al., 2001; Noah et al., 2015; Ono et al., 2015; Piper et al., 2014; Suzuki, Miyai, Ono, & Kubota, 2008). Naturalistic imaging paradigms more closely recapitulate real-life conditions than experiments relying on tightly controlled stimuli, such as assessing speech perception with single sentence presentations, or mapping retinotopic organization of visual cortex using flashing checkerboard patterns (Hamilton & Huth, 2018; Hassanpour, Eggebrecht, Culver, & Peelle, 2015; Heer, Huth, Griffiths, Gallant, & Theunissen, 2017; Lerner, Honey, Silbert, & Hasson, 2011; White & Culver, 2010a). Further, naturalistic paradigms are highly engaging, contain multi-modal content, and may be particularly well suited for populations (e.g. young children) unable make overt behavioral responses or perform a repetitive or predictable task (Church, Petersen, & Schlaggar, 2010; Karim & Perlman, 2017; Vanderwal, Eilbott, & Castellanos, 2018; Zaki & Ochsner, 2009). In addition to social interactions and natural movements, naturalistic imaging paradigms have included free viewing of movies and television shows (Bartels &

Zeki, 2004; Hasson, Malach, & Heeger, 2010; Hasson, Nir, Levy, Fuhrmann, & Malach, 2004). Naturalistic viewing paradigms employing movies or television shows enable repeatability and control over stimulus presentation, like experiments incorporating simplified and distilled stimuli, but preserve the richness and greater ecological validity associated with more unconstrained naturalistic paradigms.

Naturalistic viewing tasks have been extensively studied using other brain imaging modalities, including fMRI (Hasson et al., 2004), EEG (Poulsen, Kamronn, Dmochowski, Parra, & Hansen, 2017) and MEG (K. Lankinen, Saari, Hari, & Koskinen, 2014). Work using fMRI has established both practical and neuroscientific advantages of naturalistic viewing experiments. From a practical perspective, participants passively viewing a movie during brain imaging, particularly children, tend to move less relative to other passive tasks, such as resting-state paradigms, thereby reducing the pernicious effects of image artifacts related to head motion (Greene et al., 2018; Power, Barnes, Snyder, Schlaggar, & Petersen, 2012; Vanderwal, Kelly, Eilbott, Mayes, & Castellanos, 2015). In the cognitive neuroscience literature, naturalistic viewing tasks have been shown to reliably provide synchronized cortical responses across participants, show sensitivity to subsequent memory of the movie content, and modulate across typical and atypical developmental trajectories (Hasson et al., 2004; Hasson, Furman, Clark, Dudai, & Davachi, 2008; Byrge, Dubois, Tyszka, Adolphs, & Kennedy, 2015; Ki, Kelly, & Parra, 2016; Moraczewski, Chen, & Redcay, 2018; Salmi et al., 2013). Further, comprehension of the narrative elements of the stimulus is not constrained to a single sensory modality, further emphasizing the richness contained within naturalistic stimuli such as movies (Nguyen, Vanderwal, & Hasson, 2019). Though some optical studies have utilized naturalistic settings such as

real-life interactions, the methodological and scientific appeal of repeatable and tunable narrative movie viewing paradigms, in general, have yet to be fully leveraged using optical neuroimaging (Liu et al., 2017).

Naturalistic viewing simultaneously and reliably engages multiple cortical processing systems, including those related to processing the movie's auditory/visual content and narrative structure (Bartels & Zeki, 2004; Hasson et al., 2004). These systems are spatially distributed across the cortex, underscoring the need for a large field-of-view to capture the multi-modality responses. Furthermore, the complexity of information contained within the stimulus demands high spatial resolution, in order to map features within a modality (e.g. visual categories) to cortical structures related to processing those features. As with other whole-brain paradigms, such as resting state functional connectivity, imaging systems with higher space bandwidth product (~FOV/Resolution) provide more powerful readouts of movie-evoked responses. Therefore, in comparison to traditional sparse fNIRS systems, optical neuroimaging techniques such as high-density diffuse optical tomography (HD-DOT), which utilize a densely arranged array of measurements across a broad field-of-view, are better suited for mapping movie-evoked responses (Eggebrecht et al., 2014, 2012; White & Culver, 2010b).

Therefore, the central goal of the present work is to evaluate the functional mapping performance of naturalistic movie viewing combined with a large field-of-view HD-DOT system in healthy young adults. Cortical synchronization, as indexed by the correlation coefficient between the brain responses to repeated movie viewings, has been demonstrated using other imaging modalities including EEG (Poulsen et al., 2017), ECoG

(Honey et al., 2012), MEG (K. Lankinen et al., 2014), and fMRI (Chang et al., 2015; Hasson et al., 2004; Kaisu Lankinen et al., 2018). Cortical maps of the correlation strength between runs during naturalistic viewing highlight the broad constellation of regions reliably involved in stimulus processing. Further, if HD-DOT is sensitive to complex, multi-modal cortical responses associated with naturalistic viewing, we hypothesize that highly reproducible, synchronized, cortical responses will be measurable across regions related to both sensory (auditory/visual) and higher-order cognitive (e.g. linguistic) processing.

A limitation of spatially mapping the correlation coefficient between brain responses measured across repeated viewings is that this style of analysis is agnostic to specific components of the stimulus, such as speech or visual motion, that are relevant to mapping cortical information processing. In contrast, feature extraction tools provide a powerful technique for parameterizing individual movie features and subsequently identifying regions related to processing those features during naturalistic viewing (Bartels & Zeki, 2004; Kauttonen, Hlushchuk, & Tikka, 2015; Russ & Leopold, 2015). Accordingly, the second analysis developed in this paper is an approach that maps feature-specific cortical responses during naturalistic viewing. Like cortical responses mapped with reductive, non-naturalistic stimuli, these feature maps relate measured brain responses to task-related information processing demands.

4.3 Methods

4.3.1 Participants

Participants in this experiment were healthy young adults, recruited from the Washington University community. All participants gave written informed consent to participate in the experiment, which was approved by and carried out in accordance to the Human

Research Protection Office at Washington University School of Medicine. Participants, all right-handed native English speakers, self-reported no history of neurological or psychiatric illness. In total, 12 participants were enrolled in the naturalistic viewing experiment (aged 23.5-29.4 years; 6 female). Of the 12 initial participants, 10 are included in the analyses reported below, as two participants were excluded due to falling asleep during one of the two imaging sessions.

4.3.2 Stimuli and experimental procedure

Participants underwent an HD-DOT cap fit procedure lasting approximately 5-10 minutes, guided by real-time readouts of measurement light level, signal-to-noise, and optode-scalp coupling coefficients. Following cap fit, participants began the naturalistic viewing experiment. Informed by previous fMRI studies (Hasson et al., 2004), all participants in this experiment viewed a 30-minute segment from the feature film, *The Good, the Bad, and the Ugly*, directed by Sergio Leone. As published previously using this stimulus, participants viewed minutes 16:48 to 46:48 (Hasson et al., 2004). During an imaging session, participants viewed the same 30-minute segment two times, and each participant completed at least two imaging sessions on separate days. During passive movie viewing, unless otherwise specified, participants were instructed to relax, remain still, and watch the movie as they would normally, outside of the laboratory. The stimulus was presented on a 20-inch (diagonal) liquid-crystal display with 1080x760 pixels, positioned 75 cm from the participant's nasion, subtending a vertical view angle of 23 degrees, and a horizontal view angle of 30 degrees. The stimulus was presented using the Psychophysics Toolbox 3 package for MATLAB (2010b) (Brainard, 1997).

4.3.3 HD-DOT instrumentation

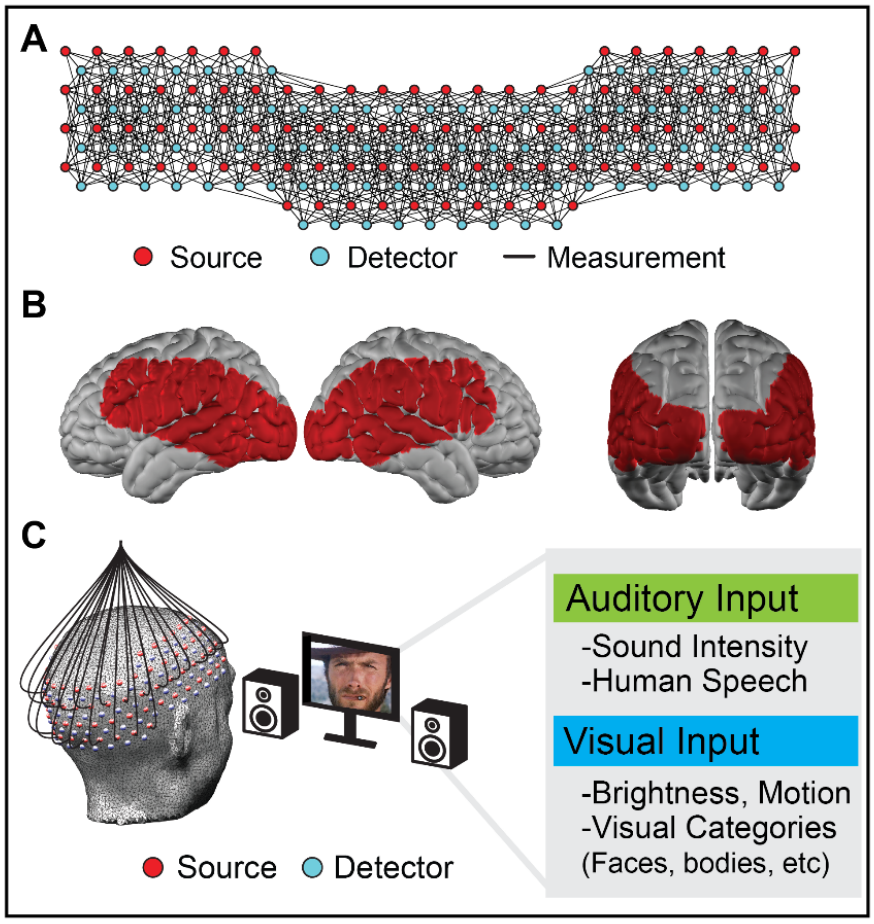

Figure 4.1. HD-DOT Instrumentation. A: The HD-DOT instrument used in the naturalistic viewing experiments consisted of a 96 source, 92 detector array, resulting in a dense grid of measurements used to produce spatially-resolved maps of brain hemodynamics. Black lines indicate measurements used in image reconstruction from a representative participant. B: The cortical field-of-view resulting from the optode arrangement. C: During naturalistic viewing, participants watched a clip from a feature film, while undergoing multi-modal sensory stimulation resulting from a hierarchical set of visual and auditory features.

The large field-of-view HD-DOT instrument used in this experiment (Figure 4.1) has been described in detail in prior work using this instrument (Eggebrecht et al., 2014). In brief, this custom-built continuous wave instrument consists of 96 LED sources illuminating the head at two wavelengths (750 nm and 850 nm), and 92 avalanche photo diode detectors (Hamamatsu C5460-01), coupled to the head using 4.2 m long fiber-optic bundles

(CeramOptec, 2.5-mm diameter bundles of 50 μm fibers). The weight of the 188 fibers was managed using an extruded aluminum frame and series of collinear rings surrounding the participant, ensuring that participants do not bear any of the fiber weight.

Fibers were affixed to the scalp using a custom-built imaging cap, which positions optodes such that first-through fourth-nearest neighbor separations are 1.3, 3.0, 3.9, and 4.7 cm, respectively. Using previously published temporal, frequency, and spatial encoding patterns, the HD-DOT system achieves an overall framerate of 10 Hz (Eggebrecht et al., 2014). In a typical participant, this system configuration yielded over 1,200 source-detector measurements (per wavelength), which were then converted into voxelated movies of brain hemodynamics as specified below.

4.3.4 HD-DOT image reconstruction

Image reconstruction occurs in five separate phases: light-level measurement pre-processing, anatomical light modeling, image reconstruction, spectroscopy and spatial normalization. The measurement pre-processing and image reconstruction steps followed previously published procedures using the same HD-DOT instrument (Eggebrecht et al., 2014). Raw detector light levels were first converted to time-series log-ratio data. Log-ratio data was generated by taking the logarithm of the ratio of the instantaneous light level and the source-detector measurement's mean value across the entire run. In this approach, the baseline is therefore defined as the measurement's mean value across the entire run. Next, any measurements with a temporal variance exceeding 7.5% were considered to be contaminated by non-physiological variance (e.g. head motion) and excluded from image reconstruction for the entire run. The percentage of measurements retained for each source-detector separation in this sample was (Mean ±

SD): 99.7±1% of first nearest-neighbors, 97.0±3% of second nearest-neighbors, 83.6±11% of third-nearest neighbors, and 40.0±9% of fourth nearest-neighbors. Consequently, the exact set of measurements used in image reconstruction varied on a run-by-run basis (Figure 4.8, Appendix). However, the measurement density afforded by the HD-DOT instrument ensures that a given voxel is over-sampled by multiple measurements and minimizes any potential sampling dropout caused by the removal of any single measurement. The measurements that passed the variance threshold were then high-pass filtered (f > 0.02 Hz) to remove long term drift. Next, systemic and superficial signals, which were approximated by averaging all first nearest-neighbor measurements, were regressed out of all measurements. Measurements were then low-pass filtered (f < 0.5 Hz).

For anatomical light modeling, the non-linear ICBM152 atlas from the Montreal Neurological Institute was used to generate a wavelength-dependent forward model of light propagation through five non-uniform tissue compartments with tissue specific optical properties: scalp ($\mu_{a,750}$ = 0.017 ; $\mu_{a,850}$ = 0.019; $\mu_{s,750}'$ = 0.74; $\mu_{s,850}'$ = 0.64), skull ($\mu_{a,750}$ = 0.012; $\mu_{a,850}$ = 0.014; $\mu_{s,750}'$ = 0.94; $\mu_{s,850}'$ = 0.84), grey matter ($\mu_{a,750}$ = 0.018; $\mu_{a,850}$ = 0.019; $\mu_{s,750}'$ = 0.84; $\mu_{s,850}'$ = 0.67), white matter ($\mu_{a,750}$ = 0.018; $\mu_{a,850}$ = 0.021; $\mu_{s,750}'$ = 1.19; $\mu_{s,850}'$ = 1.01), and cerebrospinal fluid ($\mu_{a,750}$ = 0.004; $\mu_{a,850}$ = 0.004; $\mu_{s,750}'$ = 0.3; $\mu_{s,850}'$ = 0.3) (Fonov, Evans, McKinstry, Almli, & Collins, 2009). This light modeling accounts for the wavelength dependence of both the illumination patterns (light fluence), and the collection sensitivity patterns, as published previously with HD-DOT (Eggebrecht et al., 2014). These modelling steps, combined with superficial signal regression (Gregg, White, Zeff, Berger, & Culver, 2010; Saager & Berger, 2005) and optimal wavelength

choice (λ = 750 and 850 nm) provide accurate unmixing of oxy- and deoxy-hemoglobin (Boas et al., 2001).

The atlas-based forward modeling technique eliminates the need for subject-specific forward modeling using individual anatomical images, and results in individual and group level image quality with localization errors on the order of millimeters (Ferradal, Eggebrecht, Hassanpour, Snyder, & Culver, 2014). Using the atlas anatomy combined with the 188 optode positions, the sensitivity matrix was generated using NIRFAST (Dehghani et al., 2008). The sensitivity matrix was then inverted using Tikhonov regularization (Eggebrecht et al., 2012). The conversion from differential absorption to differential hemoglobin was made using spectroscopy values from the literature (Bluestone, Abdoulaev, Schmitz, Barbour, & Hielscher, 2001).

For image reconstruction, the measurement data was converted to voxel space using the inverted sensitivity matrix and spectroscopy parameters described above, which resulted in volumetric time-series data of three hemodynamic contrasts: oxyhemoglobin (ΔHbO_2), deoxyhemoglobin (ΔHbR) and total hemoglobin (ΔHbT) at a framerate of 1 Hz. All analyses performed on these images utilize the oxyhemoglobin (ΔHbO_2) contrast, unless otherwise specified (see Figure 4.9 for results with all three hemoglobin contrasts).

Hemoglobin spectroscopy performance was verified using an independent dataset collected from a subset (N=5) of participants in this study. These participants viewed a rotating wedge consisting of a black and white checkerboard that flickered at a 10 Hz reversal rate to produce an evoked response in visual cortex, following previously published procedures (White & Culver, 2010a; Zeff, White, Dehghani, Schlaggar, & Culver, 2007). The ratios of the ΔHbO_2, ΔHbR, and ΔHbT responses in visual cortex follow

previously reported responses obtained with near-infrared tissue spectroscopy using similar stimulation protocols (Figure 4.9, Appendix). Utilizing a more traditional stimulation paradigm to evaluate spectroscopy performance confirms that the light modeling and spectroscopy parameters are appropriate for the more novel naturalistic viewing analyses.

4.3.5 Data analysis of movie responses

The image reconstruction procedure resulted in a volumetric time-series of brain responses time-locked to the stimulus presentation. Two analyses were performed on these HD-DOT images. First, we evaluated the inter- and intra-subject synchronization between multiple viewings of the movie stimulus following procedures previously used with fMRI (Hasson et al., 2004). Second, we evaluated the correlation between parameterized features of the movie stimulus and the measured cortical responses (Bartels & Zeki, 2004; Russ & Leopold, 2015). For correlation maps resulting from both the synchronization and feature-based analyses, the voxelwise correlation coefficients were assessed using the T-statistic. The observed Pearson product-moment correlations were transformed to a normally distributed statistic using the Fisher Z-transformation,

$$z' = 0.5\,[\ln(1 + r) - \ln(1 - r)]$$

Examples of Z-transformed maps are presented in Figure 4.9 (Appendix). For a given voxel, the Z-transformed correlation coefficient was then mean subtracted and divided by the standard error, $\sigma/\sqrt{n}$, where σ is the sample standard deviation, and *n* is the number of images included in a given analysis. The resulting contrast-to-noise T-maps therefore indicate the extent to which an observed correlation coefficient deviates from a null distribution in which there is no observed correlation between signals.

4.3.5a Inter- and intra-subject synchronization

To assess the extent to which an individual exhibited synchronized responses across repeated presentations (intra-subject synchronization), as well as the extent to which an individual synchronized with others in the sample (inter-subject synchronization) we performed a correlation analysis. For each voxel, we calculated the correlation coefficient between the voxel's ΔHbO_2 timeseries for two separate movie presentations(Hasson et al., 2004). Repeating this procedure across all voxels in the field-of-view produces a spatial map of synchronization across the cortex.

4.3.5b Feature-based analysis

The movie stimulus was decomposed into both visual and auditory features in order to more precisely relate features of the stimulus to observed ΔHbO_2 responses. Visual features included features based on image statistics calculated based on individual movie frames (luminance, flow). Luminance was indexed by the mean pixel intensity for a single frame, after converting the full-color image to a grayscale image (Russ & Leopold, 2015). Motion was parametrized by calculating optical flow, using the Lucas-Kanade algorithm for solving the optical flow constraint equation:

$$I_x u + I_y v + I_t = 0,$$

where I_x, I_y, and I_t, are spatiotemporal image brightness derivatives, and u and v are horizontal and vertical optical flow, respectively. The Lucas-Kanade algorithm was implemented using the opticalFlowLK class in the MATLAB Computer Vision Toolbox (noise threshold = 0.0039). For each frame, the average magnitude of optical flow across all pixels was used to track changes in visual motion intensity for the duration of the stimulus.

A second set of visual features included manually coded features: visually presented faces, bodies, and hands. For manually coded features, three human raters viewed the stimulus in 1-second bins and made a binary judgment regarding the presence of the three visual features of interest: Faces, bodies, and hands. Bins during which the raters' judgments were discordant were subsequently re-evaluated to reach a consensus.

Auditory features included the envelope of the stimulus audio, as well as moment-to-moment changes in the presence of human-generated speech. The envelope of the stimulus audio was used to track overall changes in audio intensity, regardless of the content of the audio, and implemented in MATLAB. Following previously published methods, the envelope of audio intensity was calculated by computing power modulations across 25 frequency bands (center frequencies: 200 Hz – 5 kHz; width: 200 Hz; sampling rate: 50 ms) (Honey et al., 2012). Within each band, the logarithm of the power time course was taken, and then all frequency bands were averaged, resulting in a single time course representing the audio envelope of the stimulus audio. The presence of human speech (excluding human-generated non-speech sounds) was manually coded by three raters, using binary judgments on 1-second bins of audio. Discordant judgments were subsequently re-evaluated to reach a consensus.

To model the response to each feature, we convolved the raw feature time-series with a canonical hemodynamic response and then bandpass filtered ($0.02 \text{ Hz} < f < 0.5$ Hz) the feature time-series to match the measurement filtering parameters (Hassanpour et al., 2014). To relate feature dynamics to measured cortical responses, we calculated the temporal correlation between the modeled time-course for each feature and the ΔHbO_2 response time-course for each voxel across the field-of-view. This procedure

generated a spatial map of the correlation strength between the brain responses and each feature time-course. To differentially assess pairs of features, a paired-samples T-test between sets of two feature correlation maps was used to identify cortical regions with differential responses between a pair of features.

4.4 Results

4.4.1 Inter- and intra-subject synchronization

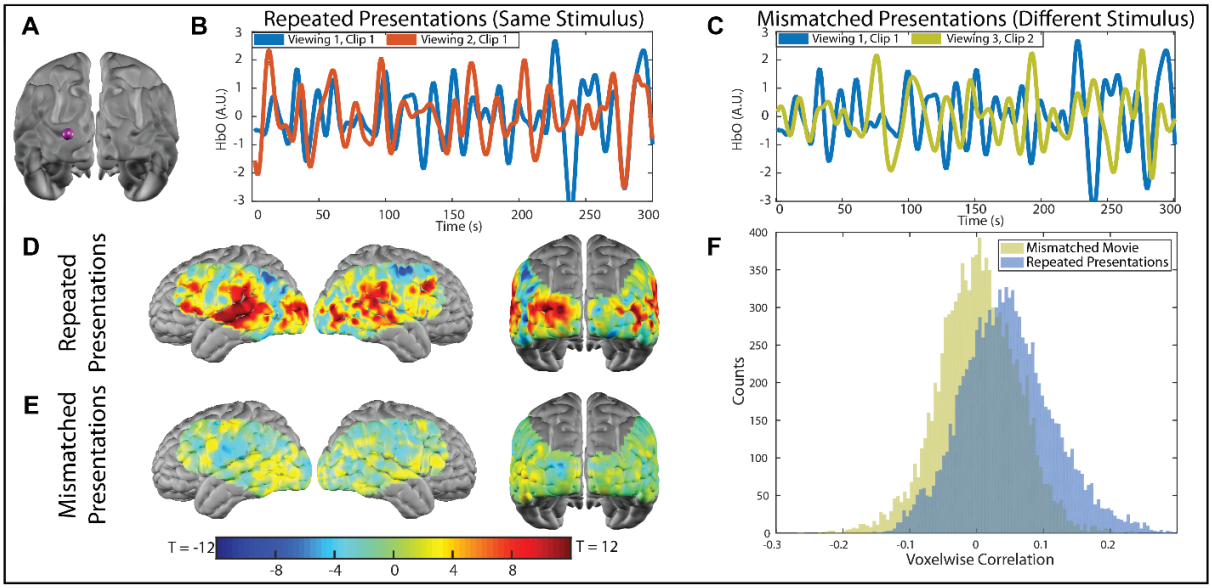

Figure 4.2. **Intra-subject synchronization.** A: Seed region (purple sphere) used to extract an exemplar oxy-hemoglobin timeseries during viewing of repeated movie stimuli (B) and mismatched movie stimuli (C) from a single subject's data (i.e. two repetitions of the movie stimulus). D: During repeated presentations of the stimulus, the group average of individual viewers' synchronization maps shows elevated synchronization in regions across the cortical field-of-view, particularly auditory and visual processing regions, as shown in this unthresholded T-map. E: During mismatched stimulus presentations, the synchronization values are greatly reduced, as shown in this unthresholded T-map. F: Voxelwise distributions of Pearson correlation values during repeated and mismatched movie presentations.

For a single voxel, intra-subject, between-viewing synchronization is indexed and quantified by the Pearson product-moment correlation coefficient between ΔHbO_2

timeseries, obtained during two separate repetitions of the same stimulus within the same participant (Figure 4.2, A-C). Repeating this procedure across the field-of-view generates a correlation map. Averaging these correlation maps across participants (N = 10 participants; 2 stimulus repetitions per participant) reveals regions of elevated correlation coefficients, or synchronization, across the entire HD-DOT field-of-view (Figure 4.2, D). In particular, elevated correlation coefficients are observed in regions related to auditory and visual processing, underscoring that the strongest correlations observed are due to sensory processing of the multi-modal movie stimulus. For a given participant, intra-subject synchronization was assessed using stimulus repetitions obtained within and across imaging sessions, meaning that an individual participant's intra-subject synchronization map could include responses measured during movie viewings of the same repeated clip, across multiple days.

Obtaining multiple runs during repetitions of the same stimulus across multiple imaging sessions enables assessment of potential habituation effects, which would result in diminished activation magnitudes as the number of stimulus repetitions increases (Buckner et al., 1998). In the intra-subject synchronization analysis, these effects would be evident in diminished intra-subject synchronization between viewings across disparate sessions, relative to viewings within a session (i.e. when there have been fewer stimulus repetitions). To assess this potential habituation effect, the intra-subject synchronization analysis was repeated with runs that were (1) obtained within the same session and (2) obtained across separate sessions (Figure 4.10, Appendix). While the average value of the Fisher z-transformed correlation was slightly lower across sessions (mean z(r) = 0.038) than it was within sessions (mean z(r) = 0.041), the voxelwise topographies and

distributions of correlation coefficients are largely overlapping, (Figure 4.10, Appendix), indicating no observed habituation effect across the repeated stimulus presentations in this dataset.

If the observed synchronization between voxelwise responses is related to processing repetitions of the same stimulus, then the magnitude of the correlation should be diminished when the analysis is repeated with ΔHbO_2 timeseries obtained during disparate viewing conditions (i.e. different movie clips). Indeed, when participants view non-overlapping movie segments, the correlation coefficients are diminished both within a single region (Figure 4.2, C) and across the entire HD-DOT field-of-view (Figure 4.2, E). The dramatic reduction in the correlation coefficients is also evident in the distributions of correlation values observed during both matched and mis-matched viewing conditions (Figure 4.2, F). Voxelwise responses in individual viewers show the greatest reliability, or synchronization, during repetitions of the same stimulus (Figure 4.2, D).

Cortical responses measured within single individuals reveal movie-driven responses with high correlation coefficients in regions related to stimulus processing. To assess whether this effect extended beyond individual viewers to disparate pairs of viewers, the synchronization analysis was repeated across all possible pairs of the ten viewers. The voxelwise correlation coefficient between the ΔHbO_2 time-series in each participant was calculated for each pair of viewers, which revealed a synchronization topography comparable to the intra-subject analysis (Figure 4.3). In other words, not only does the naturalistic stimulus reliably drive cortical responses within an individual, it also reliably drives cortical responses across individuals.

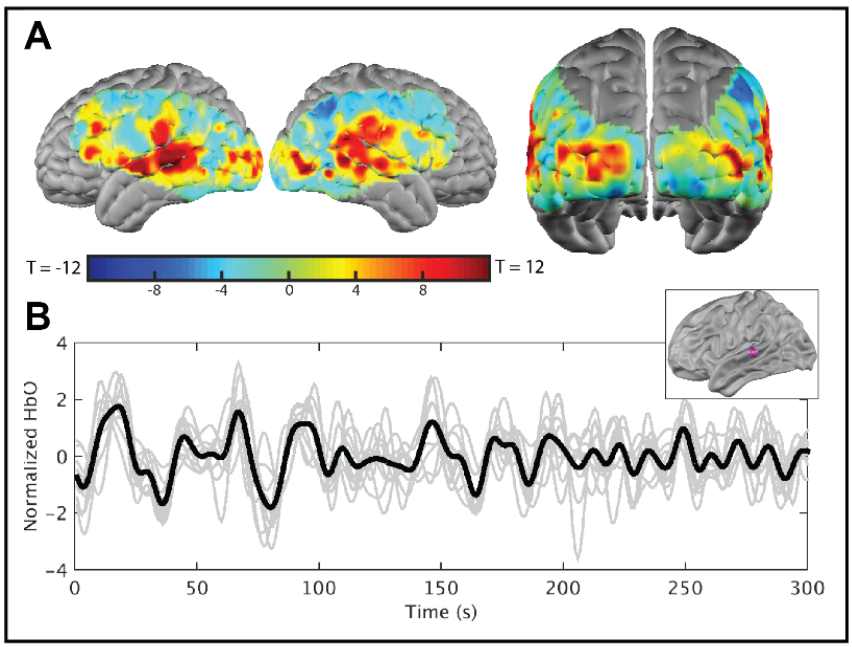

Figure 4.3. Inter-subject synchronization. A: Pairs of separate viewers also show synchronized cortical responses in regions related to visual and auditory processing during naturalistic viewing, as shown in the unthresholded map of synchronization averaged across all possible pairs of 10 viewers (45 pairs in total). B: Oxy-hemoglobin timeseries from a seed region in the left superior temporal gyrus (inset) for individual viewers (grey lines) and the group average (black line).

4.4.2 Gaze-based synchronization modulations

To demonstrate the sensitivity of naturalistic viewing experiments to eye position, a subset of participants (N = 4) in the present work repeated the experiment under modified viewing conditions. These participants viewed the stimulus once under natural conditions, and a second time while maintaining central fixation throughout the entire viewing period, during which a crosshair was overlaid over the center of the movie stimulus. Within both of the viewing conditions, synchronization in visual cortex was preserved, as indexed by the high correlation coefficients in visual cortex (Figure 4.4). However, when the correlation coefficient between ΔHbO_2 time-series from disparate viewing conditions was calculated, synchronization was diminished, highlighting that the synchronization effect in

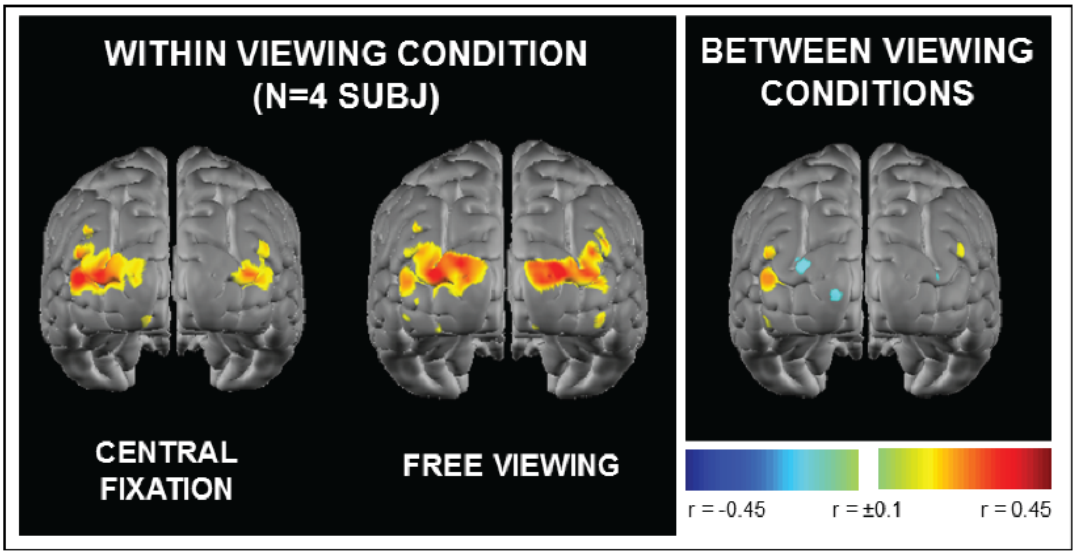

Figure 4.4. Gaze-based synchronization modulations. A subset of participants (N = 4) viewed an additional repetition of the stimulus under experimenter-imposed viewing conditions, in which participants were instructed to maintain central fixation during movie viewing. Voxelwise maps display raw Pearson correlation coefficients, which provide a quantification of cortical synchronization during both central fixation viewing and free viewing. Synchronization is observable when viewing conditions are held constant. Synchronization is abolished when comparing across viewing conditions that impose different gaze patterns during naturalistic viewing.

visual cortex, in part, depends on consistent viewing conditions. This result is consistent with the observation that eye position during unconstrained viewing of professionally produced movie is reproducible across viewers (Dorr, Martinetz, Gegenfurtner, & Barth, 2010).

4.4.3 Feature-based analysis

The feature extraction procedure, applied across visual and auditory modalities, resulted in a set of seven features (Figure 4.5). Inspection of the content of the movie clips at the times corresponding to the minima and maxima (labels 1-4 in Figure 4.5, A) indicated that the extraction procedures reliably parameterize the features of interest. In general, features were not strongly correlated with each other, with the exception of the two features derived from image statistics, luminance and optical flow (Figure 4.5 ,C).

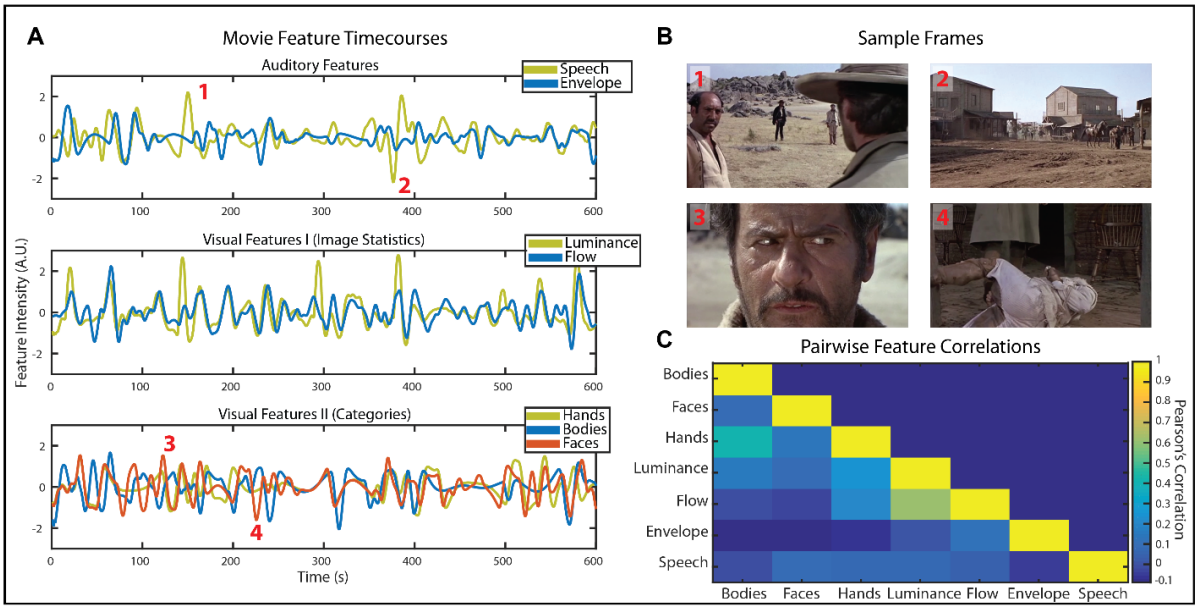

Figure 4.5. Feature extraction procedure. A: Seven features of varying complexity across visual and auditory processing were extracted from the stimulus using a combination of automated and manual approaches. B: Sample frames from the maxima and minima of two features, human-produced speech and visually presented faces, illustrate that the feature extraction procedures quantify changes in perceived feature intensity. For instance, a peak in human speech intensity corresponds to a conversation, while a valley corresponds to a landscape. A peak in visually presented face corresponds to a full-frame face, while a valley corresponds to a body with an obscured face. C: The correlation between pairs of features was generally weak, with the exception of the two visual features based on image statistics: luminance and optical flow.

Correlation maps generated from the time-series for each feature category were in agreement with known functional neuroanatomy (Figure 4.6) (Eggebrecht et al., 2014; Wilson, Molnar-Szakacs, & Iacoboni, 2008), and were evaluated using a T-statistic to identify voxels with correlation coefficients that deviate from a null distribution in which there is no observed correlation between signals (see methods). For instance, in the auditory domain, voxels in the bilateral superior temporal gyrus (STG) had the highest correlation coefficients to the audio envelope feature time-series, while the correlation

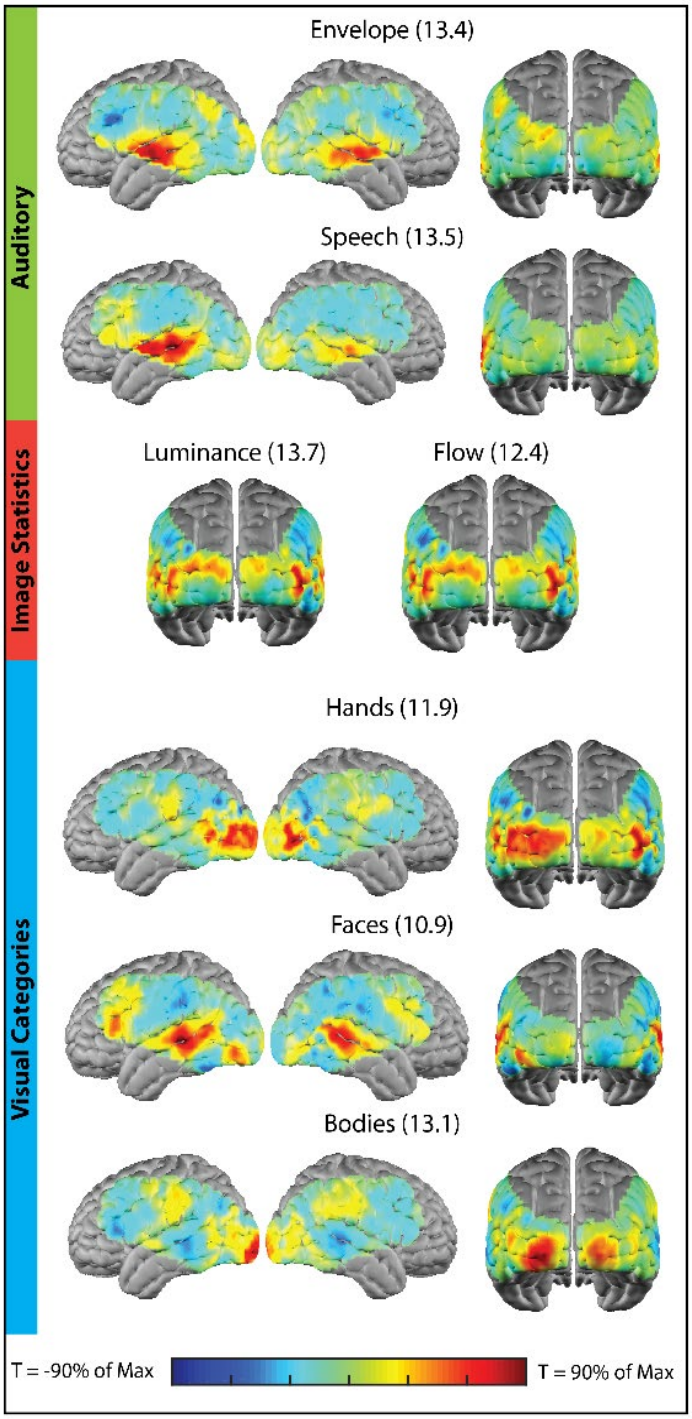

Figure 4.6. Correlation maps for individual movie features. Maps represent the group averaged map across individual feature maps for each of the 10 subjects included in the analysis. Correlation maps for each of the seven visual and auditory movie features highlight cortical regions related to processing those features during naturalistic viewing. Individual maps are scaled to 90% of the maximum T-statistic for each map, indicated in parentheses next to each map title.

between voxelwise ΔHbO_2 and the speech feature revealed a left-lateralized response in the STG and left prefrontal cortex.

For visual features generated by image statistics (luminance and flow), voxels in visual cortex have the highest correlation coefficients between the ΔHbO_2 time-series in these regions and the feature time-series. Conversely, the set of visual feature time-courses for higher-level visual features revealed patterns of elevated correlation coefficients across broader constellations of regions. For instance, the map of face processing during naturalistic viewing, generated by computing the voxelwise correlation between the ΔHbO_2 time-series and the visually presented faces time series, not only involved extrastriate visual regions, but also auditory and speech processing regions, underscoring that features were not present in isolation during the naturalistic viewing task (Wilson et al., 2008). Similarly, the correlation coefficient between voxelwise ΔHbO_2 and the time-course of visually presented bodies was elevated in voxels in the visual cortex and voxels in the inferior regions surrounding the central sulcus.

4.4.4 Hierarchical feature contrasts

Within the set of features used for functional mapping, individual features differed in complexity. For instance, the audio envelope, a low-level feature, indexed non-specific changes in stimulus audio intensity. Changes in audio intensity during movie viewing may be driven by factors such as environmental sounds, music, or human produced speech. Processing human produced speech is a more complex auditory task with both auditory and linguistic components, and was indexed by a dedicated, higher-level language feature (Juha M. Lahnakoski et al., 2012). Consequently, the set of auditory features used in this analysis was both hierarchical and potentially overlapping. To evaluate the

relationship between these hierarchical auditory features, a paired T-test was computed between the correlation maps for the audio envelope and speech features (Figure 4.7), resulting in a map of regions that preferentially respond to speech relative to other sounds indexed by the envelope feature. Relative to the correlation map for the speech feature alone (Figure 4.6), the contrasted map in Figure 4.7 evaluates a region's selectivity for one feature over another and provided more detailed mapping of regions (e.g. left prefrontal cortex, or Broca's area) involved in naturalistic speech processing.

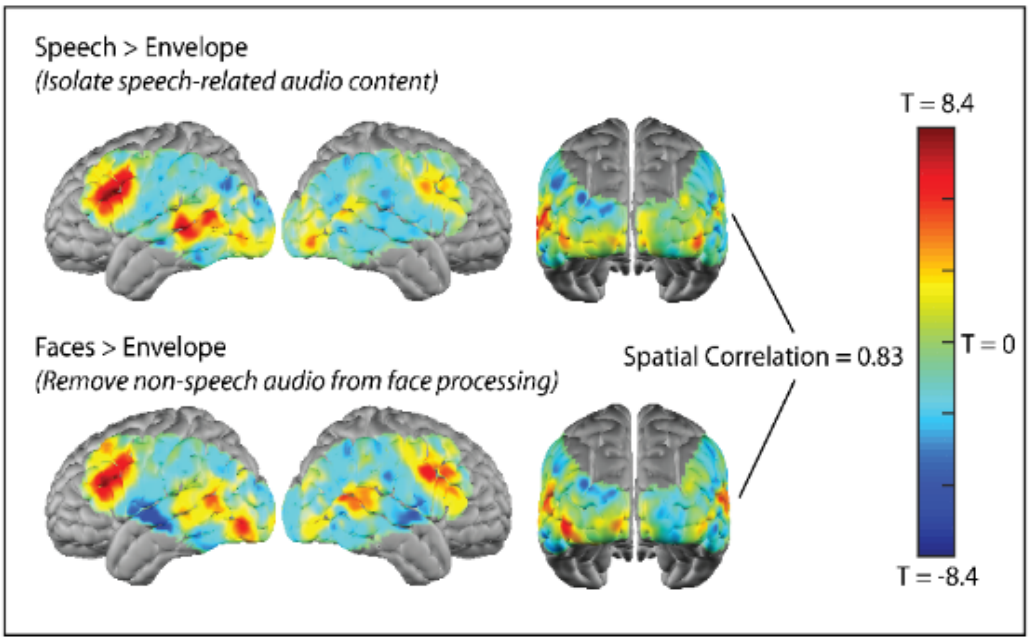

Figure 4.7. Maps for pairwise feature contrasts. Maps represent the group averaged map across individual feature maps for each of the 10 subjects included in the analysis. Paired T-tests between sets of features aimed at identifying regions related to speech processing during naturalistic viewing reveal that spatially convergent maps can be generated by contrasting disparate, but conceptually related features. Top: Contrast between the speech and auditory envelope features. Bottom: Contrast between the visually presented faces and auditory envelope features.

Hierarchical features were not limited to features within a single modality. During naturalistic viewing of the stimulus, visually presented human faces co-occurred with auditorily presented human speech. Consequently, the correlation map for the visually

presented face feature may serve as a surrogate feature for mapping cortical responses to social information, specifically human speech (Juha Marko Lahnakoski et al., 2012). However, other ambient sounds may also co-occur with visually presented faces, which are indexed by the auditory envelope. To test this hypothesis, the paired T-test described above was repeated for the face and auditory envelope features (Figure 4.7).

The spatial correlation between the maps generated using these two approaches to isolating speech processing (or contrasted feature maps) was r = 0.83, indicating good agreement. Therefore, by contrasting individual features, cortical responses to movie stimuli were further dissected, evaluating a given region's preference for one feature over another.

4.5 Discussion

In the present study, we used passive movie viewing, a naturalistic sensory stimulation paradigm, to evaluate the feasibility of measuring synchronized, movie-evoked cortical responses in healthy adult participants using HD-DOT. This synchronization, as indexed by the voxelwise correlation coefficient between oxy-hemoglobin responses measured across repeated viewings, was most prominent in auditory and visual cortex, highlighting that passive movie viewing is an effective tool for engaging distributed, multi-modal cortical regions (Hasson et al., 2004). Further, the spatial maps of correlation coefficients generated within participants and between participants both demonstrated elevated correlations during repeated stimulus viewings, underscoring that naturalistic stimuli reliably drive cortical activity despite the task's highly unconstrained conditions. The magnitude of the correlation coefficients was greatly diminished when participants viewed different, non-overlapping movie segments.

While high synchronization was observed both within and between participants over the HD-DOT field of view, this analysis approach did not relate features contained within the movie to specific cortical areas. In order to leverage the reliable cortical responses to the stimulus and relate them to naturalistic information processing, a feature decomposition strategy was employed to parameterize the movie stimulus (Bartels & Zeki, 2004; Juha M. Lahnakoski et al., 2012; Russ & Leopold, 2015). In the initial feature set, seven visual and auditory features of varying complexity were extracted from the stimulus. These features were subsequently used to functionally map cortical regions related to feature-specific processing; highlighting that, despite the richness and concurrent multi-modal stimulation associated with naturalistic tasks, tracking the intensity of individual features encountered during naturalistic viewing provides an effective strategy for parameterizing and mapping the complex movie stimulus.

Both synchronization and feature-based mapping strategies have been successfully incorporated in neuroimaging research using other modalities. Inter- and intra-subject synchronization during naturalistic viewing was first demonstrated using fMRI and has been shown in subsequent studies investigating the reproducibility of movie-evoked cortical responses (Hasson et al., 2010, 2004). Similarly, feature-based decomposition of naturalistic stimuli, using both manual and automated decoding approaches, has been incorporated in imaging work in both humans and non-human primates, highlighting that naturalistic tasks are suitable for mapping brain activity in a manner comparable to more constrained stimuli commonly utilized in functional mapping experiments (Bartels & Zeki, 2004; Russ & Leopold, 2015).

The present work is extension of these analytic tools to optical neuroimaging modalities, leveraging the relatively high resolution and broad coverage of the superficial cortex that HD-DOT offers compared to sparse fNIRS. Stimuli such as *The Good, the Bad, and the Ugly*, are narrative movies produced for entertainment; consequently, the "tasks" embedded in processing a feature film are complex, rich, and concurrent. Prior work using fNIRS has also used video stimuli, although generally with the goal of understanding a targeted and constrained information processing task. For example, fNIRS experiments investigating the development of specialized cortical responses to social stimuli have successfully leveraged the richness of video stimuli with human actors (S. Lloyd-Fox et al., 2017; Sarah Lloyd-Fox et al., 2009). Further, these responses have been shown to be sensitive to altered developmental trajectories (S. Lloyd-Fox et al., 2013). Depending on the study, these targeted videos can be optimized for the specific task of interest. On the other hand, because social interactions are inherently rich, multi-modal experiments, video stimuli are an effective tool for recapitulating this richness in a repeatable and controlled manner. By replacing a video stimulus tailored for assessing a specific domain with a feature film, as done in the present work, multiple sensory and cognitive processing domains can be assessed concurrently using a single, integrated movie stimulus. Outside of the laboratory, information is rarely encountered in a single sensory domain under rigidly controlled stimulus presentation parameters, underscoring the ecological relevance associated with free viewing tasks as implemented in this work.

Movie viewing tasks also afford practical advantages for special populations of interest. For instance, toddlers and school age children may find measurements of task-evoked brain activity relying on highly constrained and isolated stimuli to be boring,

repetitive, or predictable (Vanderwal et al., 2018). Indeed, work using fMRI indicates that naturalistic viewing tasks in toddlers and school age children reduces head motion, a substantial source of artifact. Further, the extent to which a child shows synchronized brain responses during naturalistic viewing correlates with behavioral assessments of mathematical and linguistic ability. Future work using naturalistic viewing tasks in conjunction with optical neuroimaging can leverage the practical advantages and scientific value of these paradigms alongside comfortable and wearable instrumentation, such as HD-DOT, that is particularly well suited for pediatric imaging (Ferradal et al., 2016).

One limitation of the naturalistic viewing task, as implemented in this work, is the lack of measured behavioral responses. Behavioral responses can track participant comprehension and attentiveness throughout the task, two variables that have been previously shown to modulate cortical responses measured during naturalistic viewing (Byrge et al., 2015; Campbell et al., 2015; Hasson et al., 2008). Possible behavioral responses include comprehension assessments following the experiment (Hasson et al., 2008) and recording eye position during the experiment (Wang, Freeman, Merriam, Hasson, & Heeger, 2012). Indeed, while eye position during viewing of a professionally produced movie is generally reproducible across subjects, gaze position has been reported to vary in special populations, including participants with Autism spectrum disorder (Norbury et al., 2009).

In the present work, the importance of eye position during naturalistic viewing was assessed during a separate experiment during which a subset of participants viewed an additional repetition of the stimulus while maintaining central fixation during the entire

viewing session. The correlation magnitude between voxelwise responses in visual cortex within viewing conditions indicated synchronized brain responses across participants; however, cortical responses from mismatched viewing conditions did not show the synchronization effect (Figure 4.4). In this experiment, participants confirmed their ability to comply with the fixation instructions by self-report. In future work, eye tracking can confirm compliance with experimenter-imposed gaze conditions and provide better characterization of eye position during free viewing.

An additional limitation of the present experiments is the utilization of a single movie clip. Importantly, not all movies are equally suitable for mapping particular features of interest. For instance, an animated movie with animal characters (e.g. *Finding Nemo*) would likely be poorly suited for mapping cortical responses to visually presented hands. Further, a boring or difficult to understand movie (e.g. *Waiting for Godot*) may result in diminished synchronization resulting from poor attentiveness or comprehension (Campbell et al., 2015). Future work employing naturalistic viewing paradigms can assess the efficacy of differing stimuli in performing functional brain mapping within a given domain of interest, as well as expand the set of features used for a given movie clip. In addition to the low and high-level sensory features used in this work, movie stimuli contain rich social, emotional, and narrative content that engage higher-order brain functions (Juha M. Lahnakoski et al., 2012; Juha Marko Lahnakoski et al., 2012). Sex-related differences have been reported in social and emotional processing in imaging and behavioral studies using non-naturalistic designs (Lang et al., 1998; Rodway, Wright, & Hardie, 2003). While the sample in this study was neither sufficiently powered nor balanced to assess potential sex-related effects, naturalistic designs such as passive

movie viewing offer a convergent experimental strategy to further explore these sex-related differences in social and emotional processing.

Using optical neuroimaging tools to study the brain during naturalistic viewing conditions has broad applicability for experimental questions demanding rich, engaging stimuli alongside wearable and ergonomic imaging tools (Pinti et al., n.d.; Vanderwal et al., 2018). Developmental cognitive neuroscience has benefitted from the broad applicability of optical neuroimaging tools for imaging the developing brain (Cristia et al., 2014; Emberson, Zinszer, Raizada, & Aslin, 2017; Karim & Perlman, 2017; S. Lloyd-Fox et al., 2017, 2013; Sarah Lloyd-Fox et al., 2009; Perlman, Luna, Hein, & Huppert, 2014). Paired with optical neuroimaging, the movie-based imaging paradigm described in this paper provides engaging and ecologically relevant study designs for understanding information processing across the lifespan, highlighting the richness of this paradigm for interrogating “real-life” brain function.

4.6 Acknowledgements

I would like to thank the participants in the naturalistic viewing experiments, as well as Ashley Nielsen, Broc Burke, Zachary Markow, Arefeh Sherafati, and Kalyan Tripathy for helpful comments regarding data collection and analysis. Further, the following funding sources for supported this research (across multiple investigators involved with the study): NIH R01EB009223, R01NS090874, R21NS098020, R21DC015884, U01EB027005, Bill & Melinda Gates Foundation OPP1184813; K01MH103594, R21MH109775; McDonnell Center for Systems Neuroscience.

4.7 Appendix

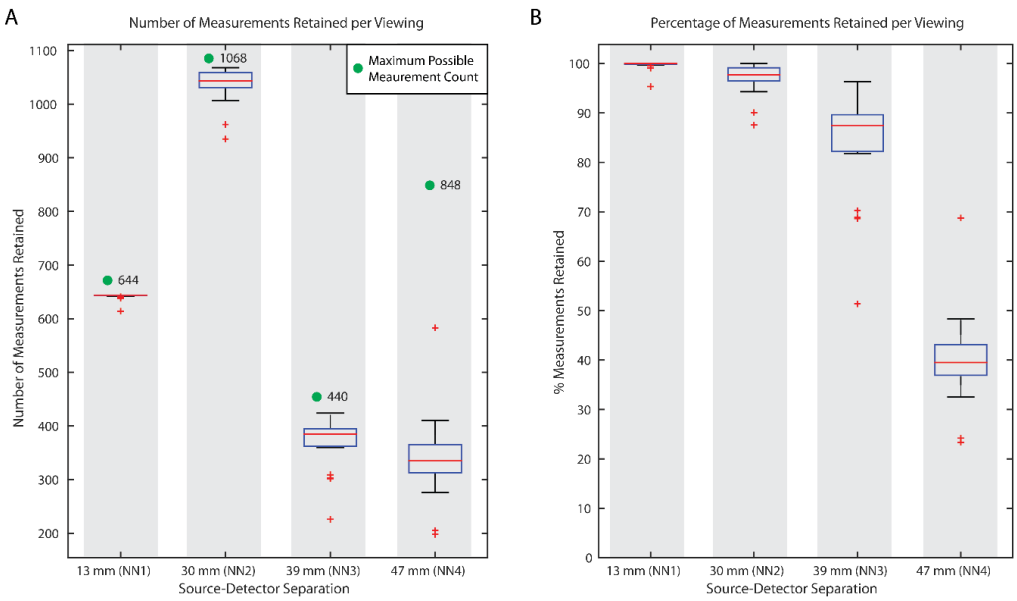

Figure 4.8. Measurement retention across all passive movie viewing runs. A: Box plots show the distributions for the number of measurements retained at the first four nearest-neighbor separations, with a mean of 642/644 NN1, 1034/1065 NN2, 368/440 NN3, and 339/848 NN4 measurements retained across all runs. B: Box plots show the percentage of measurements retained for the first four nearest-neighbor separations.

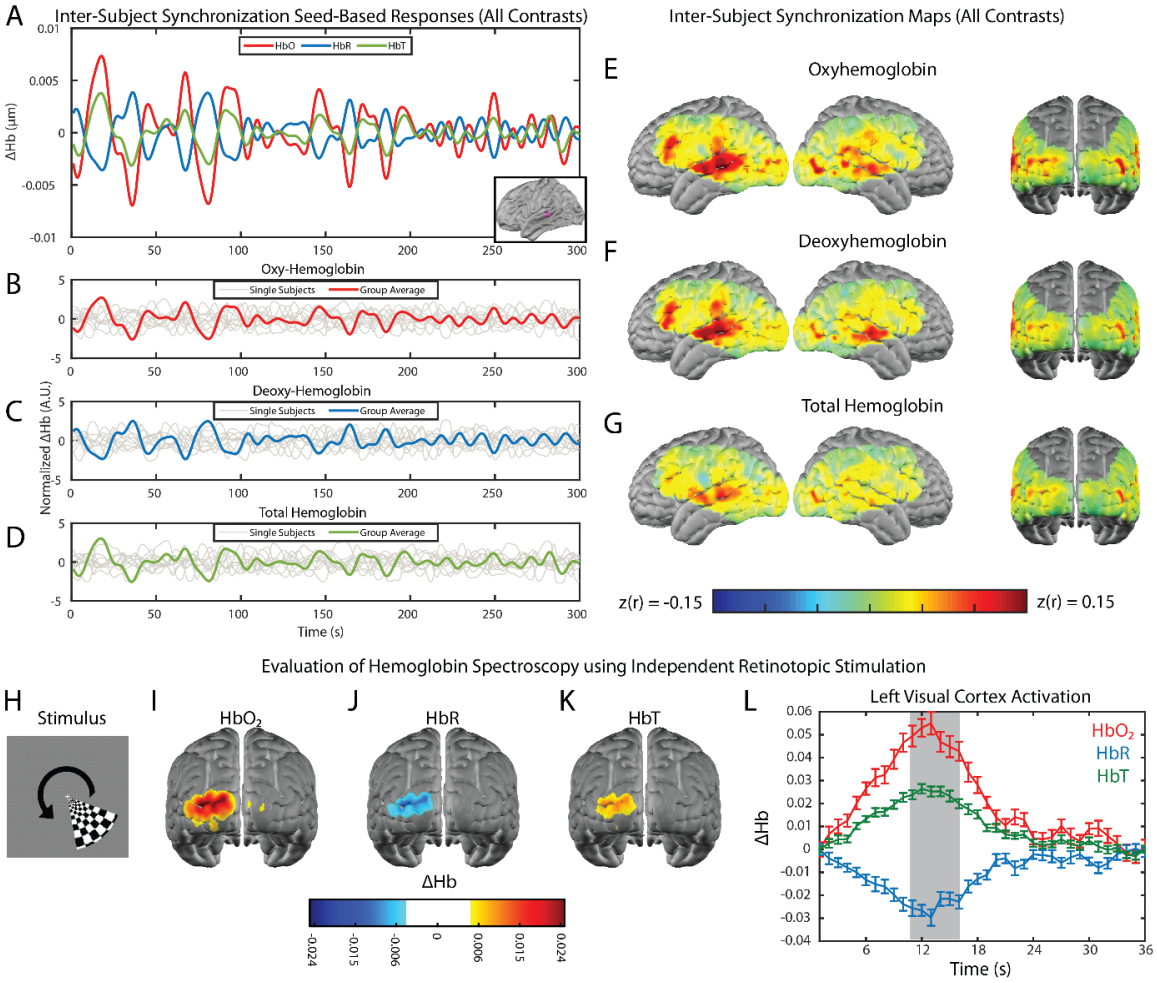

Figure 4.9. Inter-subject synchronization assessed across oxy-hemoglobin, deoxy-hemoglobin, and total hemoglobin contrasts. **A**: Timeseries for all three contrasts from a seed region in temporal cortex (inset) during a five-minute subset of the passive movie viewing experiment. **B**: The oxy-hemoglobin timeseries from the seed region during passive movie viewing in all 10 individual subjects (grey lines) and the group averaged oxy-hemoglobin response (red line). **C**: The deoxy-hemoglobin timeseries from the seed region during passive movie viewing in all 10 individual subjects (grey lines) and the group averaged deoxy-hemoglobin response (blue line). **D**: The total-hemoglobin timeseries from the seed region during passive movie viewing in all 10 individual subjects (grey lines) and the group averaged total-hemoglobin response (green line). **E**: Group averaged spatial map of correlation coefficients for the inter-subject synchronization analysis performed using the oxy-hemoglobin contrast. Voxel values represent Fisher's Z-transformed correlation coefficients. **F**: Group averaged spatial map of correlation coefficients for the inter-subject synchronization analysis performed using the deoxy-hemoglobin contrast. **G**: Group averaged spatial map of correlation coefficients for the inter-subject synchronization analysis performed using the total hemoglobin contrast.

H: Retinotopic mapping stimulus used for evaluation of hemoglobin spectroscopy in a subset of passive movie viewing participants (N = 5). **I:** Posterior view of the group-level block-averaged oxy-hemoglobin response, averaged over the shaded timepoints in Panel L. **J:** Posterior view of the group-level block-averaged deoxy-hemoglobin response, averaged over the shaded timepoints in Panel L. **I:** Posterior view of the group-level block-averaged total-hemoglobin response, averaged over the shaded timepoints in Panel L. **L:** Activation time traces from left visual cortex for the oxy-hemoglobin, deoxy-hemoglobin, and total hemoglobin contrasts.

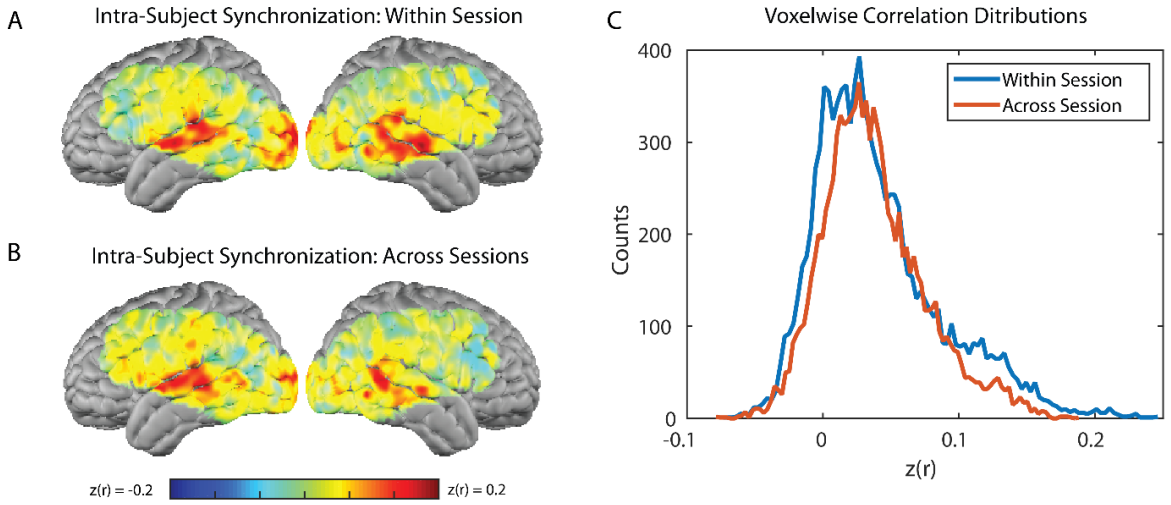

Figure 4.10. Run-dependent synchronization effects. Intra-subject synchronization was assessed separately for runs collected within the same session and runs collected across separate imaging sessions. A: Map of Fisher z-transformed Pearson's correlations for passive movie viewing runs within a single imaging session. B: Map of Fisher z-transformed Pearson's correlations for passive movie viewing runs across multiple imaging sessions. C: Voxelwise distributions of Fisher z-transformed Pearson's correlations for maps shown in A and B.

4.8 References

Bartels, A., & Zeki, S. (2004). Functional brain mapping during free viewing of natural scenes. *Human Brain Mapping*, *21*(2), 75–85. https://doi.org/10.1002/hbm.10153

Bluestone, A., Abdoulaev, G., Schmitz, C., Barbour, R., & Hielscher, A. (2001). Three-dimensional optical tomography of hemodynamics in the human head. *Optics Express*, *9*(6), 272–286.

Boas, D. A., Gaudette, T., Strangman, G., Cheng, X., Marota, J. J., & Mandeville, J. B. (2001). The accuracy of near infrared spectroscopy and imaging during focal

changes in cerebral hemodynamics. *NeuroImage*, *13*(1), 76–90. https://doi.org/10.1006/nimg.2000.0674

Brainard, D. H. (1997). The Psychophysics Toolbox. *Spatial Vision*, *10*(4), 433–436.

Buckner, R. L., Goodman, J., Burock, M., Rotte, M., Koutstaal, W., Schacter, D., … Dale, A. M. (1998). Functional-anatomic correlates of object priming in humans revealed by rapid presentation event-related fMRI. *Neuron*, *20*(2), 285–296.

Byrge, L., Dubois, J., Tyszka, J. M., Adolphs, R., & Kennedy, D. P. (2015). Idiosyncratic Brain Activation Patterns Are Associated with Poor Social Comprehension in Autism. *Journal of Neuroscience*, *35*(14), 5837–5850. https://doi.org/10.1523/JNEUROSCI.5182-14.2015

Campbell, K. L., Shafto, M. A., Wright, P., Tsvetanov, K. A., Geerligs, L., Cusack, R., … Tyler, L. K. (2015). Idiosyncratic responding during movie-watching predicted by age differences in attentional control. *Neurobiology of Aging*, *36*(11), 3045–3055. https://doi.org/10.1016/j.neurobiolaging.2015.07.028

Cantlon, J. F., & Li, R. (2013). Neural Activity during Natural Viewing of Sesame Street Statistically Predicts Test Scores in Early Childhood. *PLOS Biology*, *11*(1), e1001462. https://doi.org/10.1371/journal.pbio.1001462

Chang, W.-T., Jääskeläinen, I. P., Belliveau, J. W., Huang, S., Hung, A.-Y., Rossi, S., & Ahveninen, J. (2015). Combined MEG and EEG show reliable patterns of electromagnetic brain activity during natural viewing. *NeuroImage*, *114*, 49–56. https://doi.org/10.1016/j.neuroimage.2015.03.066

Church, J. A., Petersen, S. E., & Schlaggar, B. L. (2010). The “Task B problem” and other considerations in developmental functional neuroimaging. *Human Brain Mapping*, *31*(6), 852–862. https://doi.org/10.1002/hbm.21036

Cristia, A., Minagawa-Kawai, Y., Egorova, N., Gervain, J., Filippin, L., Cabrol, D., & Dupoux, E. (2014). Neural correlates of infant accent discrimination: an fNIRS study. *Developmental Science*, *17*(4), 628–635. https://doi.org/10.1111/desc.12160

Dehghani, H., Eames, M. E., Yalavarthy, P. K., Davis, S. C., Srinivasan, S., Carpenter, C. M., … Paulsen, K. D. (2008). Near infrared optical tomography using NIRFAST: Algorithm for numerical model and image reconstruction. *Communications in Numerical Methods in Engineering*, *25*(6), 711–732. https://doi.org/10.1002/cnm.1162

Dorr, M., Martinetz, T., Gegenfurtner, K. R., & Barth, E. (2010). Variability of eye movements when viewing dynamic natural scenes. *Journal of Vision*, *10*(10), 28–28. https://doi.org/10.1167/10.10.28

Eggebrecht, A. T., Ferradal, S. L., Robichaux-Viehoever, A., Hassanpour, M. S., Dehghani, H., Snyder, A. Z., … Culver, J. P. (2014). Mapping distributed brain function and networks with diffuse optical tomography. *Nature Photonics*, *8*(6), 448–454. https://doi.org/10.1038/nphoton.2014.107

Eggebrecht, A. T., White, B. R., Ferradal, S. L., Chen, C., Zhan, Y., Snyder, A. Z., … Culver, J. P. (2012). A quantitative spatial comparison of high-density diffuse optical tomography and fMRI cortical mapping. *NeuroImage*, *61*(4), 1120–1128. https://doi.org/10.1016/j.neuroimage.2012.01.124

Emberson, L. L., Zinszer, B. D., Raizada, R. D. S., & Aslin, R. N. (2017). Decoding the infant mind: Multivariate pattern analysis (MVPA) using fNIRS. *PLOS ONE*, *12*(4), e0172500. https://doi.org/10.1371/journal.pone.0172500

Ferradal, S. L., Eggebrecht, A. T., Hassanpour, M., Snyder, A. Z., & Culver, J. P. (2014). Atlas-based head modeling and spatial normalization for high-density diffuse optical tomography: in vivo validation against fMRI. *NeuroImage*, *85 Pt 1*, 117–126. https://doi.org/10.1016/j.neuroimage.2013.03.069

Ferradal, S. L., Liao, S. M., Eggebrecht, A. T., Shimony, J. S., Inder, T. E., Culver, J. P., & Smyser, C. D. (2016). Functional Imaging of the Developing Brain at the Bedside Using Diffuse Optical Tomography. *Cerebral Cortex*, *26*(4), 1558–1568. https://doi.org/10.1093/cercor/bhu320

Fonov, V., Evans, A., McKinstry, R., Almli, C., & Collins, D. (2009). Unbiased nonlinear average age-appropriate brain templates from birth to adulthood. *NeuroImage*, *47*, S102. https://doi.org/10.1016/S1053-8119(09)70884-5

Greene, D. J., Koller, J. M., Hampton, J. M., Wesevich, V., Van, A. N., Nguyen, A. L., … Dosenbach, N. U. F. (2018). Behavioral interventions for reducing head motion during MRI scans in children. *NeuroImage*, *171*, 234–245. https://doi.org/10.1016/j.neuroimage.2018.01.023

Gregg, N. M., White, B. R., Zeff, B. W., Berger, A. J., & Culver, J. P. (2010). Brain specificity of diffuse optical imaging: improvements from superficial signal regression and tomography. *Frontiers in Neuroenergetics*, *2*. https://doi.org/10.3389/fnene.2010.00014

Hamilton, L. S., & Huth, A. G. (2018). The revolution will not be controlled: natural stimuli in speech neuroscience. *Language, Cognition and Neuroscience*, *0*(0), 1–10. https://doi.org/10.1080/23273798.2018.1499946

Hassanpour, M. S., Eggebrecht, A. T., Culver, J. P., & Peelle, J. E. (2015). Mapping cortical responses to speech using high-density diffuse optical tomography. *NeuroImage*, *117*, 319–326. https://doi.org/10.1016/j.neuroimage.2015.05.058

Hassanpour, M. S., White, B. R., Eggebrecht, A. T., Ferradal, S. L., Snyder, A. Z., & Culver, J. P. (2014). Statistical analysis of high density diffuse optical tomography. *NeuroImage*, *85*, 104–116. https://doi.org/10.1016/j.neuroimage.2013.05.105

Hasson, U., Furman, O., Clark, D., Dudai, Y., & Davachi, L. (2008). Enhanced intersubject correlations during movie viewing correlate with successful episodic encoding. *Neuron*, *57*(3), 452–462. https://doi.org/10.1016/j.neuron.2007.12.009

Hasson, U., Malach, R., & Heeger, D. J. (2010). Reliability of cortical activity during natural stimulation. *Trends in Cognitive Sciences*, *14*(1), 40–48. https://doi.org/10.1016/j.tics.2009.10.011

Hasson, U., Nir, Y., Levy, I., Fuhrmann, G., & Malach, R. (2004). Intersubject Synchronization of Cortical Activity During Natural Vision. *Science*, *303*(5664), 1634–1640. https://doi.org/10.1126/science.1089506

Heer, W. A. de, Huth, A. G., Griffiths, T. L., Gallant, J. L., & Theunissen, F. E. (2017). The hierarchical cortical organization of human speech processing. *Journal of Neuroscience*, 3267–16. https://doi.org/10.1523/JNEUROSCI.3267-16.2017

Hirsch, J., Zhang, X., Noah, J. A., & Ono, Y. (2017). Frontal temporal and parietal systems synchronize within and across brains during live eye-to-eye contact. *NeuroImage*, *157*, 314–330. https://doi.org/10.1016/j.neuroimage.2017.06.018

Honey, C. J., Thesen, T., Donner, T. H., Silbert, L. J., Carlson, C. E., Devinsky, O., … Hasson, U. (2012). Slow Cortical Dynamics and the Accumulation of Information over Long Timescales. *Neuron*, *76*(2), 423–434. https://doi.org/10.1016/j.neuron.2012.08.011

Karim, H. T., & Perlman, S. B. (2017). Neurodevelopmental maturation as a function of irritable temperament. *Human Brain Mapping*, *38*(10), 5307–5321. https://doi.org/10.1002/hbm.23742

Kauttonen, J., Hlushchuk, Y., & Tikka, P. (2015). Optimizing methods for linking cinematic features to fMRI data. *NeuroImage*, *110*, 136–148. https://doi.org/10.1016/j.neuroimage.2015.01.063

Ki, J. J., Kelly, S. P., & Parra, L. C. (2016). Attention Strongly Modulates Reliability of Neural Responses to Naturalistic Narrative Stimuli. *Journal of Neuroscience*, *36*(10), 3092–3101. https://doi.org/10.1523/JNEUROSCI.2942-15.2016

Lahnakoski, Juha M., Salmi, J., Jääskeläinen, I. P., Lampinen, J., Glerean, E., Tikka, P., & Sams, M. (2012). Stimulus-Related Independent Component and Voxel-Wise Analysis of Human Brain Activity during Free Viewing of a Feature Film. *PLOS ONE*, *7*(4), e35215. https://doi.org/10.1371/journal.pone.0035215

Lahnakoski, Juha Marko, Glerean, E., Salmi, J., Jääskeläinen, I. P., Sams, M., Hari, R., & Nummenmaa, L. (2012). Naturalistic fMRI Mapping Reveals Superior Temporal Sulcus as the Hub for the Distributed Brain Network for Social Perception. *Frontiers in Human Neuroscience*, *6*. https://doi.org/10.3389/fnhum.2012.00233

Lang, P. J., Bradley, M. M., Fitzsimmons, J. R., Cuthbert, B. N., Scott, J. D., Moulder, B., & Nangia, V. (1998). Emotional arousal and activation of the visual cortex: An fMRI analysis. *Psychophysiology*, *35*(2), 199–210.

Lankinen, K., Saari, J., Hari, R., & Koskinen, M. (2014). Intersubject consistency of cortical MEG signals during movie viewing. *NeuroImage*, *92*, 217–224. https://doi.org/10.1016/j.neuroimage.2014.02.004

Lankinen, Kaisu, Saari, J., Hlushchuk, Y., Tikka, P., Parkkonen, L., Hari, R., & Koskinen, M. (2018). Consistency and similarity of MEG- and fMRI-signal time courses during movie viewing. *NeuroImage*, *173*, 361–369. https://doi.org/10.1016/j.neuroimage.2018.02.045

Lerner, Y., Honey, C. J., Silbert, L. J., & Hasson, U. (2011). Topographic mapping of a hierarchy of temporal receptive windows using a narrated story. *The Journal of Neuroscience: The Official Journal of the Society for Neuroscience*, *31*(8), 2906–2915. https://doi.org/10.1523/JNEUROSCI.3684-10.2011

Liu, Y., Piazza, E. A., Simony, E., Shewokis, P. A., Onaral, B., Hasson, U., & Ayaz, H. (2017). Measuring speaker–listener neural coupling with functional near infrared spectroscopy. *Scientific Reports*, *7*, 43293. https://doi.org/10.1038/srep43293

Lloyd-Fox, S., Begus, K., Halliday, D., Pirazzoli, L., Blasi, A., Papademetriou, M., … Elwell, C. E. (2017). Cortical specialisation to social stimuli from the first days to

the second year of life: A rural Gambian cohort. *Developmental Cognitive Neuroscience*, *25*, 92–104. https://doi.org/10.1016/j.dcn.2016.11.005

Lloyd-Fox, S., Blasi, A., Elwell, C. E., Charman, T., Murphy, D., & Johnson, M. H. (2013). Reduced neural sensitivity to social stimuli in infants at risk for autism. *Proc. R. Soc. B*, *280*(1758), 20123026. https://doi.org/10.1098/rspb.2012.3026

Lloyd-Fox, Sarah, Blasi, A., Volein, A., Everdell, N., Elwell, C. E., & Johnson, M. H. (2009). Social Perception in Infancy: A Near Infrared Spectroscopy Study. *Child Development*, *80*(4), 986–999. https://doi.org/10.1111/j.1467-8624.2009.01312.x

Matusz, P. J., Dikker, S., Huth, A. G., & Perrodin, C. (2018). Are We Ready for Real-world Neuroscience? *Journal of Cognitive Neuroscience*, 1–12. https://doi.org/10.1162/jocn_e_01276

Miyai, I., Tanabe, H. C., Sase, I., Eda, H., Oda, I., Konishi, I., … Kubota, K. (2001). Cortical Mapping of Gait in Humans: A Near-Infrared Spectroscopic Topography Study. *NeuroImage*, *14*(5), 1186–1192. https://doi.org/10.1006/nimg.2001.0905

Moraczewski, D., Chen, G., & Redcay, E. (2018). Inter-subject synchrony as an index of functional specialization in early childhood. *Scientific Reports*, *8*(1), 2252. https://doi.org/10.1038/s41598-018-20600-0

Nguyen, M., Vanderwal, T., & Hasson, U. (2019). Shared understanding of narratives is correlated with shared neural responses. *NeuroImage*, *184*, 161–170. https://doi.org/10.1016/j.neuroimage.2018.09.010

Noah, J. A., Ono, Y., Nomoto, Y., Shimada, S., Tachibana, A., Zhang, X., … Hirsch, J. (2015). fMRI Validation of fNIRS Measurements During a Naturalistic Task. *Journal of Visualized Experiments : JoVE*, (100). https://doi.org/10.3791/52116

Norbury, C. F., Brock, J., Cragg, L., Einav, S., Griffiths, H., & Nation, K. (2009). Eye-movement patterns are associated with communicative competence in autistic spectrum disorders. *Journal of Child Psychology and Psychiatry*, *50*(7), 834–842. https://doi.org/10.1111/j.1469-7610.2009.02073.x

Ono, Y., Noah, J. A., Zhang, X., Nomoto, Y., Suzuki, T., Shimada, S., … Hirsch, J. (2015). Motor learning and modulation of prefrontal cortex: an fNIRS assessment. *Journal of Neural Engineering*, *12*(6), 066004. https://doi.org/10.1088/1741-2560/12/6/066004

Perlman, S. B., Luna, B., Hein, T. C., & Huppert, T. J. (2014). fNIRS evidence of prefrontal regulation of frustration in early childhood. *NeuroImage*, *85*, 326–334. https://doi.org/10.1016/j.neuroimage.2013.04.057

Pinti, P., Tachtsidis, I., Hamilton, A., Hirsch, J., Aichelburg, C., Gilbert, S., & Burgess, P. W. (n.d.). The present and future use of functional near-infrared spectroscopy (fNIRS) for cognitive neuroscience. *Annals of the New York Academy of Sciences*, *0*(0). https://doi.org/10.1111/nyas.13948

Piper, S. K., Krueger, A., Koch, S. P., Mehnert, J., Habermehl, C., Steinbrink, J., … Schmitz, C. H. (2014). A wearable multi-channel fNIRS system for brain imaging in freely moving subjects. *NeuroImage*, *85 Pt 1*, 64–71. https://doi.org/10.1016/j.neuroimage.2013.06.062

Poulsen, A. T., Kamronn, S., Dmochowski, J., Parra, L. C., & Hansen, L. K. (2017). EEG in the classroom: Synchronised neural recordings during video presentation. *Scientific Reports*, *7*, 43916. https://doi.org/10.1038/srep43916

Power, J. D., Barnes, K. A., Snyder, A. Z., Schlaggar, B. L., & Petersen, S. E. (2012). Spurious but systematic correlations in functional connectivity MRI networks arise from subject motion. *NeuroImage*, *59*(3), 2142–2154. https://doi.org/10.1016/j.neuroimage.2011.10.018

Rodway, P., Wright, L., & Hardie, S. (2003). The valence-specific laterality effect in free viewing conditions: The influence of sex, handedness, and response bias. *Brain and Cognition*, *53*(3), 452–463. https://doi.org/10.1016/S0278-2626(03)00217-3

Russ, B. E., & Leopold, D. A. (2015). Functional MRI mapping of dynamic visual features during natural viewing in the macaque. *NeuroImage*, *109*, 84–94. https://doi.org/10.1016/j.neuroimage.2015.01.012

Saager, R. B., & Berger, A. J. (2005). Direct characterization and removal of interfering absorption trends in two-layer turbid media. *Journal of the Optical Society of America. A, Optics, Image Science, and Vision*, *22*(9), 1874–1882.

Salmi, J., Roine, U., Glerean, E., Lahnakoski, J., Nieminen-von Wendt, T., Tani, P., … Sams, M. (2013). The brains of high functioning autistic individuals do not synchronize with those of others. *NeuroImage: Clinical*, *3*, 489–497. https://doi.org/10.1016/j.nicl.2013.10.011

Suzuki, M., Miyai, I., Ono, T., & Kubota, K. (2008). Activities in the frontal cortex and gait performance are modulated by preparation. An fNIRS study. *NeuroImage*, *39*(2), 600–607. https://doi.org/10.1016/j.neuroimage.2007.08.044

Vanderwal, T., Eilbott, J., & Castellanos, F. X. (2018). Movies in the magnet: Naturalistic paradigms in developmental functional neuroimaging. *Developmental Cognitive Neuroscience*. https://doi.org/10.1016/j.dcn.2018.10.004

Vanderwal, T., Kelly, C., Eilbott, J., Mayes, L. C., & Castellanos, F. X. (2015). Inscapes: A movie paradigm to improve compliance in functional magnetic resonance imaging. *NeuroImage*, *122*, 222–232. https://doi.org/10.1016/j.neuroimage.2015.07.069

Wang, H. X., Freeman, J., Merriam, E. P., Hasson, U., & Heeger, D. J. (2012). Temporal eye movement strategies during naturalistic viewing. *Journal of Vision*, *12*(1), 16–16. https://doi.org/10.1167/12.1.16

White, B. R., & Culver, J. P. (2010a). Phase-encoded retinotopy as an evaluation of diffuse optical neuroimaging. *NeuroImage*, *49*(1), 568–577. https://doi.org/10.1016/j.neuroimage.2009.07.023

White, B. R., & Culver, J. P. (2010b). Quantitative evaluation of high-density diffuse optical tomography: in vivo resolution and mapping performance. *Journal of Biomedical Optics*, *15*(2), 026006. https://doi.org/10.1117/1.3368999

Wilson, S. M., Molnar-Szakacs, I., & Iacoboni, M. (2008). Beyond Superior Temporal Cortex: Intersubject Correlations in Narrative Speech Comprehension. *Cerebral Cortex*, *18*(1), 230–242. https://doi.org/10.1093/cercor/bhm049

Yücel, M. A., Selb, J. J., Huppert, T. J., Franceschini, M. A., & Boas, D. A. (2017). Functional Near Infrared Spectroscopy: Enabling routine functional brain imaging. *Current Opinion in Biomedical Engineering*, *4*, 78–86. https://doi.org/10.1016/j.cobme.2017.09.011

Zaki, J., & Ochsner, K. (2009). The Need for a Cognitive Neuroscience of Naturalistic Social Cognition. *Annals of the New York Academy of Sciences*, *1167*(1), 16–30. https://doi.org/10.1111/j.1749-6632.2009.04601.x

Zeff, B. W., White, B. R., Dehghani, H., Schlaggar, B. L., & Culver, J. P. (2007). Retinotopic mapping of adult human visual cortex with high-density diffuse optical tomography. *Proceedings of the National Academy of Sciences of the United States of America*, *104*(29), 12169–12174. https://doi.org/10.1073/pnas.0611266104

Chapter 5: Discussion

5.1 Summary

High-density diffuse optical tomography is an optical neuroimaging technique that uses near-infrared light to measure cortical tissue oxygenation, which is an indirect readout of local neuronal activity (Raichle & Mintun, 2006). These measurements, taken on the surface of the head, are tomographically reconstructed into three-dimensional images of hemodynamics (Eggebrecht et al., 2014, 2012). Like other optical neuroimaging instruments, HD-DOT enables human neuroimaging in a variety of settings unavailable to other commonly used imaging modalities, including a patient's bedside, open/naturalistic environments, and regions where other imaging modalities are unavailable. Additionally, populations who find other modalities frightening or are contraindicated for other modalities are suitable for HD-DOT, including awake children and patients with implanted metal. Unlike other optical neuroimaging modalities, HD-DOT offers an expanded field-of-view and greater measurement density, enabling fMRI-comparable mapping of distributed brain function with a wearable and portable device.

To date, neuroimaging research using HD-DOT has focused on two avenues of work. The first avenue is validating the functionality of the instrument against established imaging paradigms, showing that unlike fNIRS, HD-DOT can be considered a surrogate for commonly used imaging modalities such as fMRI. This validation work relied on classic paradigms mapping stereotyped responses implemented with fMRI, such as the

retinotopic organization of visual cortex (White & Culver, 2010a; Zeff, White, Dehghani, Schlaggar, & Culver, 2007). In other studies that have included subject-matched fMRI, spatial agreement between the modalities is quantifiable, and shows excellent localization accuracy (Eggebrecht et al., 2014, 2012). The second line of research involves implementing HD-DOT in studies with research questions demanding the unique advantages of optical neuroimaging. For instance, studies of speech perception using HD-DOT are unencumbered by scanner noise, providing an acoustic environment more readily optimized for studies of audition (Hassanpour, Eggebrecht, Culver, & Peelle, 2015). Further, where as other modalities require patients to be transported to imaging equipment, HD-DOT instrumentation can be utilized in the clinical environment, such as the neonatal intensive care unit (Ferradal et al., 2016).

This thesis work was conducted in a lab focused on technology development and optimization and is therefore targeted at identifying and validating novel applications for HD-DOT. The first question addressed in this work is the extent to which measurement density in an optical neuroimaging array impacts the reconstruction of fMRI-comparable images (Chapter 2). This work uses *in* vivo data to extend prior work using simulated reconstructions (White & Culver, 2010b) and indicates that sparse measurement arrays are prone to distorted or mis-localized activations to a greater extent than dense arrays. Having established the importance of dense measurement arrays for localization of cortical activations, the remainder of the thesis aims to establish methods to localize and map brain function in another population considered to be exceptionally suitable for optical neuroimaging: children (Aslin & Mehler, 2005; S. Lloyd-Fox, Blasi, & Elwell, 2010).

This objective was accomplished in two steps. First, HD-DOT performance was evaluated in a cohort of 7-10-year-old children (Chapter 3). This work was conducted in Cali, Colombia, and had the dual purpose of establishing HD-DOT as a method suitable for field-based neuroimaging assessments aimed at identifying malnutrition-related cortical deficits. However, instrumentation that is acceptable for developmental neuroimaging solves only half of the challenge. In addition to suitable instrumentation, developmental neuroimaging requires paradigms that are more engaging and stimulating than traditional block or event-related task designs. The naturalistic imaging tasks established in Chapter 4 are an attempt to fulfill this need, by using HD-DOT to measure cortical responses during a passive movie viewing task.

In this chapter, I provide a brief overview of the principal results shown in each chapter. Within each of the body chapters, the respective discussion section contextualizes the results within the current neuroimaging literature and highlights the implications of the results. Consequently, in this closing chapter, my discussion is more pointed towards the future research directions created by each of these lines of research.

5.2 Commentary on optical neuroimaging instrumentation

Unlike HD-DOT, other optical neuroimaging tools such as fNIRS use a sparse array of sources and detectors. This means that the measurement separation is usually at a single distance, and the measurements are usually not spatially overlapping (Boas, Chen, Grebert, & Franceschini, 2004; Boas et al., 2001). The results of these two factors is that brain hemodynamics measured with fNIRS are susceptible to contamination by superficial

and systemic nuisance physiology (Saager & Berger, 2005), and that lateral resolution afforded by non-overlapping measurements permits only coarse localization of activations. Consequently, while an fNIRS instrument may successfully detect an activation resulting from neuronal activity, localization of that activation may be less reliable than localizations detected using denser measurement arrays. Using subject-matched fMRI, the work in this chapter aimed to evaluate the effect of measurement density on reconstruction of fMRI comparable images.

We found that in general, using a set of three image agreement metrics, across three language processing tasks, that images reconstructed with HD-DOT agreed with fMRI more so than images reconstructed with sparse arrays. We also found that accounting for superficial and systemic nuisance physiology in the sparse arrays improved the image agreement between sparsely-constructed images and subject-matched fMRI.

The results of this work indicate that if a study aims to localize brain activity with fMRI-comparable accuracy, then measurement density must be considered as a critical imaging system speficifcation. Minimally, in the absence of a dense measurement array, incorporation of superficial signal regression methods is a practical and important data quality improvement technique, where data quality is here operationalized as the agreement between an image and subject-matched fMRI.

An important contextualizing factor for this work is that many fNIRS studies do not explicitly wish to localize fMRI-comparable images. This factor is illustrated that while

some fNIRS studies using sparse arrays do use image reconstruction techniques (Jackson et al., 2019), many more studies do not, and instead present channel-wise statistics or topographically reconstructed images (Sarah Lloyd-Fox et al., 2009). While some techniques do exist to optimize array design and placement to better attribute the measured fNIRS signal to underlying cortical signals (Brigadoi, Salvagnin, Fischetti, & Cooper, 2018; Morais, Balardin, & Sato, 2018; Yamamoto et al., 2002), the reality remains that signal detection, not localization, remains the principal capability of many fNIRS studies. While some studies do attempt to attribute observed signal changes to underlying cortical structures, in the absence of an anatomical registration method (Singh, Okamoto, Dan, Jurcak, & Dan, 2005), these attributions are generally subjective and of limited precision. This anatomical localization capability stands in stark contrast to the emphasis placed on careful attention to brain anatomy espoused by fMRI researchers (Devlin & Poldrack, 2007) and may represent a reason why some neuroimaging researchers are hesitant to include fNIRS techniques in the suite of tools utilized in their laboratories.

Of course, detection of a hemodynamic change in a given fNIRS channel presupposes that (1) the array is consistently positioned across participants and (2) the array is appropriately designed such that it samples the cortical regions related to the experimental question. Consequently, even in studies that do not wish to localize a cortical response, and instead aim to simply detect a signal related to some brain state, task manipulation, or stimulus presentation, array geometry and placement represents a source of variance. One example of such a study that might prioritize the detection of a relevant signal over attribution or localization of that signal is the emerging use of fNIRS

in brain-computer interfaces, which aim to leverage the wearability and portability of these devises in this burgeoning application (Naseer & Hong, 2015).

One solution to the potential confound of array placement and design is to use tools to optimize these design decisions, as stated above. Another solution is, of course, to increase the resolution of the system using a dense measurement grid and incorporate image reconstruction steps that account for subject-specific brain anatomy. This solution increases the number of fibers associated with a system; therefore, instrument size increases accordingly. In situations demanding high portability, such as the brain-computer interface described above, fiberless systems (Chitnis et al., 2016) or systems using detection methods that permit more lightweight fibers (Bergonzi et al., 2018) are two solutions that enable researchers to overcome the potential trade-off between image quality and wearability.

Currently, HD-DOT systems utilized by the lab generate approximately 1,200 measurements per wavelength. Future evaluations of optical measurement density may continue exploring the relationship between cortical activation localization and measurement density by increasing the number of measurements, rather than decreasing the number of measurements. Rather than eroding image quality, this work would test whether the current measurement configuration is at the ceiling for activation localization precision, or whether further improvements are available. As has been done previously, such work may be carried out in simulation prior to constructing a new instrument. However, while theoretical image quality improvements may be achievable using greater measurement density, the theoretical improvements must be considered alongside

practical limitations, such as participant's hair, which may interact negatively with denser arrays with reduced combing ability, relative to instruments with less densely packed arrays.

Ultimately, the goals of this dissertation are better served by fMRI-quality localization, as they involve complex tasks or situations in which *a priori* decisions about cortical field-of-view are undesirable. Consequently, through a quantitative assessment of image overlap using optical data and fMRI, the work completed in this chapter supports the intuition that the results presented in subsequent chapters would not have been achievable with a sparse fNIRS system.

5.3 Commentary on using neuroimaging to predict malnutrition status

Optical neuroimaging instruments are substantially more portable than neuroimaging instruments such as MRI or PET. Consequently, researchers have used these instruments to interrogate brain function in settings that demand portability, due to the lack of nearby neuroimaging infrastructure capable of housing larger brain imaging tools (Sarah Lloyd-Fox et al., 2014; Roberts et al., 2017a; Wijeakumar, Kumar, Reyes, Tiwari, & Spencer, n.d.). In essence, tools such as fNIRS enable the establishment of mobile, field-based neuroimaging laboratories. An emerging application of this capability has been to use optical neuroimaging tools, including fNIRS, to study brain development in low-resource regions of the world, where traditional neuroimaging modalities are too expensive and too resource-intensive to be readily available. In these regions, conditions

such as childhood malnutrition are extremely prevalent. Extensive behavioral studies (Barrett, Radke-Yarrow, & Klein, 1982; Grantham-McGregor, 1995) and limited imaging research (Odabaş et al., 2005) show that malnutrition during early brain development has pervasive effects on cognition, socialization, emotion, motor abilities, and other domains, providing strong motivation for the need to fully characterize these deleterious and life-long consequences.

Relative to fNIRS, HD-DOT offers a broader cortical field-of-view, greater lateral resolution, and three-dimensional images of brain hemodynamics. Consequently, the goal of the work presented in Chapter 3 was to evaluate the performance of an HD-DOT instrument in Colombia, with the ultimate objective of eventually using HD-DOT to understand the neurological consequences associated with childhood malnutrition. One of the first portable fNIRS laboratories was established in The Gambia (Sarah Lloyd-Fox et al., 2014), and the first results from this field laboratory focused on feasibility of imaging, using a paradigm that produces stereotyped brain responses. Similarly, the work presented in Chapter 3 used a passive sensory paradigm (Eggebrecht et al., 2014; Petersen, Fox, Posner, Mintun, & Raichle, 1989) and measures of bilateral functional connectivity (Ferradal et al., 2016; Smyser et al., 2010; Thomason et al., 2013) to establish the performance of this instrument in a completely novel imaging environment. Relative to other work introducing optical neuroimaging instruments in field-environments, the work in Chapter 3 places an emphasis on data quality, using a set of real-time and post-hoc image quality metrics (Sherafati, Eggebrecht, Burns-Yocum, & Culver, 2017) to quantitatively evaluate HD-DOT performance in a field setting, showing that data quality

in Cali is comparable to data in St. Louis. Finally, because HD-DOT instruments incorporate a larger number of fiber optic cables to support a greater channel count, we evaluate the effect of reducing the channel count on the resulting reconstructed images.

The results of this work indicate that task-evoked and resting-state imaging in the cohort of 7-10-year-old children used in this sample produces the expected results and is of high quality. Relative to images reconstructed using sparser measurement arrays, the densely reconstructed images consistently localize cortical responses to stimuli, indicating that other instruments with fewer fibers and channels may successfully detect an activation, but localize the activation with substantially more variability than instruments using dense arrays. Further, the dense arrays incorporate a broader cortical field-of-view than other optical neuroimaging instruments, potentially reducing the need for subjective, *a priori* decisions about which structures to image and which structures to exclude from imaging.

The results of this initial field-based HD-DOT study set the stage for future investigation of a child's malnutrition burden. These investigations could rely in task-based imaging, in which a particular domain (e.g. social cognition (Sarah Lloyd-Fox et al., 2015, 2014); visual working memory (Wijeakumar et al., n.d.)) that is thought to be affected by a child's malnutrition status is interrogated using a task that probes the neural system underlying that domain. Selection of an appropriate task should likely be informed by behavioral data from the same population, which would enable formulation of an appropriate hypothesis. A complementary approach would be to leverage functional connectivity to assess the cortical systems within the field-of-view and use assessments

of an individual's network structure to classify an individual's malnutrition status. Functional connectivity during development is also predictive of future outcomes, highlighting the potential to identify individuals with developmental trajectories that are most seriously compromised by their malnutrition burden (Smyser et al., 2013; Wheelock et al., 2018).

While the potential for future study of malnutrition using HD-DOT is promising and includes multiple, complementary strategies for mapping the malnourished brain, these studies are limited by their descriptive nature. In other words, if successful, these future studies will provide a detailed characterization of how the brains of a malnourished individual differ from the brains of a well-nourished individual. Within the context of an academic teaching hospital, these descriptive studies are critical for providing a systems-level characterization of how brains differ between individuals and populations, and individuals in patient populations generally participate in imaging while potentially undergoing treatment. In the context of field imaging, prioritizing the largely scientific task of performing imaging to characterize or describe a patient population may not fully serve the needs of individuals and families who volunteer their time to participate in these studies. Neuroimaging in a global context, if implemented with the needs of the local communities who participate in imaging studies in mind, must push beyond the more constrained goal of describing disrupted brain function using novel imaging tools, and ensure that studies are designed such that potential future impact on local communities is maximized.

Future studies that not only characterize disrupted brain function but aim to improve the condition of global communities that participate in the studies may utilize several strategies to achieve this goal, including interventional studies and more critical methodological evaluation. Brain imaging may be used in conjunction with an intervention, such as a therapeutic food (Linneman et al., 2007; Manary, Ndkeha, Ashorn, Maleta, & Briend, 2004), to serve the dual purpose of (1) characterizing malnutrition status using imaging and (2) using imaging as one of multiple potential endpoints in a trial of various foods. This dual purpose has been implemented in only a limited number of global neuroimaging studies (Roberts et al., 2017b). Assessing intervention efficacy, even at a traditional teaching hospital, is a complex and resource-intensive question, and implementing such a study in a novel setting will only intensify those challenges. It requires expanding an imaging research team to include researchers developing interventions and is a goal a single lab may not realistically be expected to achieve in isolation. Consequently, other entities such as funding agencies, may have a larger role to play in ensuring that research teams have the resources necessary to conduct research that is both scientifically impactful and impactful to local communities who play host to research teams.

If the goal of a study is to make predictions about a child's developmental trajectory, then the use of neuroimaging over other methods must be critically evaluated and justified. This is not to say that neuroimaging is tool with limited predictive power or a limited role in clinical decision making, as both of these applications have been articulated extensively (Eggebrecht et al., 2017; Greene et al., 2016; Lee, Smyser, &

Shimony, 2013; Marrus et al., 2018). However, taking the unique demands of performing field research into account, groups that welcome neuroimaging researchers into their communities have a reasonable expectation that the researchers will positively impact their community, above and beyond intangible benefits such as publicity that is associated with being the site of a global neuroimaging study. If this expectation is valid, then the use of neuroimaging over other equally predictive tools should be a methodological decision that is explicitly evaluated and justified.

Outside of global neuroimaging studies, brain-computer interfaces are one orthogonal application that has benefitted from critically evaluating the methods used to create tools that read out physiological signals and use those signals in a computation, broadly construed. For instance, one goal of a brain-computer interface may be to read out and decode signals related to an individual's intended speech. As the organ system responsible for generating behavior, the central nervous system, particularly the brain, certainly contains signals related to intended speech. However, the signal generated by this system is of course repropagated to the periphery through the efferent pathways that carry centrally generated speech signals to articulatory structures. Engineers who have used electrical activity in these structures (e.g. jaw musculature) have been able to successfully implement a computer interface that reads out intended speech (Kapur, Kapur, & Maes, 2018). Of course, this result may have limited clinical utility for individuals with paralysis and consequently no readable signals in the musculature, but a key advantage of obtaining decodable signals from the periphery is the ease of implementation, relative to obtaining and decoding potentially more complex and noisy

signals from the central nervous system. This result provides a case study in critically evaluating whether the highest fidelity signal, whether it is to be used for brain-computer interface or a predictive algorithm, is localized to the central nervous system or elsewhere in the body. If the objective of a study is to obtain a signal that is to be used subsequently for prediction or in a computer interface, then the engineers developing the system should necessarily seek a high-fidelity signal for that purpose.

Consequently, returning to the global health context, if a study's stated objective is to predict malnutrition status, then the choice of neuroimaging must be justified against other measures such as anthropometry, and the advantages consequent from choosing an imaging-based signal over another signal must be stated. Similarly, if a study's stated goal is to predict future behavioral deficits or developmental trajectories, the choice of the signal supporting the predictive algorithm must be justified and contextualized among other available signals. For instance, in the case of a neonatal subject population, imaging is a potentially attractive signal choice, as it provides a signal that is available to be read out much earlier than a signal that would rely on overt or performed behavior (Smyser et al., 2013; Wheelock et al., 2018). While this imaging application is achievable in a research hospital, researchers are becoming increasingly aware of the amount of imaging data required to achieve appropriate signal-to-noise (Laumann et al., 2015), in addition to these tools' exquisite sensitivity to head motion (Power, Barnes, Snyder, Schlaggar, & Petersen, 2012). It is therefore reasonable to hypothesize that data collected in a non-academic setting will not meet these same stringent data quality criteria, making

achievability of adequate data quality another design consideration as methods move from the laboratory to non-laboratory settings.

The behavioral and neural system of interest further constrains the signal selection. For instance, early detection of motor deficits may be possible using accelerometer-based techniques, as continuous accelerometry provides a readout from the motor system that does not require completion of a specific task or imaging study (Hoyt et al., 2019). While this accelerometry study was implemented in an academic research setting, participants wore the accelerometers continuously, in contexts extending beyond the clinic. It is therefore reasonable to predict that data quality demands posed by a wearable accelerometer would be achievable in a variety of non-clinical settings. Furthermore, the method's low implementation cost means that actigraphy may readily achieve widespread adoption if deemed useful to implement in a low-resource context to monitor the motor system for diagnostic and predictive purposes.

The purpose of this discussion is to promote the intuition that research context matters. It is a critical consideration in study design; in particular, low-resource settings cause considerations to arise that may be unfamiliar or unnecessary relative to traditional academic research settings. Low-resource contexts demand more robust justification of chosen research methods than traditional academic contexts. This necessity arises because clinical research in an academic context generally unfolds concurrently with patient care, while the role of a clinical researcher may not be as distinctly compartmentalized in a low-resource context. Without this compartmentalization between clinical care and clinical research, researchers must consider both scientifically valuable

and clinically actionable components of their research with greater acuity. The results of the HD-DOT work in Colombia presented in Chapter 3 demonstrate that HD-DOT is feasible in a global, non-academic context, potentially enabling HD-DOT to be included in the suite of tools available for malnutrition research. However, assessing a method's *feasibility* is a distinct question from assessing a method's *suitability* for a given research question. This work aimed to address the former topic, and was therefore not intended to, and did not establish HD-DOT as the most appropriate method or signal source for patient classification, prediction of developmental trajectories, or intervention assessment. These questions must be addressed by future work using HD-DOT in field settings and should incorporate an assessment of methodological suitability and actionability of the research question as essential study design parameters.

5.4 Commentary on naturalistic brain imaging paradigms

In this work, the motivation for imaging the brain during passive movie viewing was a practical one. While optical neuroimaging instruments such as HD-DOT offer an imaging environment that is likely more comfortable for imaging task-evoked brain responses in children relative to more constrained and noisy environments associated with fMRI, task imaging paradigms used with HD-DOT are not similarly well-suited for children. Consequently, in an effort to design an imaging paradigm that incorporated sensory stimulation as well as higher-order cognitive processing in an engaging design, we identified passive movie viewing as a potential solution for imaging task-evoked cortical responses in children using an engaging, fun, and rich paradigm.

Movie viewing during functional brain imaging is part of a larger field of research using stimuli that more closely resemble the day-to-day naturalistic environment, relative to stimuli that are highly distilled, probe a targeted set of cognitive processing domains, and are presented under strictly controlled timing conditions. This field, naturalistic brain imaging, includes sensory processing tasks such as viewing rich, professionally-produced stimuli (Kauttonen, Hlushchuk, & Tikka, 2015; Juha Marko Lahnakoski et al., 2012; Moraczewski, Chen, & Redcay, 2018) (e.g. movies or television shows), but also investigates other domains including interacting with real environments, natural movements, and social interactions (Hirsch, Zhang, Noah, & Ono, 2017; Liu et al., 2017; Ono et al., 2015; Piper et al., 2014).

Passive viewing of movies or television shows offers an ideal blend of naturalistic features as well as features from more temporally controlled (i.e. block or event-related design) paradigms. Passive movie viewing is rich in the sense that it simultaneously engages multiple sensory domains in the context of a broader narrative structure that includes social, linguistic, and emotional processing to fully comprehend. However, unlike imaging using even more unconstrained stimuli or processing tasks, such as naturalistic social interactions, movie stimuli are repeatable and tunable, thereby permitting a degree of experimenter control unavailable with other naturalistic tasks. For instance, the same stimulus can be repeatedly presented to multiple participants without concern that the stimulus may vary from presentation to presentation, thereby inducing additional variance into measured cortical responses. Further, movie stimuli are tunable, in the sense that experimenters can manipulate the professionally-produced stimulus to address an

experimental question. For instance, to address how speech intelligibility impacts cortical processing in a naturalistic context where other communicative cues (e.g. facial expressions, body gestures) are available, an experimenter may present a stimulus with noise vocoded speech, which eliminates the intelligibility of the speech while holding other low-level acoustic features relatively constant. In contrast to a stimulus with fully intelligible speech, this contrast could probe cortical structures that respond differentially to speech intelligibility. This tunability stands in contrast to other, fully naturalistic imaging contexts, where experimental manipulations have to unfold in real-time, imposing more complex design demands upon the experimenter.

However, a key advantage of experimenter-designed stimuli relative to movie stimuli is that stimuli designed by the experimenter have known stimulus presentation parameters. This enables the experimenter to average together repetitions of the same stimulus type using a block design. Using more sophisticated event-related designs, experimenters may model expected cortical responses to presented stimuli and perform contrasts between pre-determined stimulus types. Consequently, naturalistic brain imaging paradigms generally demand more careful attention to the analysis of cortical responses to naturalistic stimuli, as these stimuli lack pre-designed presentation parameters for different types of stimuli. Often, the naturalistic stimulus itself must be analyzed to uncover the features and timing structures contained within the stimulus before proceeding to analysis of cortical responses related to stimulus processing.

In the passive movie viewing work introduced in Chapter 4, two complementary analysis approaches were used to analyze cortical hemodynamics during passive movie

viewing. The approaches are complementary in that one approach, inter/intra-subject synchronization makes no assumptions about the content of the stimulus, while the other approach, feature-based analysis, requires analysis of the stimulus itself in order to identify features that map onto information processing demands during movie viewing.

Given the unconstrained nature of free movie viewing, one may hypothesize that cortical responses may vary considerably across viewers, reflecting individual differences in viewing patters and idiosyncrasies in stimulus processing. Consequently, many cognitive neuroscientists were surprised by the result that, in the context of free viewing of a feature film, cortical responses to the stimulus are highly reproducible, both within and across individual viewers (Hasson, Nir, Levy, Fuhrmann, & Malach, 2004). This result has been explored using other imaging modalities (e.g. EEG, MEG) (Chang et al., 2015), and also using additional readouts such as eye-tracking (Dorr, Martinetz, Gegenfurtner, & Barth, 2010). In healthy-adults, eye-tracking convergently confirms that gaze patterns during free viewing are remarkably consistent across individual viewers, underscoring the notion that these stimuli direct viewers' attention in a controllable, reproducible manner (Norbury et al., 2009).

Using HD-DOT, we found reproducible, or synchronized patterns of brain activity during viewing of a feature film in healthy young adults. This reproducibility was observable both within subjects and across subjects, and included cortical regions implicated in sensory (i.e. visual and auditory) processing, as well as cortical systems required to process the narrative content of the stimulus (e.g. linguistic and social processing). Crucially, while eye-tracking in a limited number of participants revealed

reproducible gaze patterns across individuals, a gaze-based manipulation during movie viewing provided further insight into the origins of the reproducible cortical responses observed during movie viewing. During some repetitions, participants were directed to maintain central fixation over the course of the entire stimulus viewing, by foveating on a fixation cross overlaid on the center of the stimulus. Relative to free viewing conditions, in which participants can scan the full visual scene and fixate on the most relevant or dynamic regions, this gaze constraint introduced a distinct and artificial viewing pattern. The contrast between the two viewing patterns was evident by assessing cortical synchronization in visual cortex. When synchronization was assessed between runs with the same viewing condition, correlated hemodynamic responses were observable in visual cortex. However, when synchronization was assessed across disparate viewing conditions, synchronization was diminished. Consequently, this result indicates that synchronization in visual cortex, depends in part, on consistent gaze position during stimulus viewing. Accordingly, in stimuli that do not direct eye position as effectively as feature films, fixation patterns may vary more across subjects, resulting in diminished cortical synchronization (Ki, Kelly, & Parra, 2016).

We observed the synchronization effect over broad swaths of cortex, causing these maps to be poorly suited for attributing cortical responses seen in a set of regions to a particular processing domain contained within the stimulus. Feature extraction strategies provide one approach for parameterizing processing domains within the stimulus, permitting greater interpretability of the movie-evoked responses (Bartels & Zeki, 2004; Russ & Leopold, 2015). The feature approaches we used in the HD-DOT

work involved both manual feature extraction (e.g. annotation of frames containing visual features) as well as automated feature extraction (e.g. quantification of image parameters such as motion and brightness and quantification of sound intensity). As media annotation algorithms become more sophisticated, it is likely that more features, including those related to narrative content, will be amenable to automated annotation (McNamara, De La Vega, & Yarkoni, 2017).

The feature-based mapping strategies introduced in Chapter 4 resulted in a set of seven features that parametrized low and high-level visual and auditory features contained within the movie. Contrasts between pairs of features enabled more sophisticated comparisons, and implicated distributed sets of regions, a result that is likely attributable to the multi-modal nature of the stimulus. The complexity of these feature maps further highlight that brain regions recruited during naturalistic processing likely differ from processing characterized using more distilled stimuli. Crucially, both cortical mapping approaches are complementary: More controlled stimuli and contrasts enable more precise mappings between cortical regions and underlying information processing, while richer naturalistic stimuli enable mapping of brain activity as it unfolds in real-life contexts, using constellations of region that have been rigorously characterized using other paradigms.

Feature-based mapping approaches face two principal limitations. First, the stimulus chosen constrains the available features. As an extreme example, a silent movie would be inappropriately suited for understanding naturalistic auditory processing. Consequently, if experimenters have a hypothesis-driven question regarding a specific

processing domain, it is critical to assess whether the content of the movie is appropriate for question at hand. Second, the set of features extracted from a stimulus, using the procedures described in Chapter 4, is limited by the experimenter's capability to identify, quantify, and subsequently extract those features. Parameters that map onto sensory domains are more straightforward to quantify than parameters that describe social processing domains. Consequently, more sophisticated tools may enable extraction of more complex features, but it is incumbent on the experimenter to address the interpretability of those more complex features and the resulting correlation maps.

One approach that was not used in the passive movie viewing work described in Chapter 4 was data-driven approaches to decompose the cortical responses measured during movie viewing using approaches such as independent component analysis. Unlike the feature-based mapping approach, which requires an *a priori* decision about which features to map, data-driven approaches extract independent patterns of brain activity that concurrently unfold during stimulus viewing (Lahnakoski et al., 2012; Mantini, Corbetta, Romani, Orban, & Vanduffel, 2012). Like independent component analysis procedures implemented in other brain imaging applications, such as functional connectivity, the maps of the resultant independent components are usually then subject to the experimenter's identification and annotation. Thus, while data-driven approaches could identify related sets of regions that a feature-based approach may not be able to as easily extract, the attribution of a given independent component to a processing domain during naturalistic viewing still depends on an experimenter's judgment.

So far, the naturalistic imaging conducted with HD-DOT has focused largely on repeating paradigms established with fMRI, which is an important step to demonstrate image quality and instrument performance. Future directions with naturalistic imaging paradigms using HD-DOT include extending these paradigms to populations more easily imaged with HD-DOT than other methods, such as children (Bartels & Zeki, 2004; Hasson et al., 2004; Vanderwal, Eilbott, & Castellanos, 2018). Because synchronized cortical responses seem to depend, in part, on an individual's ability to interpret, understand, and follow the stimulus's narrative content in a reproducible way (Ki et al., 2016), cortical reproducibility may follow a developmental trajectory as a child gains the ability to process the stimulus in an adult-like way (Cantlon & Li, 2013; Moraczewski et al., 2018; Nguyen, Vanderwal, & Hasson, 2019). Indeed, prior work has demonstrated more adult-like patterns of cortical activity during movie viewing over development, which may be attributable to comprehension (particularly of content containing linguistic or mathematical information). Consequently, passive movie viewing may provide an attractive solution to image multi-domain cortical processing as it develops from idiosyncratic patterns (i.e. low comprehension) to reproducible patters (i.e. high comprehension).

An alternative to naturalistic imaging with HD-DOT that reliant on paradigms developed with fMRI is to extend these naturalistic tasks to incorporate imaging environments that leverage the bore-free environment of HD-DOT (Zaki & Ochsner, 2009). Indeed, naturalistic imaging using fNIRS has usually leveraged the ability of these techniques to image neural responses accompanying behaviors that are not able to be

performed within a bore, such as conversations or locomotion (Liu et al., 2017; Miyai et al., 2001; Piper et al., 2014). The approaches used to analyze HD-DOT images obtained during movie viewing are well-suited for these even more naturalistic tasks as well. For instance, during conversations, reproducibility of cortical responses across speakers and listeners may index comprehensibility. Further, in environments in which participants are freely moving through environments, a video recording of the participant's behavior that is time-locked to the imaging acquisition enables feature annotation during the imaging session. In this case, the features reflect the participant's actual behavior, rather than the content of a presented stimulus. However, the "feature" concept, as introduced here, is intentionally general, enabling applications in a variety of naturalistic imaging paradigms.

5.5 Closing Comments

This section is the culmination of approximately 10 years spent as a student at WashU. When I first came to WashU in 2009, it was to learn about brains. Specifically, it was because WashU had a program called "Philosophy-Neuroscience-Psychology" that basically guaranteed I would never be bored, and also guaranteed that I would always have a fun fact to tell people about everyone's favorite organ: the brain. Although I have no points of comparison, I will still happily make the claim that WashU is the best place to learn about brains, simply because I have not had to experience boredom for the past 10 years. I am immensely grateful to the faculty and my fellow students for that.

When I learned that you could put a brain in a scanner and obtain all sorts of (potentially) useful information about said person while they stare at a plus sign, I was

shocked, and also decided to pursue graduate education. The Culver Lab simultaneously fulfilled my interest in tinkering with technology with my interest in neuroscience, and I enjoyed being mostly unable to predict what questions would come my way in lab. What's the best way to distill a stroke patient's functional connectome into a single metric? What on earth is going on that causes "$y = A\,x$" to take so long for my computer to solve? How can we understand what the brain is doing during a totally unconstrained task with no behavioral output? While I could rarely predict what the next question was going to be, I was grateful that I could count on it being an interesting question, and that I could count on those around me to help me understand the nuances of it.

As Dr. Ashley Nielsen stated in her dissertation, "While not necessarily ground-breaking for the field of neuroscience as a whole, this series of projects taught me a lot about the scientific process." It is likely not surprising that Ashley has articulated something that also resonates deeply with me. In addition to learning more about biophotonics, instrumentation design, and human neuroimaging than I could even imagine, my graduate education also taught me that the scientific process is much more incremental than I initially appreciated. Despite that incremental progress, I hope that this dissertation contains work that advances the field, however incrementally, towards the goals of using neuroimaging to improve and inform clinical outcomes, learn about how the brain functions in naturalistic conditions, and develop instrumentation to make neuroimaging available for more routine assessments.

When I first joined the Culver Lab, I did not know that "photonics" was a word. Now, it is one of my favorite words--partially because no one else knows that it is a word. Just

as my naïveté towards the field optical neuroimaging nevertheless resulted in what I hope is perceived as a fruitful five or so years in the lab, I am convinced that some of the most interesting pursuits are probably the ones of which I currently have no awareness. While I have chosen to pursue a career in outside of academia, I feel it is important to note that this choice was driven not by a rejection of or disdain for research, but rather in pursuit of my interest in consulting, and my belief that the depth of graduate training combined with the breadth of consulting will provide exposure to those other interesting, but currently unknown interests. Because my time in the lab was so rich and so jam-packed with information, skills, and life lessons, I have no doubt that I will find ways to apply the knowledge I've gained as a graduate student the unexpected situations that have yet to come.

5.6 References

Aslin, R. N., & Mehler, J. (2005). Near-infrared spectroscopy for functional studies of brain activity in human infants: promise, prospects, and challenges. *Journal of Biomedical Optics*, *10*(1), 011009. https://doi.org/10.1117/1.1854672

Barrett, D. E., Radke-Yarrow, M., & Klein, R. E. (1982). Chronic malnutrition and child behavior: Effects of early caloric supplementation on social and emotional functioning at school age. *Developmental Psychology*, *18*(4), 541–556. https://doi.org/10.1037/0012-1649.18.4.541

Bartels, A., & Zeki, S. (2004). Functional brain mapping during free viewing of natural scenes. *Human Brain Mapping*, *21*(2), 75–85. https://doi.org/10.1002/hbm.10153

Bergonzi, K. M., Burns-Yocum, T. M., Bumstead, J. R., Buckley, E. M., Mannion, P. C., Tracy, C. H., … Culver, J. P. (2018). Lightweight sCMOS-based high-density diffuse optical tomography. *Neurophotonics*, *5*(3), 035006. https://doi.org/10.1117/1.NPh.5.3.035006

Boas, D. A., Chen, K., Grebert, D., & Franceschini, M. A. (2004). Improving the diffuse optical imaging spatial resolution of the cerebral hemodynamic response to brain activation in humans. *Optics Letters*, *29*(13), 1506–1508.

Boas, D. A., Gaudette, T., Strangman, G., Cheng, X., Marota, J. J., & Mandeville, J. B. (2001). The accuracy of near infrared spectroscopy and imaging during focal changes in cerebral hemodynamics. *NeuroImage*, *13*(1), 76–90. https://doi.org/10.1006/nimg.2000.0674

Brigadoi, S., Salvagnin, D., Fischetti, M., & Cooper, R. J. (2018). Array Designer: automated optimized array design for functional near-infrared spectroscopy. *Neurophotonics*, *5*(3), 035010. https://doi.org/10.1117/1.NPh.5.3.035010

Cantlon, J. F., & Li, R. (2013). Neural Activity during Natural Viewing of Sesame Street Statistically Predicts Test Scores in Early Childhood. *PLOS Biology*, *11*(1), e1001462. https://doi.org/10.1371/journal.pbio.1001462

Chang, W.-T., Jääskeläinen, I. P., Belliveau, J. W., Huang, S., Hung, A.-Y., Rossi, S., & Ahveninen, J. (2015). Combined MEG and EEG show reliable patterns of electromagnetic brain activity during natural viewing. *NeuroImage*, *114*, 49–56. https://doi.org/10.1016/j.neuroimage.2015.03.066

Chitnis, D., Cooper, R. J., Dempsey, L., Powell, S., Quaggia, S., Highton, D., … Everdell, N. L. (2016). Functional imaging of the human brain using a modular, fibre-less, high-density diffuse optical tomography system. *Biomedical Optics Express*, *7*(10), 4275–4288. https://doi.org/10.1364/BOE.7.004275

Devlin, J. T., & Poldrack, R. A. (2007). In praise of tedious anatomy. *NeuroImage*, *37*(4), 1033–1041; discussion 1050-1058. https://doi.org/10.1016/j.neuroimage.2006.09.055

Dorr, M., Martinetz, T., Gegenfurtner, K. R., & Barth, E. (2010). Variability of eye movements when viewing dynamic natural scenes. *Journal of Vision*, *10*(10), 28–28. https://doi.org/10.1167/10.10.28

Eggebrecht, A. T., Elison, J. T., Feczko, E., Todorov, A., Wolff, J. J., Kandala, S., … Pruett, J. R. (2017). Joint Attention and Brain Functional Connectivity in Infants and Toddlers. *Cerebral Cortex*, *27*(3), 1709–1720. https://doi.org/10.1093/cercor/bhw403

Eggebrecht, A. T., Ferradal, S. L., Robichaux-Viehoever, A., Hassanpour, M. S., Dehghani, H., Snyder, A. Z., … Culver, J. P. (2014). Mapping distributed brain function and networks with diffuse optical tomography. *Nature Photonics*, *8*(6), 448–454. https://doi.org/10.1038/nphoton.2014.107

Eggebrecht, A. T., White, B. R., Ferradal, S. L., Chen, C., Zhan, Y., Snyder, A. Z., … Culver, J. P. (2012). A quantitative spatial comparison of high-density diffuse optical tomography and fMRI cortical mapping. *NeuroImage*, *61*(4), 1120–1128. https://doi.org/10.1016/j.neuroimage.2012.01.124

Ferradal, S. L., Liao, S. M., Eggebrecht, A. T., Shimony, J. S., Inder, T. E., Culver, J. P., & Smyser, C. D. (2016). Functional Imaging of the Developing Brain at the Bedside

Using Diffuse Optical Tomography. *Cerebral Cortex*, *26*(4), 1558–1568. https://doi.org/10.1093/cercor/bhu320

Grantham-McGregor, S. (1995). A Review of Studies of the Effect of Severe Malnutrition on Mental Development. *The Journal of Nutrition*, *125*(suppl_8), 2233S-2238S. https://doi.org/10.1093/jn/125.suppl_8.2233S

Greene, D. J., Church, J. A., Dosenbach, N. U. F., Nielsen, A. N., Adeyemo, B., Nardos, B., … Schlaggar, B. L. (2016). Multivariate pattern classification of pediatric Tourette syndrome using functional connectivity MRI. *Developmental Science*, *19*(4), 581–598. https://doi.org/10.1111/desc.12407

Hassanpour, M. S., Eggebrecht, A. T., Culver, J. P., & Peelle, J. E. (2015). Mapping cortical responses to speech using high-density diffuse optical tomography. *NeuroImage*, *117*, 319–326. https://doi.org/10.1016/j.neuroimage.2015.05.058

Hasson, U., Nir, Y., Levy, I., Fuhrmann, G., & Malach, R. (2004). Intersubject Synchronization of Cortical Activity During Natural Vision. *Science*, *303*(5664), 1634–1640. https://doi.org/10.1126/science.1089506

Hirsch, J., Zhang, X., Noah, J. A., & Ono, Y. (2017). Frontal temporal and parietal systems synchronize within and across brains during live eye-to-eye contact. *NeuroImage*, *157*, 314–330. https://doi.org/10.1016/j.neuroimage.2017.06.018

Hoyt, C. R., Van, A. N., Ortega, M., Koller, J. M., Everett, E. A., Nguyen, A. L., … Dosenbach, N. U. F. (2019). Detection of Pediatric Upper Extremity Motor Activity and Deficits With Accelerometry. *JAMA Network Open*, *2*(4), e192970–e192970. https://doi.org/10.1001/jamanetworkopen.2019.2970

Jackson, E. S., Wijeakumar, S., Beal, D. S., Brown, B., Zebrowski, P., & Spencer, J. P. (2019). A fNIRS Investigation of Speech Planning and Execution in Adults Who Stutter. *Neuroscience*, *406*, 73–85. https://doi.org/10.1016/j.neuroscience.2019.02.032

Kapur, A., Kapur, S., & Maes, P. (2018). AlterEgo: A Personalized Wearable Silent Speech Interface. *23rd International Conference on Intelligent User Interfaces*, 43–53. https://doi.org/10.1145/3172944.3172977

Kauttonen, J., Hlushchuk, Y., & Tikka, P. (2015). Optimizing methods for linking cinematic features to fMRI data. *NeuroImage*, *110*, 136–148. https://doi.org/10.1016/j.neuroimage.2015.01.063

Ki, J. J., Kelly, S. P., & Parra, L. C. (2016). Attention Strongly Modulates Reliability of Neural Responses to Naturalistic Narrative Stimuli. *Journal of Neuroscience*, *36*(10), 3092–3101. https://doi.org/10.1523/JNEUROSCI.2942-15.2016

Lahnakoski, Juha M., Salmi, J., Jääskeläinen, I. P., Lampinen, J., Glerean, E., Tikka, P., & Sams, M. (2012). Stimulus-Related Independent Component and Voxel-Wise

Analysis of Human Brain Activity during Free Viewing of a Feature Film. *PLOS ONE*, *7*(4), e35215. https://doi.org/10.1371/journal.pone.0035215

Lahnakoski, Juha Marko, Glerean, E., Salmi, J., Jääskeläinen, I. P., Sams, M., Hari, R., & Nummenmaa, L. (2012). Naturalistic fMRI Mapping Reveals Superior Temporal Sulcus as the Hub for the Distributed Brain Network for Social Perception. *Frontiers in Human Neuroscience*, *6*. https://doi.org/10.3389/fnhum.2012.00233

Laumann, T. O., Gordon, E. M., Adeyemo, B., Snyder, A. Z., Joo, S. J., Chen, M.-Y., … Petersen, S. E. (2015). Functional System and Areal Organization of a Highly Sampled Individual Human Brain. *Neuron*, *87*(3), 657–670. https://doi.org/10.1016/j.neuron.2015.06.037

Lee, M. H., Smyser, C. D., & Shimony, J. S. (2013). Resting-State fMRI: A Review of Methods and Clinical Applications. *American Journal of Neuroradiology*, *34*(10), 1866–1872. https://doi.org/10.3174/ajnr.A3263

Linneman, Z., Matilsky, D., Ndekha, M., Manary, M. J., Maleta, K., & Manary, M. J. (2007). A large-scale operational study of home-based therapy with ready-to-use therapeutic food in childhood malnutrition in Malawi. *Maternal & Child Nutrition*, *3*(3), 206–215. https://doi.org/10.1111/j.1740-8709.2007.00095.x

Liu, Y., Piazza, E. A., Simony, E., Shewokis, P. A., Onaral, B., Hasson, U., & Ayaz, H. (2017). Measuring speaker–listener neural coupling with functional near infrared spectroscopy. *Scientific Reports*, *7*, 43293. https://doi.org/10.1038/srep43293

Lloyd-Fox, S., Blasi, A., & Elwell, C. E. (2010). Illuminating the developing brain: The past, present and future of functional near infrared spectroscopy. *Neuroscience & Biobehavioral Reviews*, *34*(3), 269–284. https://doi.org/10.1016/j.neubiorev.2009.07.008

Lloyd-Fox, Sarah, Blasi, A., Volein, A., Everdell, N., Elwell, C. E., & Johnson, M. H. (2009). Social Perception in Infancy: A Near Infrared Spectroscopy Study. *Child Development*, *80*(4), 986–999. https://doi.org/10.1111/j.1467-8624.2009.01312.x

Lloyd-Fox, Sarah, Halliday, D., Begus, K., Darboe, M., Prentice, A., Moore, S., & Elwell, C. (2015). Measuring Brain Function in Newborns in Rural Gambia. *The FASEB Journal*, *29*(1_supplement), 899.5. https://doi.org/10.1096/fasebj.29.1_supplement.899.5

Lloyd-Fox, Sarah, Papademetriou, M., Darboe, M. K., Everdell, N. L., Wegmuller, R., Prentice, A. M., … Elwell, C. E. (2014). Functional near infrared spectroscopy (fNIRS) to assess cognitive function in infants in rural Africa. *Scientific Reports*, *4*, 4740. https://doi.org/10.1038/srep04740

Manary, M. J., Ndkeha, M. J., Ashorn, P., Maleta, K., & Briend, A. (2004). Home based therapy for severe malnutrition with ready-to-use food. *Archives of Disease in Childhood*, *89*(6), 557–561. https://doi.org/10.1136/adc.2003.034306

Mantini, D., Corbetta, M., Romani, G. L., Orban, G. A., & Vanduffel, W. (2012). Data-driven analysis of analogous brain networks in monkeys and humans during natural vision. *NeuroImage*, *63*(3), 1107–1118. https://doi.org/10.1016/j.neuroimage.2012.08.042

Marrus, N., Eggebrecht, A. T., Todorov, A., Elison, J. T., Wolff, J. J., Cole, L., … Pruett, J. R. (2018). Walking, Gross Motor Development, and Brain Functional Connectivity in Infants and Toddlers. *Cerebral Cortex*, *28*(2), 750–763. https://doi.org/10.1093/cercor/bhx313

McNamara, Q., De La Vega, A., & Yarkoni, T. (2017). Developing a Comprehensive Framework for Multimodal Feature Extraction. *Proceedings of the 23rd ACM SIGKDD International Conference on Knowledge Discovery and Data Mining*, 1567–1574. https://doi.org/10.1145/3097983.3098075

Miyai, I., Tanabe, H. C., Sase, I., Eda, H., Oda, I., Konishi, I., … Kubota, K. (2001). Cortical Mapping of Gait in Humans: A Near-Infrared Spectroscopic Topography Study. *NeuroImage*, *14*(5), 1186–1192. https://doi.org/10.1006/nimg.2001.0905

Moraczewski, D., Chen, G., & Redcay, E. (2018). Inter-subject synchrony as an index of functional specialization in early childhood. *Scientific Reports*, *8*(1), 2252. https://doi.org/10.1038/s41598-018-20600-0

Morais, G. A. Z., Balardin, J. B., & Sato, J. R. (2018). fNIRS Optodes' Location Decider (fOLD): a toolbox for probe arrangement guided by brain regions-of-interest. *Scientific Reports*, *8*(1), 3341. https://doi.org/10.1038/s41598-018-21716-z

Naseer, N., & Hong, K.-S. (2015). fNIRS-based brain-computer interfaces: a review. *Frontiers in Human Neuroscience*, *9*. https://doi.org/10.3389/fnhum.2015.00003

Nguyen, M., Vanderwal, T., & Hasson, U. (2019). Shared understanding of narratives is correlated with shared neural responses. *NeuroImage*, *184*, 161–170. https://doi.org/10.1016/j.neuroimage.2018.09.010

Norbury, C. F., Brock, J., Cragg, L., Einav, S., Griffiths, H., & Nation, K. (2009). Eye-movement patterns are associated with communicative competence in autistic spectrum disorders. *Journal of Child Psychology and Psychiatry*, *50*(7), 834–842. https://doi.org/10.1111/j.1469-7610.2009.02073.x

Odabaş, D., Caksen, H., Sar, S., Unal, O., Tuncer, O., Ataş, B., & Yilmaz, C. (2005). Cranial MRI findings in children with protein energy malnutrition. *The International Journal of Neuroscience*, *115*(6), 829–837. https://doi.org/10.1080/00207450590882082

Ono, Y., Noah, J. A., Zhang, X., Nomoto, Y., Suzuki, T., Shimada, S., … Hirsch, J. (2015). Motor learning and modulation of prefrontal cortex: an fNIRS assessment. *Journal of Neural Engineering*, *12*(6), 066004. https://doi.org/10.1088/1741-2560/12/6/066004

Petersen, S. E., Fox, P. T., Posner, M. I., Mintun, M., & Raichle, M. E. (1989). Positron Emission Tomographic Studies of the Processing of Singe Words. *Journal of Cognitive Neuroscience*, *1*(2), 153–170. https://doi.org/10.1162/jocn.1989.1.2.153

Piper, S. K., Krueger, A., Koch, S. P., Mehnert, J., Habermehl, C., Steinbrink, J., … Schmitz, C. H. (2014). A wearable multi-channel fNIRS system for brain imaging in freely moving subjects. *NeuroImage*, *85 Pt 1*, 64–71. https://doi.org/10.1016/j.neuroimage.2013.06.062

Power, J. D., Barnes, K. A., Snyder, A. Z., Schlaggar, B. L., & Petersen, S. E. (2012). Spurious but systematic correlations in functional connectivity MRI networks arise from subject motion. *NeuroImage*, *59*(3), 2142–2154. https://doi.org/10.1016/j.neuroimage.2011.10.018

Raichle, M. E., & Mintun, M. A. (2006). Brain Work and Brain Imaging. *Annual Review of Neuroscience*, *29*(1), 449–476. https://doi.org/10.1146/annurev.neuro.29.051605.112819

Roberts, S. B., Franceschini, M. A., Krauss, A., Lin, P.-Y., Braima de Sa, A., Có, R., … Muentener, P. (2017a). A Pilot Randomized Controlled Trial of a New Supplementary Food Designed to Enhance Cognitive Performance during Prevention and Treatment of Malnutrition in Childhood. *Current Developments in Nutrition*, *1*(11). https://doi.org/10.3945/cdn.117.000885

Roberts, S. B., Franceschini, M. A., Krauss, A., Lin, P.-Y., Braima de Sa, A., Có, R., … Muentener, P. (2017b). A Pilot Randomized Controlled Trial of a New Supplementary Food Designed to Enhance Cognitive Performance during Prevention and Treatment of Malnutrition in Childhood. *Current Developments in Nutrition*, *1*(11). https://doi.org/10.3945/cdn.117.000885

Russ, B. E., & Leopold, D. A. (2015). Functional MRI mapping of dynamic visual features during natural viewing in the macaque. *NeuroImage*, *109*, 84–94. https://doi.org/10.1016/j.neuroimage.2015.01.012

Saager, R. B., & Berger, A. J. (2005). Direct characterization and removal of interfering absorption trends in two-layer turbid media. *Journal of the Optical Society of America. A, Optics, Image Science, and Vision*, *22*(9), 1874–1882.

Sherafati, A., Eggebrecht, A. T., Burns-Yocum, T. M., & Culver, J. P. (2017). A global metric to detect motion artifacts in optical neuroimaging data (Conference Presentation). *Neural Imaging and Sensing*, *10051*, 1005112. https://doi.org/10.1117/12.2252417

Singh, A. K., Okamoto, M., Dan, H., Jurcak, V., & Dan, I. (2005). Spatial registration of multichannel multi-subject fNIRS data to MNI space without MRI. *NeuroImage*, *27*(4), 842–851. https://doi.org/10.1016/j.neuroimage.2005.05.019

Smyser, C. D., Inder, T. E., Shimony, J. S., Hill, J. E., Degnan, A. J., Snyder, A. Z., & Neil, J. J. (2010). Longitudinal analysis of neural network development in preterm infants. *Cerebral Cortex (New York, N.Y.: 1991)*, *20*(12), 2852–2862. https://doi.org/10.1093/cercor/bhq035

Smyser, C. D., Snyder, A. Z., Shimony, J. S., Blazey, T. M., Inder, T. E., & Neil, J. J. (2013). Effects of white matter injury on resting state fMRI measures in prematurely born infants. *PloS One*, *8*(7), e68098. https://doi.org/10.1371/journal.pone.0068098

Thomason, M. E., Dassanayake, M. T., Shen, S., Katkuri, Y., Alexis, M., Anderson, A. L., … Romero, R. (2013). Cross-Hemispheric Functional Connectivity in the Human Fetal Brain. *Science Translational Medicine*, *5*(173), 173ra24-173ra24. https://doi.org/10.1126/scitranslmed.3004978

Vanderwal, T., Eilbott, J., & Castellanos, F. X. (2018). Movies in the magnet: Naturalistic paradigms in developmental functional neuroimaging. *Developmental Cognitive Neuroscience*. https://doi.org/10.1016/j.dcn.2018.10.004

Wheelock, M. D., Austin, N. C., Bora, S., Eggebrecht, A. T., Melzer, T. R., Woodward, L. J., & Smyser, C. D. (2018). Altered functional network connectivity relates to motor development in children born very preterm. *NeuroImage*, *183*, 574–583. https://doi.org/10.1016/j.neuroimage.2018.08.051

White, B. R., & Culver, J. P. (2010a). Phase-encoded retinotopy as an evaluation of diffuse optical neuroimaging. *NeuroImage*, *49*(1), 568–577. https://doi.org/10.1016/j.neuroimage.2009.07.023

White, B. R., & Culver, J. P. (2010b). Quantitative evaluation of high-density diffuse optical tomography: in vivo resolution and mapping performance. *Journal of Biomedical Optics*, *15*(2), 026006. https://doi.org/10.1117/1.3368999

Wijeakumar, S., Kumar, A., Reyes, L. M. D., Tiwari, M., & Spencer, J. P. (n.d.). Early adversity in rural India impacts the brain networks underlying visual working memory. *Developmental Science*, *0*(0), e12822. https://doi.org/10.1111/desc.12822

Yamamoto, T., Maki, A., Kadoya, T., Tanikawa, Y., Yamada, Y., Okada, E., & Koizumi, H. (2002). Arranging optical fibres for the spatial resolution improvement of topographical images. *Physics in Medicine and Biology*, *47*(18), 3429–3440. https://doi.org/10.1088/0031-9155/47/18/311

Zaki, J., & Ochsner, K. (2009). The Need for a Cognitive Neuroscience of Naturalistic Social Cognition. *Annals of the New York Academy of Sciences*, *1167*(1), 16–30. https://doi.org/10.1111/j.1749-6632.2009.04601.x

Zeff, B. W., White, B. R., Dehghani, H., Schlaggar, B. L., & Culver, J. P. (2007). Retinotopic mapping of adult human visual cortex with high-density diffuse optical

tomography. *Proceedings of the National Academy of Sciences of the United States of America*, *104*(29), 12169–12174. https://doi.org/10.1073/pnas.0611266104